Author:
Bellamy, Jake

Title:
G9a as a potential therapeutic target in MYCN-amplified neuroblastomas

G9a as a potential therapeutic target in *MYCN*-amplified neuroblastomas

Jacob Bellamy

A thesis submitted to the University of Bristol in accordance with the requirements for award of the degree of Master of Science by Research in the Faculty of Biomedical Sciences, School of Cellular and Molecular Medicine.

November 2018

Word count – 29,952

Abstract

MYCN-amplification is a high-risk factor in neuroblastoma which contributes to a poor prognostic outcome. Here data is presented showing that both short-interfering (si) RNA depletion and treatment by small molecule inhibitors (SMI) of lysine-specific histone methyltransferase Euchromatic Histone Lysine Methyltransferase 2 (G9a) leads to impaired growth in all tested neuroblastoma cell lines. Furthermore, in cell lines representative of high-risk neuroblastomas with *MYCN*-amplification, there is a significant increase in apoptosis and cell death. There is also a significant reduction in MYCN protein in MYCN-overexpressing cells, including in SHEP-21N cell line with inducible MYCN expression, after both G9a knockdown and SMI treatment independently. This suggests there is a synthetic lethal relationship between G9a and MYCN.

G9a-associated reduction of MYCN leads to the re-expression of repressed tumour suppressor and pro-apoptotic factor BCL-2 Related Ovarian Killer (BOK). Quantitative gene expression analysis and immunoblotting of neuroblastoma cell lines shows an increase in BOK after both G9a depletion and SMI treatment independently which is only apparent in the *MYCN*-overexpressing cell lines; this increase in BOK leads to apoptosis, and BOK depletion was able to rescue G9a inhibition-associated apoptosis.

Together, these studies show that G9a is a major oncoprotein in neuroblastoma tumourigenesis and a novel regulator of MYCN protein; this suggests that together they repress pro-apoptotic factor BOK to block apoptosis in high-risk neuroblastoma.

Acknowledgements

I am grateful to everyone who has supported me over the course of the past year and a half. This support is the only thing that has given me the strength to carry on. It has not been easy with numerous unforeseen challenges from the start.

Firstly, I would like to thank my supervisor, Dr. Karim Malik, who gave me the opportunity to undertake this project in his lab. His supervision and drive to uncover new ideas has helped me expand not only my knowledge, but also my hunger and will to compete in research.

I would also like to thank all the past and present members of the CEL lab for making the laboratory a welcoming and fun place to be. Their scientific expertise and friendship have been invaluable. I am especially indebted to Dr. Madhu Kollareddy, Dr. Marianna Szemes, and Dr. Zach Dixon.

Also, I would like to thank the University for giving me the opportunity to meet life-long friends, Kelli and Bianca. They have helped me enjoy being a researcher and countless quizzes have broadened my general knowledge.

Finally, but certainly not least, I am grateful to my partner Mia and my family, who have put up with so much whilst I have been at my lowest. Your support will never be forgotten, and it is to you that I dedicate this thesis.

Author's declaration

I declare that the work in this dissertation was carried out in accordance with the requirements of the University's Regulations and Code of Practice for Research Degree Programmes and that it has not been submitted for any other academic award. Except where indicated by specific reference in the text, the work is the candidate's own work. Work done in collaboration with, or with the assistance of, others, is indicated as such. Any views expressed in the dissertation are those of the author.

SIGNED:…… DATE:……....

Contents

List of Tables and Figures

Abbreviations

AKR1C1	Aldoketo reductase family C1
AKR1C2	Aldoketo reductase family C2
AKR1C3	Aldoketo reductase family C3
ALK	Anaplastic lymphoma kinase
AMHR2	Anti-Mullerian hormone receptor II
AML	Acute myeloid leukaemia
BAK	BCL-2 homologous antagonist killer
BAX	BCL-2-associated X protein
BCA	Bicinchoninic acid assay
BH Domain	BCL-2 homology domain
BOK	BCL-2 related Ovarian Killer
BSA	Bovine serum albumin
CASP8	Caspase 8
CCBE1	Collagen and calcium-binding epidermal growth factor domains 1
CLU	Clusterin
cPARP	Cleaved PARP
DNMT1	DNA Methyltransferase 1
EHMT1	Euchromatic Histone Lysine Methyltransferase 1
EHMT2	Euchromatic Histone Lysine Methyltransferase 2
EMT	Epithelial-mesenchymal transition
ER	Endoplasmic reticulum
EZH2	Enhancer of Zeste 2

FABP3	Fatty acid binding protein 3
FBS	Foetal bovine serum
FBXW7	F-box and WD repeat domain-containing 7
FLCN	Folliculin
GR	Glucocorticoid receptor
H3K9me2	Di-methylation of Histone 3 Lysine 9
HDAC	Histone Deacetylase
HP1	Heterochromatin Protein 1
IC50	Half maximal inhibitory concentration
INRGSS	International Neuroblastoma Risk Group Strategy System
INSS	International Neuroblastoma Staging System
MAPK	Mitogen-activated protein kinase
MNA	*MYCN* amplified
MOMP	Mitochondrial outer membrane permeabilisation
MTT	3-(4,5-dimethylthiazol-2-yl)-2,5-diphenyltetrazolium bromide
NB	Neuroblastoma
NES	Nuclear export signal
Non-MNA	Non-*MYCN* amplified
NLS	Nuclear localisation signal
OMM	Outer mitochondrial membrane
PARP	Poly(ADP-ribose) polymerase
PI3K	Phosphatidylinositol-4,5-Bisphosphate 3-Kinase
PK	Pharmacokinetic

PRC2	Polycomb repressor complex 2
Q-VD-Oph	5-(2,6-Difluorophenoxy)-3-[[3-methyl-1-oxo-2-[(2-quinolinylcarbonyl)amino] butyl]amino]-4-oxo-pentanoic acid
SAM	S-adenosylmethionine
SDS	Sodium dodecyl sulphate
SEM	Standard error of the mean
SET domain	Su(var)3-9, Enhancer-of-zeste and Trithorax domain
siRNA	Short interfering RNA
SMI	Small molecule inhibitors
TBP	TATA-Box Binding Protein
TERT	Telomerase reverse transcriptase
TET	Tetracycline

Chapter 1

General introduction

1.1 The Hallmarks of Cancer

Cancer is a multistep disease that was originally thought to comprise of six biological capabilities during development of human tumours; this has now grown to ten which are illustrated in Figure 1.1, along with potential therapeutics to target them. These include sustaining proliferative signalling, evading growth suppressors, resisting cell death, enabling replicative immortality, inducing angiogenesis, and activating invasion and metastasis (1). Causal to these capabilities is genomic instability which enables the genetic diversity necessary to generate these hallmarks. Somatic evolution is the acquisition and build-up mutations and epimutations in somatic cells (2). This clonal selection and expansion based on which genetic attributes help the tumour to survive and help to drive these hallmarks.

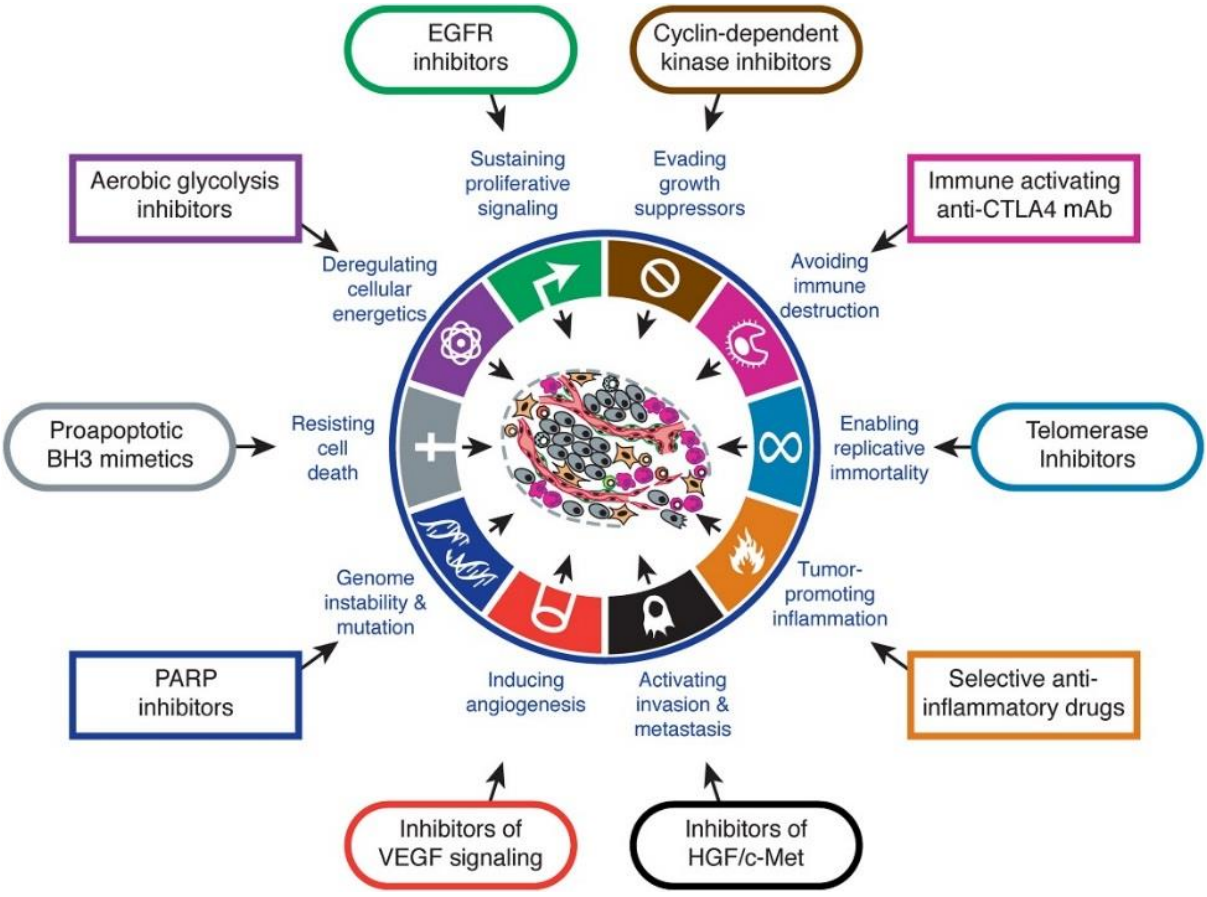

Figure 1.1– Hallmarks of cancer with targeted therapeutic treatments taken from Hanahan et al (1).

1.1.1 Oncogenes, mutations, and gene amplification

A proto-oncogene is a gene that has the potential to become oncogenic and cause cancer by becoming mutated and/or expressed at elevated levels relative to normal. Oncogenes encode proteins involved in cell proliferation and/or apoptosis. These include transcription factors, chromatin remodelers, growth factors and growth factor receptors, signal transducers, and apoptosis regulators (3). Many types of mutations can occur in oncogenes to change the structure to create an enhanced oncoprotein. For example, mutations in *RAS* gene codons 12, 13, or 61 encode for a constitutively active version of the triphosphatases that links tyrosine kinases to downstream serine and threonine kinases to induce continuous cell growth (3).

The number of mutations found in any cancer can vary from 10 or 20 to thousands. Only a few of these mutations are driver mutations that are subject to selection during tumourigenesis, for example *MYC* and *ABL1* (4). The vast majority of gene mutations are just passengers which don't actively contribute to tumourigenesis and are therefore not under a selection pressure (2).

Another oncogenic mechanism is gene amplification is an increase in copy number of a particular region of a chromosome arm. This leads to the overexpression of the amplified genes and thus these become oncogenic. An example is the amplification *ERBB1* and *ERBB2* in glioblastoma and breast cancer respectively (5).

1.1.2 Tumour Suppressors

A tumour suppressor gene is defined as a gene that normally inhibits cell division and protects the cell from becoming oncogenic. There are many examples of known tumour suppressor genes such as *TP53* (6), *APC* (7), and *PTEN* (8).

Tumour suppressors act through many biological functions to facilitate protection from tumourigenesis (9). For example, tumour suppressors can act at various stages of cell division to facilitate a smooth transition through the cell cycle. Tumour suppressor RB can act to repress genes necessary for the cell cycle to continue thus halting cell division in G_1 phase. If DNA damage is recognised, cell division will also be brought to a halt. ATM kinase for example, recognises double-strand DNA breaks and so phosphorylates substrates to initiate cell cycle checkpoint responses and DNA repair processes (10). If this DNA damage cannot be fixed, p53 can then induce apoptosis

to remove the faulty cell. A mutation in a tumour suppressor at any of these steps could potentially lead to tumourigenesis.

Unlike oncogenes, tumour suppressor genes necessitate a mutation in both alleles of the gene to render the tumour inhibitory power of the encoded protein obsolete. If only one of these alleles is damaged, the second can still generate the correct protein; this is Knudson's two-hit hypothesis in which tumour suppressor retinoblastoma protein (pRb) was first documented (11). There are exceptions to this rule however, as mutations in one allele of *TP53* can cause a dominant negative effect by inactivating the wild type function of p53. This effect was shown in transgenic mouse models expressing p53 mutated at residue 135 in a $p53^{+/-}$ background. These had a higher incidence of tumourigenesis relative to $p53^{+/-}$ mice without the transgene (12), suggesting this mutant can induce carcinogenesis in the presence of the wild type p53. This has also been observed in human cancers, as dominant negative mutations of p53 are associated with the early onset of glioblastoma (13). The mechanism for this negative dominant effect suggests that missense mutants of p53 prevent wild type p53 from binding to p53 target gene promoters, such as p21 and MDM2, which prevents it from carrying out its tumour suppressor function (14).

There are also a group of genes and proteins which prevent tumour cells from metastasising which are known as metastasis repressors. The first metastasis-suppressor gene, *NME1* (*nm23*), is active in melanoma, breast, and colon cancers and works to inhibit kinases that promote cell division (15). The proteins can be used as prognostic markers, for example, high expression of kinase *NME1* is correlated with good prognosis in breast (16, 17), gastric (18), and non-small cell carcinoma (19).

1.1.3 Apoptosis pathways

There are two main pathways that lead to caspase-dependent apoptosis (20-22), outlined in Figure 1.2. These are the extrinsic (or death-receptor) and intrinsic (or mitochondrial) pathways. The extrinsic pathway involves stimulation of death receptors by death ligands, for example Fas ligand binds to Fas receptors to trigger downstream apoptosis by activating a caspase cascade (23). The intrinsic pathway is characterised by mitochondrial outer membrane permeabilisation (MOMP) following intrinsic stimuli such as DNA damage (24) and the consequent release of cytochrome c into the cytosol through a pore in the membrane. Cytochrome c then binds with apoptosis initiator protein APAF1 to form the apoptosome which activates caspase-9 (25).

There is also evidence to suggest the two pathways are linked as both pathways activate initiator caspases which activate the executioner caspases. Cleavage of BID by caspase-8 leads to the generation of cleaved BID that is translocated to the mitochondria to drive the intrinsic pathway (26). This shows that there is some crosstalk between the intrinsic and extrinsic pathways to strengthen the apoptotic signal (21).

1.1.4 Pro- and anti-apoptotic factors

The BCL-2 family of proteins regulate cell death at the mitochondrial level. These can be split it to two antagonistic groups: pro-apoptotic and anti-apoptotic. The balance between pro- and anti-apoptotic proteins determines the sensitivity of the cells towards apoptotic stimuli; excess of pro-apoptotic factors makes the cells sensitive to apoptotic stimuli, whereas excess of anti-apoptotic factors decreases their sensitivity. Table 1.1 shows the members of each family. All anti-apoptotic proteins are multi-region proteins containing four BCL-2 homology (BH) regions, BH1-BH4. Pro-apoptotic factors are subdivided further; BAK and BAX oligomerise to perform MOMP, whereas BID, BIM/BAD, and NOXA promote apoptosis through activation of BAX or BAK or inhibition of anti-apoptotic factors (27). The structure of the BCL-2 family is defined by the presence of BH domains- short stretch of conserved sequence around 20 amino acid residues in length (28, 29). This is represented in Figure 1.3. For the purposes of this study, only BAK, BAX, and BOK will be focussed upon in more detail.

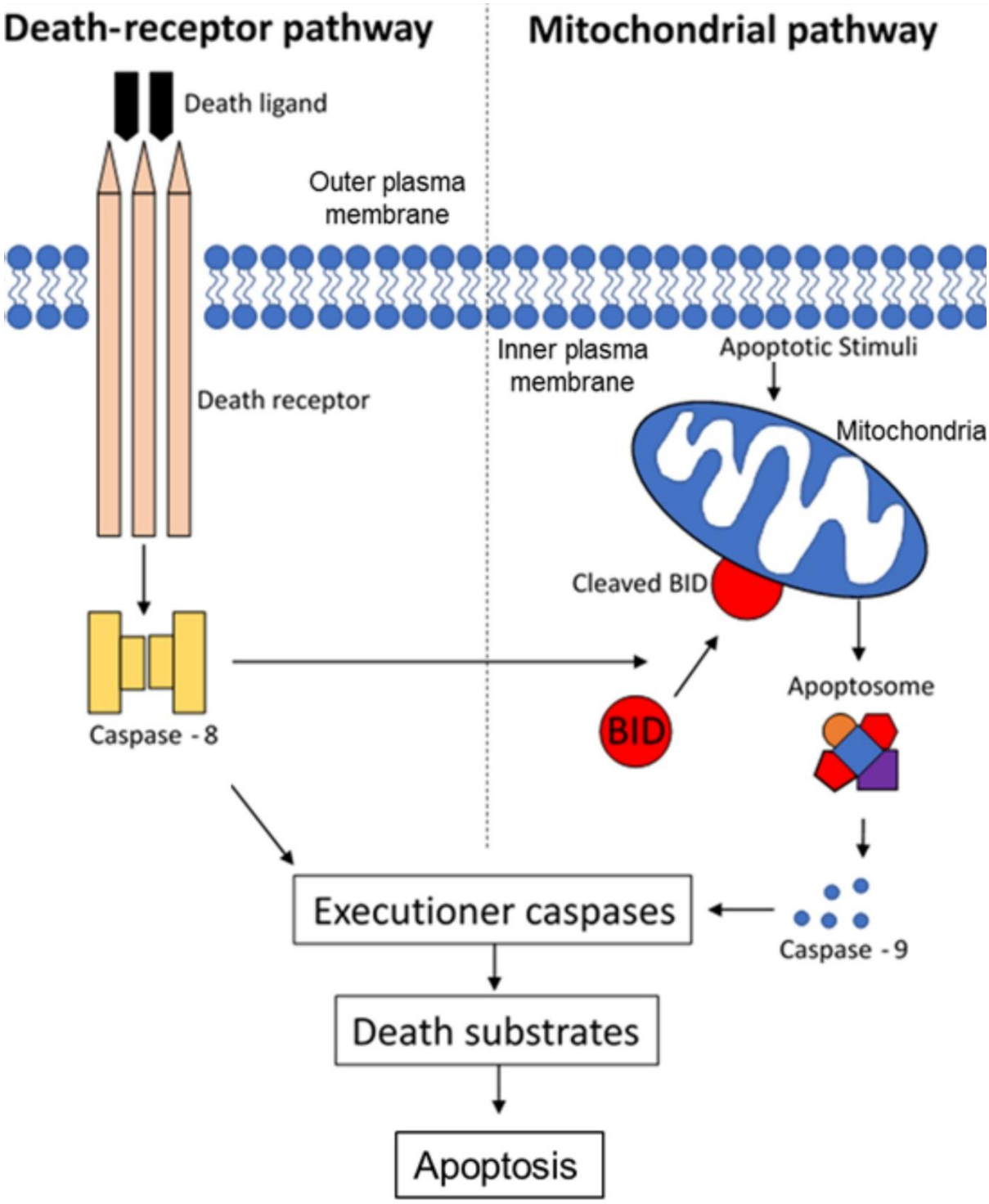

Figure 1.2 – a basic graphical representation of death-receptor (extrinsic) and mitochondrial (intrinsic) apoptotic pathways adapted from Igney et al (21).
Extrinsic pathway *– Action of death ligand binding to complementary death-ligand receptor initiates downstream apoptosis.* ***Intrinsic pathway*** *– Apoptotic stimulus, such as DNA damage, initiates MOMP which releases cytochrome c and activates the apoptosome to drive downstream apoptosis.*

Family	BCL-2			
Group	Pro-apoptotic			Pro-survival
Sub-group	Multi-region		BH3-only	Multi-region pro-survival
Members	BAK, BAX, BOK	BID	BIM, BAD, NOXA	BCL-2, BCL-XL, MCL-1, BCL-W
Regions	MBR, BH1, BH2, BH3, BH4	MBR, BH3, BH4	MBR, BH3	MBR, BH1, BH2, BH3, BH4

Table 1.1– Classification of BCL-2 family proteins adapted from Siddiqui et al (27).
Two groups of the BCL-2 family are either anti-apoptotic or pro-apoptotic. Anti-apoptotic proteins are multi-region proteins which contain four BH domains. Multi-region BAK, BAX, BOK, and BID have more than one BH domain structurally similar to the parent protein BCL-2. BIM, BAD, and NOXA contain only the BH3 region. All contain a C-terminal transmembrane domain, a membrane-bound region (MBR), that enables translocation or localisation to the MOM or ER.

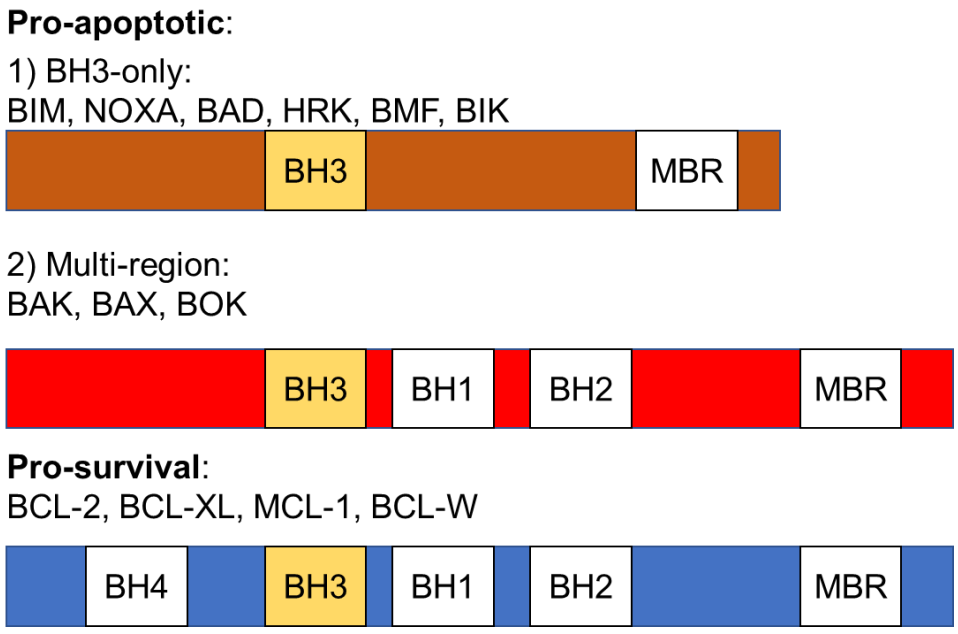

Figure 1.3 – Basic structural representation of the three branches of the BCL-2 family.
The BH domains are numbered, with BH3 common to all branches (yellow). MBR represents the membrane-bound region that enables translocation or localisation to the MOM or ER.

1.1.5 Normal regulation of multi-region apoptotic factors

There are distinct mechanisms by which these apoptotic factors are regulated. For example, following an intrinsic death stimulus, pro-apoptotic BAX and BAK homo-dimerise and translocate to the outer mitochondrial membrane (OMM) from the cytosol where they undergo a conformational change to form the structures necessary for MOMP (30-32). This homo-dimerisation is dominant irrespective of the presence of survival factors (33). Furthermore, pro-apoptotic BAK, which is normally found localised to the OMM, can form complexes with anti-apoptotic MCL-1 which negatively regulates the BAK's pro-apoptotic activity (34). This regulation is outlined in Figure 1.4.

Pro-apoptotic factor BOK is a relatively recent addition having been cloned in a yeast two-hybrid screen of ovarian cDNA (35). BOK hetero-dimerises with anti-apoptotic BCL-2-member MCL-1 which in turn regulates apoptosis. It has previously been suggested to play a role in ER-stress induced cell death (36, 37), and more recently a role in the mitochondrial apoptotic pathway (38). In addition, other transcriptional regulators of BOK expression include members of the E2F family of transcription factors as both E2F1 and E2F3 can associate with the BOK promoter *in vivo* to promote transcription (39).

1.1.6 Regulation of apoptosis in cancer

A major hallmark of cancer is evading apoptotic cell death which is normally triggered in response to physiologic stresses that cancer cells experience during the course of tumorigenesis. This plays a critical role in the initiation and progression of cancers. Tumours have been shown to use multiple mechanisms to regulate apoptosis by upregulating expression of anti-apoptotic oncogenes or downregulating pro-apoptotic tumour suppressor genes. For example, increased expression of anti-apoptotic BCL-2 in follicular lymphoma helps the tumour survive which suggests it and other anti-apoptotic proteins are potential oncogenes (40).

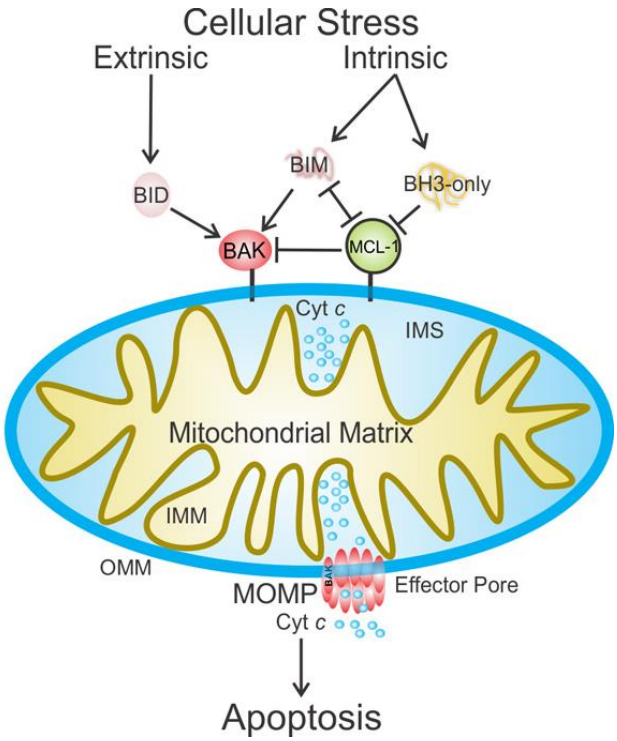

Figure 1.4 – Mediation of the mitochondrial apoptotic pathway by the BCL-2 family of proteins taken from Moldoveanu et al (41).
When cellular stress activates more pro-apoptotic BH3-only proteins to override the anti-apoptotic response, BAK and BAX are stimulated to form pores in the outer mitochondrial membrane (OMM). This releases cytochrome c (Cyt c) into the cytosol to activate the apoptosome and downstream apoptosis.

1.2 Epigenetics and cancer

1.2.1 The epigenetic machinery of normal cells

In addition to the genetic loss of tumour suppressor gene function, they can be functionally eliminated as a result of epigenetic silencing. DNA methylation, and covalent histone modifications are epigenetic mechanisms. These alter the structural dynamics of chromatin to regulate the functioning of the genome and so can silence tumour suppressor genes.

1.2.1.1 DNA methylation

DNA methylation occurs by modifying the cytosine residues in CpG dinucleotide rich stretches (CpG islands) in promoter regions of a gene (42). DNA methylation leads to gene silencing by both preventing and promoting the recruitment of regulatory proteins to DNA, for instance, blocking transcription factor c-MYC from accessing binding sites to repress gene expression (43). DNA methylation patterns are governed by the

cooperative activity of *de novo* methyltransferases DNMT3A and DNMT3B, and maintenance methyltransferase DNMT1. *De novo* adds methyl groups to unmethylated cytosines, whereas maintenance adds methyl groups to DNA that has one strand already methylated; *de novo* methyltransferases set the methylation patterns, which are maintained by the maintenance methyltransferase. Non-covalent mechanisms consist of nucleosome remodelling and the replacement of canonical histones with specialised variants. These are important in how the structure of the chromatin regulates gene activity. Nucleosome mapping has shown the precise positioning of nucleosomes with nucleosome free regions (NFRs) present at 5' and 3' ends of genes thought to provide assembly and disassembly sites of the transcription apparatus (44). The presence or absence of nucleosomes in NFRs are correlated with active and repressed gene transcription respectively (45, 46). When histone variants H3.3 and H2A.Z are incorporated into nucleosomes, they can influence nucleosome occupancy and therefore gene activity (47). These are preferentially enriched at promoters of either active genes or genes poised for activation (48).

1.2.1.2 Covalent histone modifications

Chromatin is made of multiple nucleosome components which contain ~146 base pairs of DNA wrapped around an octamer of four core histone proteins (H2A and B, H3, and H4) (49). H1 is adjacent to the nucleosome and functions to keep the DNA in place that is wrapped around the nucleosome.

Histones contain a protruding lysine rich N- terminal tail that are subject to reversible covalent modifications (Figure 1.5). These include lysine (K) and arginine (R) methylation, acetylation, ubiquitylation, and phosphorylation. There are over 60 different histone residues where modifications have been detected (50). These modifications change the chromatin state by modifying the affinity of the histone for its negatively charged back bone, thus opening and closing genes off to transcription factors and RNA polymerases, thereby repressing or activating target genes. This also suggests that there is a vast amount of potential functional responses as a result. The multitude of modifications also implies that there is a degree of crosstalk and regulation between the modifications and their relative function. Histone writers, erasers, and readers add, remove, and recognise these post-translational modifications

respectively. Writers are divided in to groups based on the specific residue they add or remove, whereas readers direct a specific translational response as a result.

1.2.1.2.1 Histone acetylation and ubiquitylation

The addition of acetyl groups to lysine residues on the histone tail changes the positive charge of histone tails to promote the opening of DNA to become more accessible to transcription factors (51, 52). Histone acetylation is mediated by histone acetyltransferases (HATs) and histone deacetylases (HDACs) which add and remove acetyl groups respectively.

Ubiquitylation of lysine residues on histone tails does not lead to proteasomal degradation as would happen normally, instead acting as a signalling molecule whose addition (ubiquitylation) and removal (deubiquitylation) denotes transcriptional activation (53).

1.2.1.2.2 Lysine methylation

Lysine residues on histone 3 and histone 4 can be methylated. This occurs by transferring one, two, or three molecules from S-adenosyl-L-methionine (SAM) to the ε-amino group of the target lysine residue (54). These methylation patterns are associated with both transcriptional activation or repression (55). For example, methylation of histone H3K4, H3K36, or H3K79 is associated with transcriptional activation (56), whereas methylation of H3K9 and H3K27 are associated with transcriptional repression. Furthermore, within this, the degree of methylation can also determine the activity of the gene. For example, tri-methylated H3K4 and mono-methylated H3K9 typifies active genes (57, 58) yet di- and tri-methylated H3K9 are associated with repressed genes. These readouts are defined more in table 1.2.

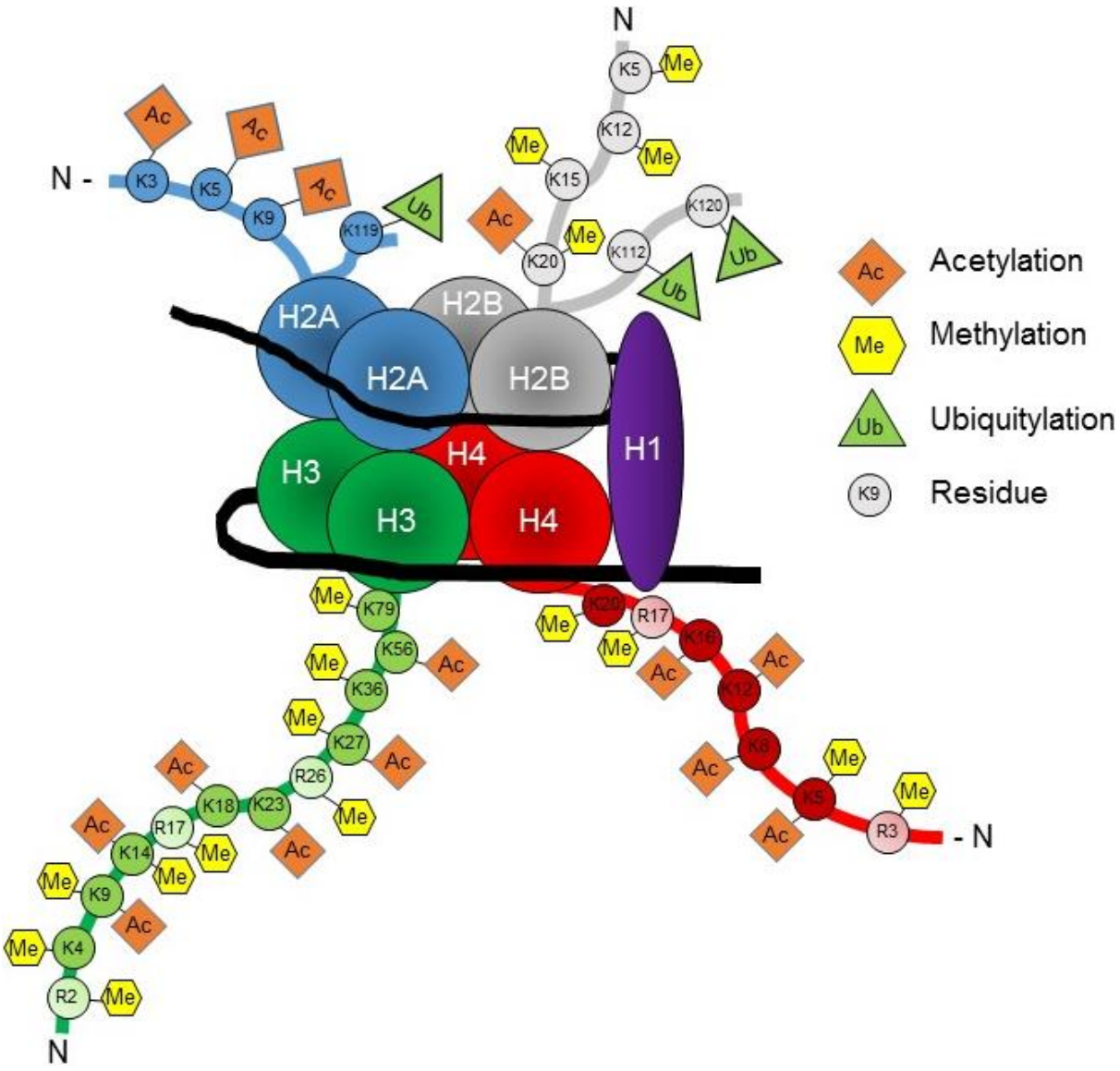

Figure 1.5 – Post-translational modifications sites on histone tails
DNA is wrapped around the core histone octamer, a nucleosome. This consists of H2A and B, H3, and H4. These histones protrude tails which are modified at specific residues, lysine (K) and arginine (R), by acetylation, methylation, ubiquitylation, and phosphorylation (not shown).

Type of histone modification		Histone and residue						
		H3K4	***H3K9***	***H3K27***	***H3K79***	***H3K36***	***H4K20***	***H2BK5***
Methylation marks	**Mono-**	*A (59)*	*A (60)*	*A (60)*	*A (60, 61)*		*A (60)*	*A (60)*
	Di-		*R (62)*	*R (62)*	*A (61)*			
	Tri-	*A (63)*	*R (60)*	*R (60)*	*A (61), R (60)*	*A (64)*		*R (62)*

Table 1.2 – Histone lysine methylation modifications in gene regulation
Lysine methylation marks can act as transcriptionally active (A) or repressive (R) marks.

The location of the methylated-lysine residue along with the degree of methylation are also associated with altering gene expression. For example, tri-methylation is associated with gene repression on H3K27 (60), however H3K4me3 is associated with active transcription (63, 65). This suggest that the effects of methylation are context-dependent.

Furthermore, there are also instances of the same modifications being associated with opposing activities, such as H3K4me2 and me3 which can both be associated with transcriptional activation and repression (66). This activity change is probably due to different chromatin effector proteins recognising the methylation marks. Table 1.3 shows all the lysine HMTs and demethylases, and their respective modifications.

1.2.1.2.3 Arginine methylation

Arginine methylation is a common PTM that is carried out by arginine methyltransferase (PRMT) family (67). These catalyse the transfer of methyl groups from S-adenosylmethionine (SAM) to arginine residues. There are three main forms of methylarginines identified in eukaryotes: mono-methylarginine (MMA), asymmetric dimethylarginine (aDMA), and symmetric dimethylarginine (sDMA). PRMTs cover three categories dependent on their catalytic activity; type I (PRMT1, PRMT2, PRMT3, PRMT4, PRMT6, and PRMT8) and II (PRMT5 and PRMT9) perform MMA before the establishment of aDMA or sDMA respectively (68). PRMT7 is a type III enzyme that only catalyses formation of MMA; only known substrate is histones thus far (69).
Arginine methylation plays a crucial role in gene regulation as the methylation marks PRMTs deposit on histones act as activating (H4R3me2a, H3R2me2s, H3R17me2a, H3R26me2a) or repressive (H3R2me2a, H3R8me2a, H3R8me2s, H4R3me2s) marks.

There are also non-histone targets of PRMTs, for example PRMT1 directly methylates Ash2L to positively regulate its transcription (70).

Lysine Methyltransferase	Residue Methylated	Mono-	Di-	Tri-
SUV39H1/ KMT1A	H3K9			(71, 72)
SUV39H2/ KMT1B	H3K9			(72)
EHMT2/G9a/ KMT1C	H3K9	(72, 73)	(72, 73)	(74, 75)
EHMT1/GLP/ KMT1D	H3K9	(72, 73)	(72, 73)	(74, 75)
SETDB1/ KMT1E	H3K9	(76, 77)	(77)	(77)
SETD1A/ KMT2F	H3K4	(78)	(78)	(78)
SETD1B/ KMT2G	H3K4			(79)
SET2/ KMT3A	H3K36	(80)	(80)	(80)
NSD2/KMT3F	H3K36	(81)	(81)	
DOT1L/ KMT4	H3K79	(82, 83)	(82, 83)	(82, 83)
PR-Set7/ KMT5A	H4K20	(84)		
SUV420H1/ KMT5B	H4K20		(85, 86)	(85, 86)
SUV420H2/ KMT5C	H4K20		(85, 86)	(85, 86)
EZH2/ KTM6A	H3K27		(87)	(87)
EZH1/ KMT6B	H3K27	(88)	(87)	(87)
RIZ1/ KMT8A	H3K9		(89)	(89)

Lysine Demethylases	Residue(s) Demethylated	Mono-	Di-	Tri-
LSD1/KDM1A	H3K4/ H3K9	(90, 91)	(90, 91)	
KDM2A	H3K36		(92)	
KDM2B	H3K36/ H3K4		H3K36 (92)	H3K4 (93)
KDM3A	H3K9	(94)	(94)	
KDM4A	H3K9, H3K36			(95)
KDM4B	H3K9			(95)
KDM4C	H3K9, H3K36			(95)
KDM4D	H3K9		(95)	(95)

Table 1.3 – Histone 3 and 4 lysine residue methyl group modifying enzymes
Histone lysine methylation writers and erasers. The residue and the type of methyl modification are shown along with the reference it is shown in.

1.2.1.2.4 Protein Demethylation

Protein demethylases were first documented in 2004 when LSD1/KDM1 was identified as part of a multiprotein corepressor complex that contains histone deacetylase-1 and-2 and demethylase activities (90, 96). Prior to this, deposited methylation marks where

thought to be irreversible. Lysine demethylation is catalysed by two families of lysine demethylases- the flavin-dependent KDM1 enzymes and the 2-oxoglutarate- and oxygen-dependent JmjC KDMs, respectively (97). Recently, a subset of JmjC lysine demethylases have also been shown to act as an arginine demethylase on both histone and non-histone targets.

1.2.2 Epigenetic deregulation in cancer

Epigenetic mechanism can be manipulated to promote a favourable tumourigenic environment, for example, CpG islands preceding tumour suppressor genes are often hypermethylated in cancer cells which then silences these genes (98). Various tumour suppressors including *p16* and *BRCA1* undergo tumour-specific silencing by hypermethylation (99). These genes are involved in cellular processes detrimental to cancer development and growth therefore silencing them favours the tumour. Promoter hypermethylation also indirectly silences other genes by silencing transcription factors. Promoter hypermethylation-induced silencing of transcription factors occurs in oesophageal cancer where *RUNX3* is silenced and its downstream target repressed as a result (100). The mechanism used to target these genes is unknown however. One theory is that a growth advantage is gained to cells with certain genes hypermethylated therefore are clonally selected (101). Another suggests a role for histone marks in tumour specific targeting of *de novo* methylation as H3K27me3 is often found to pre-mark regions that are hypermethylated and these recruit DNA methyl transferases, leading to *de novo* methylation (102).

Histone modifications can also be hijacked to alter the amount of repressive and active markers in the epigenome. For example, cancerous cells exhibit decreased mono-acetylated and tri-methylated forms of H4 relative to healthy cells (103). Decreased acetylation of H3 and H4 is associated with tumourigenesis, along with increased H3K9me1 and H3K27me3, and decreased H3K4me3. Mutations in the histone octamers also lead to cancerous cells. Histone variants of H2A are able to alter the chromatin structure; H2A.Z has a role in gene activation and repression with high levels detected in many cancers (104). Epigenetic modifiers genes are also regulated in cancerous cells. An epigenetic modifier is a gene that encodes for histone modifiers, chromatin remodelers or DNA methylators, for example *EZH2* or *DNMT1*. Mutations in these genes will render the gene unreadable so the protein is not translated, or the mutation has an oncogenic effect on the proteins function.

Mutations affecting a core component of polycomb repressive complex 2 (PRC2), histone methyltransferase *EZH2*, can have differing consequences. One such effect reported in non-Hodgkin lymphomas, is that gain-of-function mutations and amplifications lead to decreased repressive marker H3K27me3, which is necessary to promote lymphoid transformation (105, 106). Moreover, loss-of-function mutations of *EZH2* are frequently seen in head and neck squamous carcinomas and T cell leukaemia (107, 108). This supports the dual function of EZH2 as both an oncogene and a tumour suppressor which is contextual based on tissue type.

Mutations in the DNA methylation machinery are also common. DNA methyltransferase 3α (*DNMT3A*) is mutated by frameshift and point mutations in acute myeloid leukaemia (AML) (109), and mutated DNMT3A is shown to be an indicator of poor prognosis (109, 110). Furthermore, *DNMT1* is mutated in colorectal cancer with mutations in the coding exons leading to inactivation of the gene (111). Mutations in chromatin remodelers are widespread in solid tumours too. For example, *SMARCB1* is a regulator of chromatin structure that is deleted or mutated in paediatric rhabdoid tumours which leads to tumourigenesis suggesting it normally has a tumour suppressor effect (112). This all shows how cancer can manipulate the epigenome and epigenetic environment to is advantage to induce tumourigenesis.

1.3 The roles of histone lysine methyltransferase G9a

1.3.1 G9a

G9a or Enzyme Histone Methyltransferase 2 (EHMT2, from here on will be known as G9a) is a histone methyltransferase of histone 3 lysine 9 (H3K9), belonging to the SET domain containing Su(var) 3-9 family of proteins (113). The SET domain is the proteins catalytic centre where which contributes to its methyltransferase activity. G9a also has an ankyrin repeat-containing domain which is necessary for protein-protein interactions, (113, 114) and two nuclear localisation signals in the N-terminal region (115, 116). A representation of these domains is shown in Figure 1.6. G9a also contains pre-SET and post-SET domains that was suggested to be required for enzymatic activity (71). However, analysis of *S. cerevisiae* SET domain containing proteins shows that none of these contain neither pre-SET or post-SET domains (117). Yet, deletion of the pre- and SET domains has been shown to impair heterochromatin localisation of G9a suggesting that these are necessary for nuclear translocation

(115). G9a has two isoforms through alternative splicing, with the shorter isoform (isoform b) missing exon 10 of the 24 exons that encode G9a (118, 119).

G9a can form a homodimer complexes, however the endogenous preferential is to form a heterodimer with G9a-like protein (GLP), a similar histone 3 lysine 9 (H3K9) methyltransferase, via their SET domains in a near one-to-one ratio (73). GLP possesses the same activities as G9a (73), although studies using methyltransferase-defective mutants has shown that the enzymatic activity of G9a is more important than that of GLP for the *in vivo* histone methyltransferase function (120, 121). In addition, it has been shown that the ankyrin repeat domains of G9a and GLP have differing binding affinities towards H3K9me1 and H3K9me2, with G9a preferring to associate with H3K9me2 and GLP associating with H3K9me1 (122).

G9a can mono- or di-methylate H3K9 in euchromatin, the chromosome material involved in transcription closest to the centromere. It has also been known to mono-methylate H3K27, di-methylate H1.2K187, and tri-methylate H3K9 (74, 123). The mechanism behind the degree of methylation is determined by key residues in the active site of the HMTase. In human G9a, phenylalanine positioned at 1205 allows the HMTase to perform di- and tri-methylation, whereas a Tyrosine at the same position

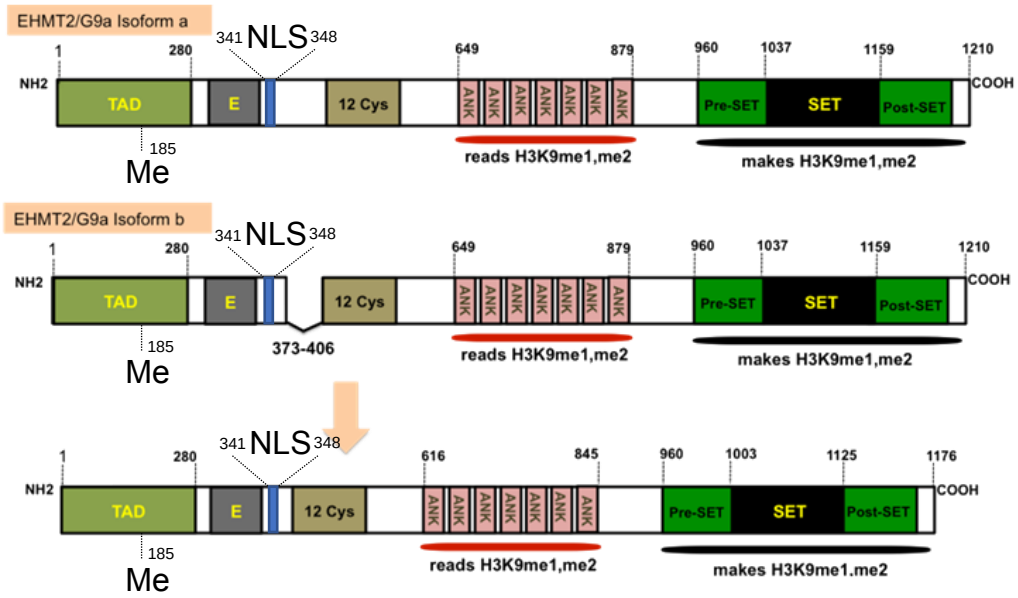

Figure 1.6 – G9a isoform structures
Representation of G9a domain structures of both isoform a and b, adapted from Shankar et al, and the Atlas of Genetics and Cytogenetics in Oncology and Haematology (http://atlasgeneticsoncology.org/) (118, 124). The denotations are as follows: The Cysteine rich region – 12 Cys, ankyrin repeats – ANK, catalytic SET domain with flanking pre- and post-SET regions. The site for methylation – Me, nuclear localisation signal – NLS, and the glutamic acid – E rich region. Numbers indicate amino acid residues.

is restrictive and so inhibits tri-methylation (74). This shows that these somatic mutations can change the activity of G9a so can act as a switch to different methyltransferase activities.

G9a also regulates gene transcription by catalysing H3K9me2 at the promoter regions of genes (58, 75, 125, 126). It has been shown that large regions of chromatin associate with H3K9me2 repressive marker in differentiated tissues (127). These regions were termed large organised chromatin K9 modifications (LOCKs) and are regulated during differentiation, with the size of the LOCKs varying in different cell types.

1.3.2 Non-histone Targets of G9a

The G9a recognition motif is the seven amino acid string-*TA**R**KSTG*- found on the tail of histone 3 where arginine (**R**) is paramount to G9a methylation activity (128, 129). This motif has also been found in non-histone proteins so G9a can methylate non-histone targets like p53 at K373 (130), WIZ at K305 and CDYL1 at K135 (131), and Reptin at K67 (54, 118, 132). In the case of Reptin, a non-histone chromatin modifier, the functional relevance of G9a methylation is well documented. It has been shown that nuclear G9a protein levels increase when cells are exposed to hypoxic conditions and thus there is an increase in methyltransferase activity and a consequential repression of hypoxia regulated genes such as *RUNX3*, *BRCA1, ARNTL, and GATA2* (133-136). Reptin methylation by G9a occurs under hypoxic conditions too. Methylated Reptin can then selectively downregulate target promoters via enhanced binding to HIF-1α (132). This has been shown to negatively regulate tumour growth (132). In contrast, G9a also methylates chromatin-remodelling factor Pontin under hypoxia. This in turn activates a different subset of HIF1α target genes that are involved in oncogenesis and cell survival (137, 138). All together this shows that G9a methylation of non-histone targets also has an activating or repressing potential similar to its histone targets. G9a also methylates other transcription factors which impairs their transcriptional activity. For example, G9a methylates transcription factor C/EBP β, at K39 to stop the activation of myeloid genes. Inactivation of G9a is able to rescue this and reactivate myeloid genes (139).

Interestingly, G9a also has a G9a recognition motif within its N-terminus which can be automethylated. This does not affect the catalytic ability of G9a and resembles

H3K9me3 in structure (118). This enables HP1γ (or CBX3) to recognise G9a as a binding partner and thus form the ternary complex GR-G9a/GLP-HP1γ to activate a subset of glucocorticoid genes (140). HP1 also interacts with DNA methyltransferase DNMT1 to silence gene promoters and so suggests G9a-HP1 complex can act as a scaffold to propagate gene repression. Moreover, WIZ protein has been shown as a core subunit of a G9a/GLP complex along with ZNF644, both of which contain multiple zinc finger motifs that recognise DNA sequences (141). These zinc finger proteins can then target the G9a/GLP dimer to chromatin to regulate transcriptional repression of genes such as *ROCK1* and *DIP2C* (141).

G9a can also act as a co-activator independent of its methyltransferase activity. It has been shown to cooperate with nuclear receptor coactivators GRIP1, CARM1 and p300 (142). Via its ankyrin repeat domain, G9a binds to the N-terminus of GRIP1 and this forms a scaffold complex to activate downstream targets. However, it was shown that G9a mutants with inactive methyltransferase domains had reduced activity at lower levels of G9a expression suggesting that whilst not required for coactivator activity, the methyltransferase activity may contribute to coactivator function (142). This all suggests that G9a can act as a transcriptional switch to activate or repress gene transcription depending on its binding partner. This is summarised below in Figure 1.7, along with examples of other activated and repressed target genes.

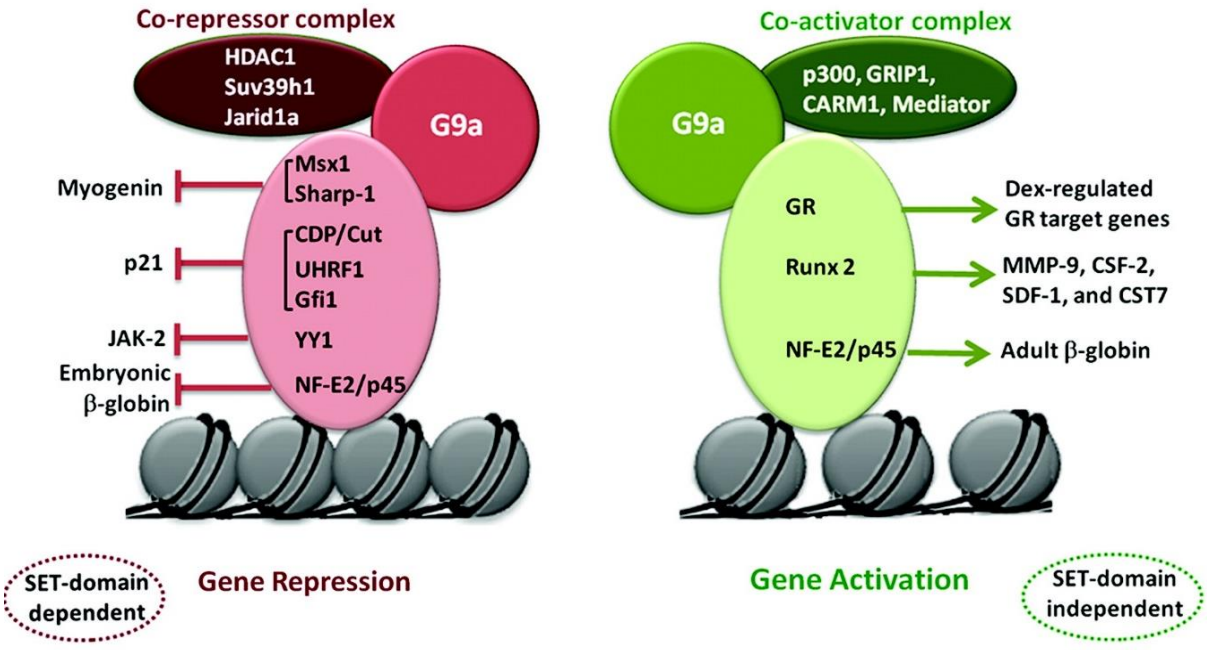

Figure 1.7 – Suggestion that the binding partner(s) of G9a determines its function as a repressor or an activator of gene transcription. This figure is taken from Shankar et al (118).

1.3.3 G9a in cancer

G9a has been implicated in cancer tumourigenesis due to overexpression in various cancers, including breast, lung, and head and neck (143) (Table 1.4). Overexpression has also been associated with poor prognosis (144) and there is a correlation with increased methylation and the silencing of tumour suppressor genes (116, 145). It has been shown that in breast cancer, G9a regulates tumour suppressor p53 by di-methylating at position K373 thus inactivating it (130), and the metastasis suppressor genes *DSC3* and *MASPIN* were reactivated upon G9a inhibition and depletion (145). Moreover, in ovarian cancer G9a activity promoted the suppression of tumour suppressors *CDH1*, *DUSP5*, *SPRY4*, and *PPP1R15A* (146). This evidence points towards G9a as a potential target for the re-expression of important tumour suppressor genes. In gastric carcinoma the depletion of G9a suppressed cell proliferation, and increased apoptosis by significantly promoting pro-apoptotic factor BAX (147).

G9a overexpression in Cancer	Reference
Oesophageal squamous cell carcinoma (ESCC)	(144)
Hepatocellular carcinoma	(130, 148)
Aggressive lung cancer	(130, 143, 149)
Aggressive ovarian carcinoma	(130, 150)
Breast cancer	(143, 151)
B cell acute lymphoblastic leukemia (ALL)	(130, 152)
Colon carcinoma	(130)
Melanoma	(130)
Prostate carcinoma	(130)
Head and neck cancer	(153)
Colorectal cancer	(154)
Bladder carcinoma	(149)

Table 1.4 – Cancers that are suggested to be influenced by G9a overexpression

In addition, it was shown in breast cancer that effective gene re-expression necessitated the inhibition of G9a and another histone methyltransferase, and Polycomb Repressive Complex (PRC2) member, EZH2. For example, dual depletion of both G9a and EZH2 dramatically increased *SPINK1* mRNA when individual depletion had no effect (155). This dual inhibition was also shown to increase growth inhibition over only G9a or EZH2 single inhibition (155). It is known that PRC2 and G9a physically interact and share several genomic targets that encode developmental

regulators such as *HOXC13* and *SIX1*, and they both colocalise at the promoters for neuronal differentiation genes too by forming a tertiary complex with neuronal regulator REST (156-158). It is suggested that G9a-mediated H3K27 mono-methylation enhances PRC2-mediated trimethylation as G9a is necessary to increase PRC2 activity, especially as EZH2, HMT part of the PRC2, recruitment and H3K27me3 trimethylation are impaired (156). This all suggests that there is an interplay between the H3K9me2/3 repressive markers governed by G9a and the H3K27me3 governed by EZH2, and that it is necessary to deplete both to reactivate co-regulated genes.

1.3.4 G9a small molecule inhibitors

To date, there are many types of G9a inhibitor with the first, BIX-01294, initially described in 2007 via high throughput biochemical screening (159). BIX-01294, a diazepin-quinazolin-amine derivative (75), consists of a central quinazoline ring linked to a seven-membered diazepane ring and a benzylated six-membered piperidine ring (160). BIX-01294 has been used to probe G9a in cellular reprogramming (161, 162), and to inhibit G9a to reactivate latent HIV-1 (163). In addition, BIX-01294 has been used to show that G9a mediates methylation of *Oct-3/4* promoter (164).

However, whilst originally being described as being G9a-specific, it has been suggested that BIX-01294 is actually more potent against GLP and acts as a competitive inhibitor of N-terminal peptides of Histone 3 (160, 165). Furthermore, BIX-01294 is now known to be toxic in cellular assays, with a study suggesting concentrations above 4.1µM is likely to cause off-target toxicity (166). This raises the possibility that from current published work with G9a inhibition via small molecule inhibitor BIX-01294 may partly attributable to off-target effects of the BIX-01294 drug and not a true effect of G9a inhibition.

Because of these off-target effects of BIX-01294, a new high-quality chemical probe with an enhanced ratio of toxicity to functional potency was necessary (167). There are a vast number of different small molecule inhibitors available. Vedadi et al optimised the 2,4-diamino-6,7-dimethoxyquinazoline scaffold template to discover new chemical probes for G9a and GLP. UNC0638 was reported as a potent and selective probe for G9a and GLP which is less toxic and more selective than BIX-01294 (168). However, this is not suitable for animal studies due to its poor in vivo pharmacokinetic (PK) properties (168). Therefore, Liu et al aimed to optimise the PK

properties of quinazoline series of inhibitors to generate UNC0642 (169). UNC0642 has improved pharmacokinetic properties that are non-toxic in 2D cell growth assays but reduced colony formation of pancreatic adenocarcinoma cells (169). UNC0638 and UNC0642 act as competitive substrate inhibitors, thus blocking the SET domain from acquiring methyl groups from SAM cofactor.

Chemical probe UNC0646 is a close analogue of UNC0638 and has been suggested to have an outstanding toxicity/function ratio in three cancer cell lines (170). Another inhibitor A366, is chemically distinct however works in the same manner of substrate competition (171). Recently, four novel SMI of G9a were discovered, with DCG066 having the best activity (172). DCG066 has a similar activity to BIX01294 (1.7±0.1μM and 3.9±0.3μM respectively in K562 leukaemia cell line) yet has a new structure allowing for further inhibitor development (172).

1.4 What is Neuroblastoma?

1.4.1 Origin

Neuroblastoma is a paediatric cancer of the sympathetic nervous system and is one of the most frequent extracranial solid tumours, as originally described by James Wright (173). It arises from developing neural crest cells that will give rise to the peripheral and enteric nervous systems, amongst others (174). These cells develop in response to extracellular signals such as growth factor Bone Morphogenetic Protein (BMP), and Shh. Furthermore, these neural crest-derived cells are highly migratory due to undergoing EMT shortly after induction. Neuroblastoma is responsible for 15% of childhood cancers deaths despite an incidence rate of 6% of all childhood cancers (175) with 90% of cases are diagnosed by the age of 5 (176) and 48% of patients have a metastatic form at diagnosis (177).

1.4.2 Clinical staging

There are various stages of neuroblastoma which are defined by two staging systems: and 1) The International Neuroblastoma Staging System (INSS) (Table 1.3), and 2) The International Neuroblastoma Risk Group Staging System (INGRSS) (Table 1.4). The INSS was developed in 1988 (178) is still the most used by cooperative groups (179) however is not suitable for pre-treatment risk classification of patients as this staging is based on the extent of tumour removal (180) suggesting that the same tumour can be classified as INSS stage 1 or 3 depending on the extent of surgical

excision (179). Thus in 2004, several major cooperative groups formed the International Neuroblastoma Risk Group Task Force and developed the INGRSS. This is designed for staging prior to surgery or treatment.

Neuroblastoma patients are stratified into risk groups at diagnosis with low-, intermediate-, or high-risk statuses. The factors that help contribute to the risk status are shown in table 1.5 (181). As shown in Figure 1.8, risk stratification schemes have successfully determined the outcomes of patients within these three groups, along with a dramatically reduced event-free survival of <50%. This suggests that targeting high-risk factors is key to helping to improve the overall survival rate of patients with high-risk neuroblastoma.

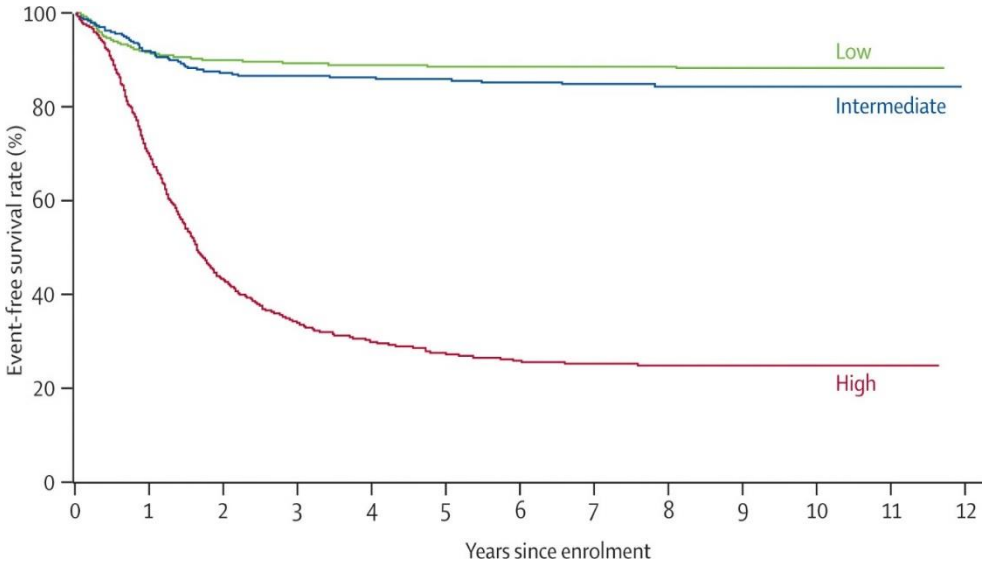

Figure 1.8 – Kaplan-Meier curve showing the survival of neuroblastoma patients based on risk group as defined by Table 1.5 (182)

Stage	Description
1	Localized tumour excision, with or without microscopic residual disease
2a	Localized tumour with incomplete gross excision
2b	Localized tumour with or without complete gross excision
3	Unresectable unilateral tumour infiltrating across the midline (beyond the opposite side of the vertebral column) with or without regional lymph node involvement, or localized unilateral tumour with contralateral regional lymph node involvement, or midline tumour with bilateral extension via infiltration (unresectable) or lymph node involvement
4	Any primary tumour with dissemination to distant lymph nodes, bone, bone marrow, liver, skin, and/or other organs (except as defined for stage 4S disease)
4S	Localized primary tumour with dissemination limited to skin, liver and/or bone marrow (limited to infants <1 year of age, marrow involvement <10% of total nucleated cell ^{123}I-metaiodobenzylguanidine scan findings negative in the marrow)

Table 1.3 – INSS Tumour Stages. Adapted from Brisse et al (179)

Stage	Description
L1	Localised tumour not involving vital structures and confined to one body compartment
L2	Loco-regional tumour with presence of one or more IDFRs
M	Distant metastatic disease (except stage MS tumour)
MS	Metastatic disease in children younger than 18 months with metastases confined to skin, liver, and/or bone marrow

Table 1.4 – INGRSS Tumour Stages. Adapted from Brisse et al (179)

High risk factors
Patient age
Stage of disease
Presence or absence of *MYCN*-amplification
Tumour cell ploidy
Chromosomal aberrations
Histopathological appearance of the tumour
Age—younger children have better survival rates

Table 1.5 – Factors associated with high-risk in neuroblastoma

1.4.3 Epigenetics in neuroblastoma

Somatic mutations are rare in neuroblastoma, so it is suggested that chromatin modification and unusual epigenetic regulation plays a key role in neuroblastoma cancer development (183). In neuroblastoma, there are several tumour suppressor and apoptosis-driving genes that are hypermethylated. These include the promoters for *RASSF1A* and *CASP8* (Caspase-8) whose silencing is well established and associated with poor prognosis (184). In addition to gene silencing, the expression of epigenetic writers can also be manipulated to fit the cancer's needs. In neuroblastoma the upregulation of Polycomb protein histone methyltransferase EZH2 is necessary to maintain an undifferentiated and poor prognostic state by increasing the repressive marker H3K27me3 on tumour suppressor proteins such as *CASZ1* (185).

1.4.4 *ALK* and *TERT* amplification

There are numerous chromosomal abnormalities associated with neuroblastoma, with deletions of chromosomes 1q and 11q, gain of 17q, and *MYCN*-amplification on 2p (186). ALK (Anaplastic Lymphoma Kinase) is a member of the insulin receptor superfamily of receptor tyrosine kinases. The discovery of activating mutations in *ALK* oncogene in both hereditary and sporadic neuroblastoma represents a druggable target. Mutations in *ALK* are frequently observed in poor prognostic *MYCN*-amplified neuroblastoma.

ALK oncogene was initially identified as a gene that fused with nuclear protein *NPM* (Nucleophosmin) through 2;5 chromosomal translocation that occurs in most anaplastic large-cell non-Hodgkin's lymphoma (187). ALK ligands include pleiotrophin (PTN) and midkine (MDK) both of which are secreted growth factors (188, 189). ALK was considered an orphan receptor until recently when ALKAL1 and ALKAL2 were shown to be bona fide ligands (190). These bind to ALK to activate downstream mitogen-activated protein kinase (MAPK) pathway and induces insulin receptor substrate 1 (IRS1) phosphorylation respectively. The latter results in MAPK and phosphoinositide 3-kinase (PI3K) activation (191, 192). It was suggested that ALK could potentiate oncogenic activity in neuroblastoma cells when its expression level exceeded a threshold (193). *ALK* can be amplified or it may possess gain of function mutations at the tyrosine kinase domain, with R1275Q and F1174L the most common (194, 195). These mutations disrupt the autoinhibitory function of ALK to keep ALK

constitutively active. MYCN and ALK synergistically cooperate to induce neuroblastoma (186, 196).

Telomere shortening is common to normal cells to restrict lifespan; cancer cells can preserve their telomere length by alternative lengthening of telomeres (ALT) or activation of telomerase reverse transcriptase (TERT). *TERT* is activated by promoter mutations (197) and upstream rearrangements, with these rearrangements in approximately 23% of examined high-stage NB (198). Alteration in *TERT* was independent of *MYCN*-amplification and is associated with poor prognosis (198).

1.4.5 High-risk transcription factor MYCN

1.4.5.1 MYCN in normal cells

MYCN is a classic oncogene transcription factor that is part of the MYC family. MYC family members are basic helix-loop-helix transcription factors who dimerise with MAX. This family is known to regulate genes associated with apoptosis, cellular proliferation, and differentiation. Upon binding to target promoters, MYCN recruits histone acetylation complexes (HATs) like TRRAP which contains HATs GCN5/PCAF or TIP60 to maintain an open chromatin state (199). Located in chromosome 2p24, MYCN was initially discovered as a paralog of C-MYC (MYC) when gene mapping in neuroblastoma cells discovered MYCN as a homologous proto-oncogene like MYCN (200). As a result, they are functionally interchangeable with MYCN expression able to replace MYC expression in developing murine models (201). Soon after, a third MYC family member MYCL was detected as being amplified in small cell lung cancers (202).

MYCN is expressed during embryogenesis in pre-B cells, kidney, intestine, and the fore and hindbrain. The developing brain is where the highest expression of MYCN is found and after embryonic development, *MYCN* is then downregulated (203). MYCN plays an essential role in normal brain development to drive the expansion of neuron precursors populations. These are derived from neuronal progenitor cells of the developing forebrain and hindbrain (204). In neural crest cells with enhanced *MYCN* expression, differentiation was downregulated in favour of the proliferation of immature neuronal precursors (205). Constitutive deletion of *MYCN* is embryonic lethal (206), and mutations causing MYCN inactivation lead to Feingold syndrome (207). This a

characterised by microcephaly, limb abnormalities, and learning difficulties, all of which can be attributed to the perturbance of normal neural development.

1.4.5.2 MYCN in neuroblastoma and other cancers

MYCN-amplification is defined by 10-500 copies of the gene and is characterised in around 25% of the most aggressive neuroblastomas. It is considered to a robust prognostic biomarker for determining outcome as it is strongly associated with prognosis (208-211). This is visualised in the Kaplan-Meier curve below, Figure 1.9. The difference between the survival probabilities between patients with low (red) and high (blue) MYCN-amplification is drastically significant demonstrating how much of a risk factor MYCN plays.

Being a transcription factor, MYCN predominantly upregulates gene transcription by binding to specific DNA sequences called E-boxes (5'-ACCGTG-3') to initiate gene transcription (212). These targets include ALK receptor tyrosine kinase which promotes proliferation and cell survival by activating downstream targets AKT/ERK (213-215). In addition, MYCN also upregulates proto-oncogenic transcription factor High mobility group A1 (HMGA1) which is overexpressed as a result (216, 217). MYCN can also act to repress gene transcription. Overexpression of *MYCN* down regulates interleukin-6 (IL-6) (218), and endothelial cell proliferation inhibitor activin A (219-221). This downregulation helps to drive tumourigenesis and proliferation, hence the aggressive nature of *MYCN*-amplified neuroblastoma.

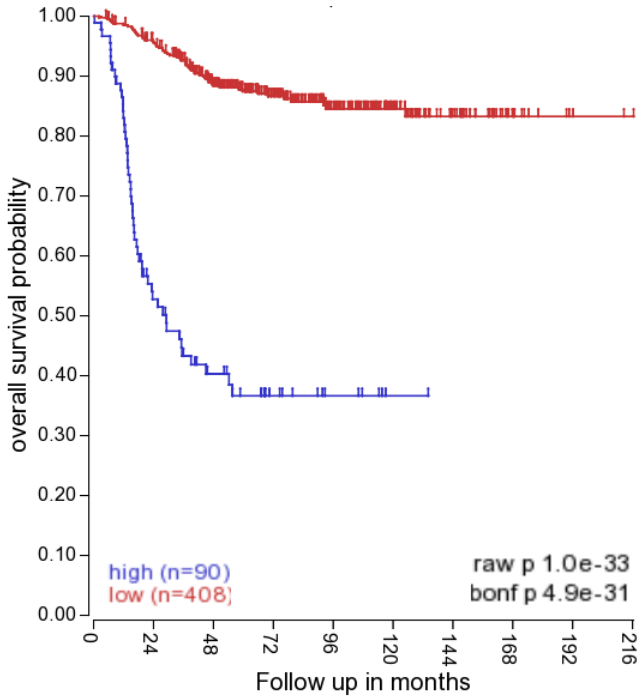

Figure 1.9 – Patients with MYCN-amplified tumours have a significantly decreased overall survival probability
Using the Genomic Analysis and Visual Platform R2 (http://r2.amc.nl), a Kaplan-Meier survival curve in neuroblastoma shows the relationship between high MYCN mRNA expression and poor prognosis. The database used was SEQC- 498 which is derived from RNA sequencing data of 498 neuroblastoma (222).

1.4.6 Regulation of MYCN

MYCN is regulated by both transcriptional and translational mechanisms. MYCN has been shown to be transcriptionally regulated by the E2F family of transcription factors. Using chromatin immunoprecipitation (ChIP) E2F-1, 2, and 3 all bound to the proximal *MYCN* promoter in *MYCN*-amplified neuroblastoma and inhibition of E2F activity was also able to reduce MYCN expression (223). Translational regulation of MYCN has been shown in neuroblastoma. Activated H-Ras through an oncogenic mutation can promote MYCN accumulation by accelerating MYCN translation (203, 224).

MYCN protein is turned-over during the interphase stage of mitosis. The half-life of MYCN is known to be very short (225) so the turnover occurs quickly. This degradation allows for neuronal precursors to undergo differentiation (226). This degradation event occurs through phosphorylation events at serine 62 and threonine 58, and subsequent ubiquitination and degradation by the proteasome. This proteasomal degradation is disrupted in *MYCN*-amplified neuroblastoma to help keep the cells in a highly proliferative state. Aurora kinase A is overexpressed in neuroblastoma cells which

hinders the interaction between phosphorylated threonine 58, and the ubiquitin ligase FBXW7 so MYCN cannot be ubiquitinated (227, 228). MYCN protein has been shown to be stabilised by other PTMs such as methylated arginine by protein arginine methyltransferase 5 (PRMT5) which increases MYCN half-life (229).

1.4.7 MYCN targets

1.4.7.1 MYCN and the cell cycle

MYCN regulates the cell cycle by shortening the time to progress through the cell cycle, specifically reducing the length of the G1 phase (208). MYCN accomplishes this by downregulating a subset of cyclin-dependent kinase inhibitors (CKIs), a class of proteins that negatively regulate progression through the cell cycle. MYCN represses the expression of $p21^{CIP1}$, a member of the Cip/Kip family of CKIs (230), by forming a complex with other transcriptional regulators, such as MIZ-1 and SP1 (231). This promotes cell growth and tumourigenesis.

1.4.7.2 MYCN and apoptosis

MYCN can regulate apoptosis by repressing pro-apoptotic genes. For example, MYCN elevates transcription of proto-oncogene *MDM2*. MDM2 is a p53 suppressor and inhibits p53-mediated apoptosis (232) which is discussed further on. In addition, methylation of (*CASP8*) promoter has also been observed in neuroblastoma at a high frequency although this is suggested to be independent of *MYCN*-amplification status (184, 233). MYCN can also repress nerve growth factor receptor (NGFR/P75NTR), a receptor that binds to neurotrophins. It is suggested that NGFR contain death domains in intracellular regions that may induce neuronal cell death; *NGFR* expression is strongly downregulated in *MYCN*-amplified neuroblastoma (234, 235). Depletion of MYCN was shown to re-express *NGFR* and sensitise the cells to NGF-mediated apoptosis (231).

However, paradoxically MYCN also represses genes that are characterised by an anti-apoptotic function. For example, MYCN has been shown to repress Galectin-3, an anti-apoptotic factor overexpressed in breast carcinoma cells resistant to cisplatin-induced apoptosis (236, 237). Furthermore, when galectin-3-negative Burkitt lymphoma cells were transfected with a plasmid expressing *Galectin-3* there was an increase in resistance to anti-Fas-induced cell death (238). In addition, increased

MYCN sensitises cells to chemotherapeutic agents like doxorubicin so can increase chemotherapy-induced apoptosis (239).

1.4.8 MYCN and chromatin modifications

MYCN is responsible not only for direct regulation of transcriptional activation or repression but can also independently regulate the modification of chromatin through maintaining the chromatin in an open state (240), and deletion of *N-MYC* in neuronal progenitor cells leads to a closed chromatin (241).

MYCN can also interact with histone modifiers to regulate gene transcription. For example, MYCN physically interacts with PRC2 histone methyltransferase EZH2 via Myc box domain 3 and this complex supresses expression of tumour suppressor *CLU* (242). As well as recruiting HATs and interacting with EZH2, MYCN can also interact with histone modifier DOT1L. MYCN has been shown to directly bind to the promoter of *DOT1L* gene to upregulate DOT1L promoter activity. Furthermore, DOT1L can also bind directly to MYCN protein to drive H3K79 di-methylation and activates target genes such as *ODC1* and *E2F2* to assist proliferation (243).

1.4.9 Targeting MYCN – Drugs and synthetic lethality

As a high-risk factor and oncoprotein involved in cell proliferation and tumourigenesis, MYCN is an obvious therapeutic target. However, due to its helical structure, there are no surfaces for ligands to bind making MYCN directly undruggable (176). Therefore, alternative methods have been developed to target MYCN and inhibit its activity.

Two genes are classed as synthetic lethal if mutation of two genes simultaneously is lethal (244). Therefore, targeting a synthetic lethal gene via pharmacological inhibitors is a potential therapeutic technique as it targets a functional interaction that is found in cancer cells (245). Figure 1.6 illustrates this. Moreover, there are combinations of gene mutations that can lead to non-lethal growth impairment, termed synthetic sickness.

The concept was developed from genetic studies in *D. melanogaster* and D. *pseudoobscura* (246, 247), and *S. cerevisiae* models (248), where combinations of non-allelic genes were lethal despite homozygous parents being viable. This is an example of Figure 1.6A. There are many examples of synthetic relationships across various cancer types. For example, breast cancers can be driven by mutations in *BRCA1* or *BRCA2* tumour suppressor genes, which impairs DNA double-strand break repair mechanisms (249). However, cells with *BRCA1* or *BRCA2* dysfunction are more

sensitive to pharmacological inhibition of Poly(ADP-ribose) polymerase (PARP), a base excision repair enzyme involved in the pathway for repair of single-strand DNA breaks. This results in the chromosomal instability, cell cycle arrest, and subsequent cell death via apoptosis as the cell accumulates DNA lesions that cannot be repaired (250, 251). This is an example of the type of synthetic lethality shown in Figure 1.10C and highlights the synthetic lethal relationship between *BRCA1* and *BRCA2*, and PARP inhibition which is the first example of a successful synthetic lethal therapy that is used in clinics.

MYCN-amplified neuroblastoma is an example of overexpression (Figure 1.10A). There have been many examples of synthetic lethal partners of MYCN in neuroblastoma published such as Aurora kinase A, PRMT5, and Cyclin dependent kinase 2 (CDK2) (227, 229, 252). For example, Aurora kinase A inhibitors target MYCN protein stability as aurora kinase A binds to MYCN to shield it from degradation. Aurora kinase A inhibitor Alisertib (MLN8237) can cause the depletion of MYCN in neuroblastoma cell lines by blocking the ability of Aurora kinase A to protect MYCN from FBXW7-mediated degradation (227, 253). Therefore, this therapeutic treatment can suppress MYCN protein levels and reduce cell growth in *MYCN*-amplified neuroblastoma. MYCN can also be targeted by controlling its activation ability. MYCN heterodimerises with MAX to recognise the E-box domains on target promoters therefore disrupting this interaction would effectively stop the transcriptional activity of MYCN. Small molecule 10058-F4 has been shown to interfere with MYCN/MAX dimerisation and reduce the tumorigenic potential of *MYCN*-amplified neuroblastoma as a result (254). However, 10058-F4 is rapidly metabolised and thus this SMI is not a suitable therapeutic agent (255).

Arginine methyltransferase PRMT5 can di-methylate MYCN to increase protein stability. When PRMT5 was depleted, MYCN protein decreased which lead to apoptotic cell death (229). Moreover, BET (bromodomain and extra-terminal domain) inhibitors JQ-1 and OTX-015 have been shown to target MYCN-driven transcription (256, 257). In addition, neuroblastoma cells are sensitive to histone 3 lysine 27 (H3K27) demethylase inhibitor GSK-J4 which inhibits ubiquitously transcribed tetratricopeptide repeat, X chromosome (UTX), and histone demethylase Jumonji D3 (JMJD3). GSK-J4 was able to induce cell death and neuroblastoma differentiation (258).

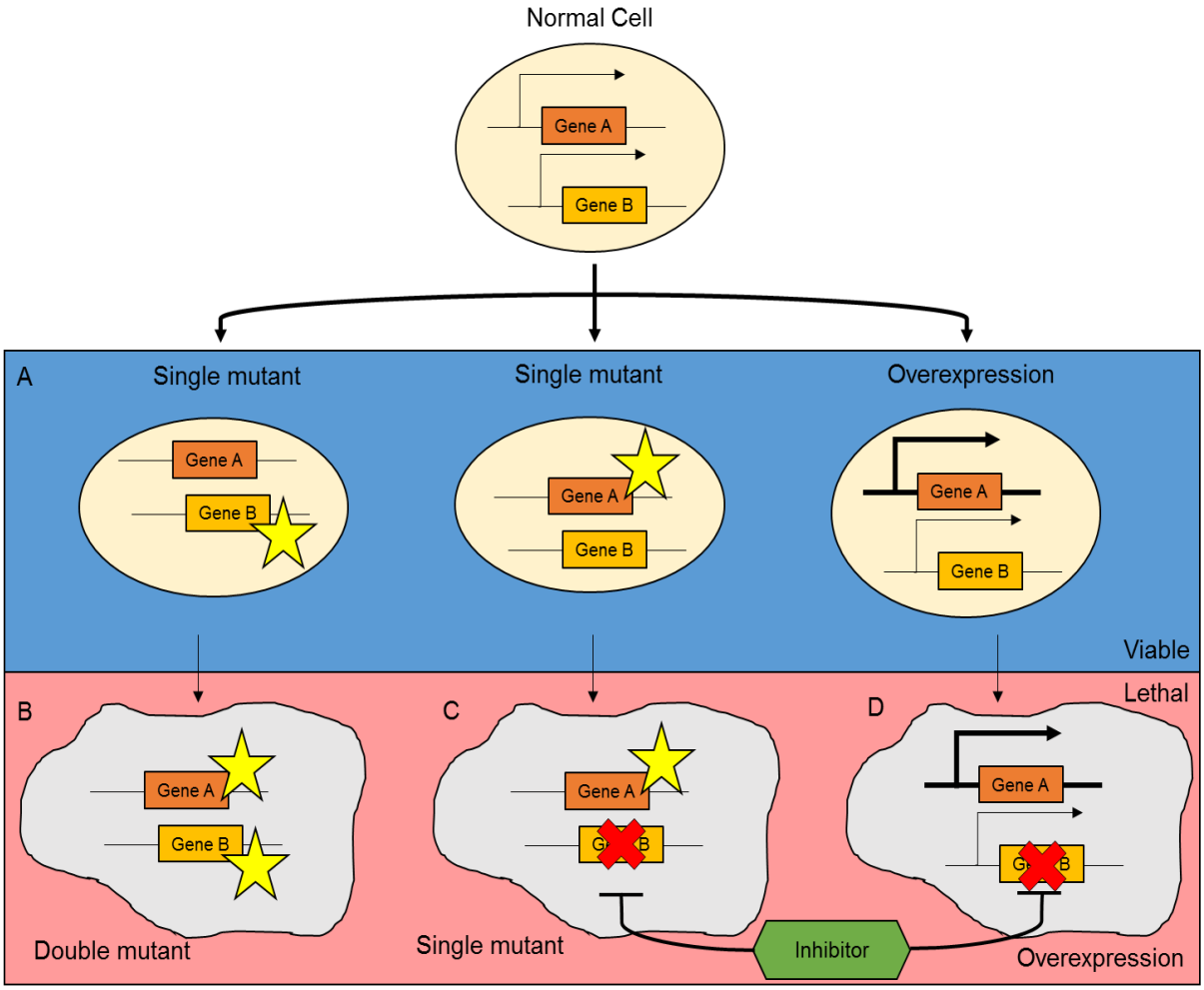

Figure 1.10 – Synthetic lethality model based on O'Neil et al (245).
A – *The loss or the inhibition of either of the proteins encoded for by gene A or gene B alone, or the overexpression of gene A is viable cancer cells.* ***B*** *– Mutation of protein encoded by gene B in cells with mutation in gene A results in synthetic lethality.* ***C*** *– Pharmacological inhibition of the protein encoded for by gene B in cells with a mutation in gene A results in synthetic lethality.* ***D*** *– Pharmacological inhibition of the protein encoded for by gene B in cells overexpression of gene A results in synthetic lethality and the subsequent death of the cell. The thicker arrow denotes increased gene expression. The star shape denotes a mutation. Red crosses denote pharmacological inhibition. Viable cells are depicted as ovals, and lethal cells are depicted as random shapes.*

1.4.10 G9a and neuroblastoma

G9a and neuroblastoma has not been well characterised with only three papers published thus far- 1) Ding et al (259), 2) Lu et al (260), and 3) Ke et al (261). This literature does suggest that G9a is a key driver of proliferation as inhibition with BIX-01294 consistently repressed cell proliferation in a variety of tested neuroblastoma cell lines. However, only Ding et al looked at the effect of G9a depletion on proliferation to confirm that BIX-01294 was targeting G9a (259).

However, this is where the similarities between the results of these papers stop suggesting that these results need re-confirming to validate their reliability. For example, when assessing if cell cycle arrest occurs following G9a inhibition, Ding et al immunoblot for two cell cycle genes cyclin A2 and cyclin B2 after 5μM BIX-01294 in SHEP-1 over the course of four days. They see a consistent decrease in these proteins with both depleted after three days thus suggesting there is cell cycle arrest. Lu et al however perform flow cytometry for cell cycle analysis alongside probing for cyclin D1. LA1-55n were treated with 2.5μg/ml (4.16μM) BIX-01294 over 24 hours and see no change in cell cycle progression or expression of cell proliferation related genes. Ke et al uses a wider range of cell lines with SK-N-AS, BE(2)-C, SK-N-DZ, SK-N-F1, and SHEP1 treated with 5μM BIX-01294 for 2-4 days. They show consistent increases in G1 phase cell cycle arrest along with downregulation of cyclinD1, CDK4 and CDK6 in all cell lines suggesting G9a inhibition does cause cell cycle arrest to inhibit proliferation. Therefore, these papers seemingly contradict one another with their overall conclusions alongside having no standard controls with which to compare these results.

Furthermore, in the context of cell survival, Ding et al suggests that G9a inhibition triggers autophagic cell death, Lu et al suggests G9a inhibition triggers apoptotic cell death, and Ke et al again suggests G9a inhibition leads to autophagy but show no cell death data. Moreover, Ke et al contradicts Ding et al by suggesting that no apoptosis is shown in their study. Therefore, these papers seem to agree that there is cell death occurring following G9a inhibition yet disagree on the method of this death.

Conversely, Ding et al also shows the effect of increased G9a expression by overexpressing G9a in SHEP1 cells. The cells with more G9a expression had increased cell proliferation and expression of cell cycle progression genes. Moreover,

overexpression of G9a activated genes involved in serine biosynthesis thus increasing serine production. This suggests a mechanistic reason for G9a promoting tumour survival and proliferation and is further evidence of the gene activator and repressor role of G9a.

The effect of G9a on MYCN regulation has only been suggested by Lu et al. They suggest that LA1-55n cells treated with 5µg/ml (8.33µM) BIX-01294 for 24 and 48 hours displays a significant change in *MYCN* mRNA expression. Moreover, LA1-55n cells were treated with 1, 2.5, and 5µg/ml (1.67, 4.17, and 8.33 µM respectively) for 24 hours show a reduction in MYCN protein in a dose dependent manner. The other papers do not test the effect of G9a on MYCN or other potential risk factors, for example ALK.

The main issue with these studies however is that these papers all inhibit G9a using small molecular inhibitor BIX-01294. BIX-01294 is a known specific inhibitor of G9a and a non-competitive with cofactor SAM (75) As previously mentioned, BIX-01294 has been shown to toxic above concentrations of 4.1µM (166), therefore the results and effects suggested by these studies may just be an artefact of off-target toxicity. This suggests that these studies need to be repeated with a more reliable small molecule inhibitor to truly assess G9a's involvement in neuroblastoma.

1.5 Aims of this research

In this thesis, the role of Histone methyltransferase G9a will be explored in *MYCN*-amplified neuroblastoma. MYCN regulates the activation and repression of its targets with the aid of histone modifiers such as histone deacetylases and methyltransferases. This cooperative mechanism is a potential target for disrupting MYCN stabilisation. Specific aims are to:

- Examine G9a as a potential oncoprotein in neuroblastoma
- Assess the efficacy of targeted G9a small molecule inhibitors in neuroblastoma
- Elucidate the involvement of G9a in gene regulation in high-risk neuroblastoma

Chapter 2

Materials and methods

2.1 Neuroblastoma Cell lines

The Neuroblastoma cell lines used for this study were derived from different sources, either as gifts from other laboratories or purchased from cell banks. The known genotype characteristics of are summarised in Table 2.1. These were used as *in vitro* models in the study.

Kelly

MYCN-amplified human neuroblastoma cell line donated from Louis Chesler's lab in The Institute of Cancer Research (ICR). Established from bone marrow metastasis of a 1-year old female with stage 4 (262).

LAN-1

MYCN-amplified human neuroblastoma cell line donated from Louis Chesler's lab in the ICR. Established from bone marrow metastasis of a 2-year-old male with stage 4 (263).

IMR-32 (IMR32)

MYCN-amplified human neuroblastoma cell line donated from Louis Chesler's lab in the ICR. They are derived from a primary tumour site in the abdomen of a 1-year-old male (264).

SH-SY5Y (SHSY5Y)

MYCN non-amplified human neuroblastoma cell line donated from Louis Chesler's lab in the ICR. It carries a single copy of *MYCN*. This cell line derived from the parental cell line, SKNSH which was established from bone marrow metastasis of a 4-year-old female with stage 4 (265).

SK-N-AS (SKNAS)

MYCN non-amplified human neuroblastoma cell line donated from Louis Chesler's lab in the ICR. established from bone marrow metastasis of an 8-year-old female with stage 4 disease (266). The cells express wild type p53 (267).

SK-N-BE(2)C (BE2C)

MYCN-amplified human neuroblastoma cell line donated from Louis Chesler's lab in the ICR. Established from parental cell line SK-N-BE(2). The parental cell line was

established in 1972 from the bone marrow biopsy of a two-year-old male with stage 4 neuroblastoma and has chromosome 1p deletion and alterations in chromosome 17 (266), and carries p53 mutation (C135F) (268).

NGP

MYCN-amplified human neuroblastoma cell line established from lung metastasis of a two-year-old male with chromosome t(1p) alterations (262, 266). The cell morphology displays neuronal-like elongated cells (N-type) (267). The cells also harbor wild type p53 protein (269).

GI-ME-N (Gimen)

MYCN non-amplified human neuroblastoma cell line that carries a single copy *MYCN*. This is from the bone marrow metastasis of a two-year-old female with stage 4 (270). Gimen has 1p deletion and express wild type p53 (271).

SHEP-21N

SHEP-21N cells are engineered by Manfred Schwab from non-MYCN-amplified SH-EP. The cell line was established by transfection of a CMV construct fused with human *MYCN*; expression is controlled by a tetracycline-off system (272). This enables the effect to be determined in two cell lines that only differ in their *MYCN*-amplification genotype.

Disease free cells

RPE-1

RPE-1 is an immortalised retinal pigment epithelial cell line, derived by transfecting RPE-340 cell line with pGRN145 hTERT-expressing plasmid (273). These cells were kindly donated from Grant Stewart's laboratory in Birmingham.

NF-TERT

NF-TERT is an immortalised human fibroblast cell line that derived from a skin biopsy. This cell line was immortalized with hTERT pBAbe retro puro. These cells were kindly donated from Grant Stewart's laboratory in Birmingham.

Name	Parental cell line	*MYCN* status	ALK mutation	*ALK* amplification	p53 status	References
KELLY	--	(+)	Mut F1174L		Mut P177T	(274-276)
LAN-1	--	(+) HSR	Mut F1174L		Mut C182X	(277-280)
IMR32	--	(+) DM	WT	(+)	WT	(264, 266, 267, 269, 281)
SHSY5Y	SKNSH	(-) SC	Mut F1174L	(-)	WT	(265, 269, 282-286)
SKNAS	--	(-) SC	WT	(-)	Mut p53ΔC	(266, 267, 275, 286)
BE(2)C	SK-N-BE(2)	(+) HSR	WT	(+)	Mut C135F	(266, 268, 275, 279, 282, 286-290)
NGP	--	(+) HSR	WT		WT	(267, 269, 275)
Gimen	--	(-) SC	WT	(-)	WT	(267, 271, 286, 291)

Table 2.1 – Characterisation of neuroblastoma cell lines
For MYCN status: (+) MYCN-amplified, (-) MYCN-unamplified, HSR- homogeneous staining region, SC- single-copy, DM- double minute.
For ALK amplification: (+): ALK-amplified, (-) ALK-unamplified, blank; unknown.
For mutation statuses: WT; wild type, Mut; mutated.
This is adapted from the table found in Thiele et al (266)

2.2 Cell Culture

Media for neuroblastoma and normal fibroblast cell culture

Neuroblastoma and disease-free cell lines were grown either in Dulbecco's modified eagle's medium: nutrient mixture F-12 (DMEM:F12) – LAN-1, IMR32, SHSY5Y, SKNAS, BE2C, RPE-1, or RPMI 1640 (Gibco) as detail in table 2.2. Each were supplemented with 10% (v/v) foetal bovine serum (FBS) (Life technologies), 2mM L-glutamine, 100 U/mL penicillin, 0.1 mg/mL streptomycin, and 1% (v/v) non-essential amino acids, unless otherwise stated. All cells were cultured as adherent monolayers at 37˚C with 5% CO_2.

Media for S21N neuroblastoma

The SHEP-21N cells were maintained in the presence of tetracycline 1:2000. They were cultured in RPMI 1640 (Gibco), supplemented with 10% (v/v) tetracycline-free FBS (Life technologies), 2 mM L-Glutamine, 100 U/mL penicillin, 0.1 mg/mL streptomycin, and 1µg/mL tetracycline.

Cell line maintenance

All cell lines were grown as adherent monolayers and incubated at 37ºC and 5% CO2 in a humidified incubator. Media was replaced every two to three days.

Cell Subculture

When cells reached 80 to 90% confluency, they would be passaged. Media was aspirated, and cells washed once in DPBS (5mL per T75) (Gibco). This was then removed, and trypsin was added (3mL per T75) and incubated at 37ºC until the cells detached from the flask. Fresh media was then added to deactivate the trypsin (7mL per T75) and this suspension was collected in a 25mL universal and centrifuged for three minutes at 1500 rpm. The supernatant was then removed, and cells resuspended in 10mL fresh media. The resuspended cells were placed in a new culture flask at a ratio of 1:10 (volume of cell suspension: total volume of media) and stored in a humidified tissue culture incubator at 37ºC with 5% CO_2.

Cell counting (live and apoptotic)

Cell-counts and cell viability were assessed using the Countess-automated cell counter (Thermo Fisher Scientific). 10µL cell suspension was mixed with 10µL trypan blue dye (Thermo Fisher), and 10µL of this mixture was then added to the disposable counting slides (Thermo Fisher). The total concentration of cells, concentration of live, concentration of dead cell population (all were per mL) and percent viability of the total cell population were obtained. The cell counts could then be analysed for statistical significance, $n \geq 2$.

Drug treatment with small molecule inhibitors

Cells were seeded the night before. Drug was then diluted in fresh media which replaced the old media. Drugs were all diluted in DMSO and stored at-20°C. Kelly cells were treated with 2.5 to 5µM of UNC0638. All other cell lines were treated with 10µM unless stated separately. Cells were treated for 24 or 72 hours. UNC0642, A366 and UNC0646 were also used in MTT viability assays from 20µM.

MTT cell viability assay

Cell lines were seeded in 96 well plate between 5000 to 15,000 cells per well in 80µL. The next day, 20µL of 5x the highest concentration of drug was added to triplicate treatments. After 72 hours, 10 µL of MTT (5 mg/mL) (Sigma) was added and incubated for a further 3 hours. Then 50 µL of SDS lysis buffer is added and the cells were incubated overnight at 37ºC.

The plates are then read the next morning with absorbance values at wavelengths 570nm and the reference wavelength of 650 nm, using SpectraMax 190 plate-reader (Molecular Devices). The percentage of survival was calculated by dividing the absorbance values of each well with absorbance value of the vehicle control and multiplying them with 100. The dose-response graphs were drawn using GraphPad Prism and used to determine the IC_{50} values for each drug and cell line.

2.3 Molecular Biology methods

RNA extraction

The RNA was extracted using the RNeasy Plus Mini Kit (Qiagen) following the manufacturer's instruction. To lyse the cells, 350µL of RLT lysis reagent with 3.5µL β-mercaptoethanol was used. Mixture was vortexed for 30 seconds and lysate transferred to a gDNA Eliminator spin column. This was centrifuged for 30s at ≥8000g (≥10,000 rpm). 350µL 70% (v/v) ethanol was then added to the flow-through, mixed, and 700µL transferred to RNeasy spin column. This was centrifuged for 15s at ≥8000g and flow-through discarded. 700µl buffer RW1 is then added to the RNeasy Mini spin column and centrifuged for 15s at ≥8000g and flow-through discarded. Next, 500µl buffer RPE is added to the RNeasy spin column. This is centrifuged for 15 s at ≥8000g and the flow-through discarded. This step is then repeated but the columns are centrifuged for 2 minutes at ≥8000g. The RNeasy columns are placed in a new 2 ml collection tube and centrifuged at full speed for 1 min to further dry the membrane. Finally, place the RNeasy spin column in a new 1.5 ml Eppendorf tube and add 30µl RNase-free water directly to the spin column membrane. This is then centrifuged for 1 minute at ≥8000g to elute the RNA.

The concentration (ng/µL) of 1µL collected RNA is then measured using the Nanodrop spectrophotometer. The Nanodrop measures absorbance at wavelengths 260nm, 280nm, and 230nm. These values are then used to determine the purity of the RNA eluted via the 260/280 and 260/230 ratios. For pure RNA, the 260/280 ratio should be around 2.1; a lower ratio indicates protein contamination. The A260/230 should be close to 2.0, with lower than 1.8 indicating significant organic contaminants.

cDNA synthesis

The cDNA was prepared using SuperScript™ IV First-Strand Synthesis System (Invitrogen). Each sample consisted of 1µg of RNA, 1µL 10mM dNTP mix, 0.5µL 50µM Oligio d(T)20 and 0.5µL 50ng/µL random hexamer primers. DEPC-treated water was added to make the total volume of each reaction 12µL. These were mixed by pipetting, briefly centrifuged, and heated at 65˚C for 5 minutes. The RNA-primer mix is then incubated on ice for 1 minute.

After, to each RNA-primer mix add the RT reaction mix which consists of 4µL briefly vortexed 5x SSIV buffer, and 1µL 100mM DTT, ribonuclease inhibitor, and SuperScript™ IV reverse transcriptase. Once mixed and centrifuged, this is heated at 23°C for 10 minutes, 50°C for 10 minutes, and 80°C for 10 minutes. The prepared cDNA was then diluted 1 in 10 with DEPC water, and stored at-20℃.

Quantitative real-time (qRT) PCR

Per reaction, a master mix consisting of the contents of table 2.3 is added to 2.5µL of diluted cDNA. 0.1% (v/v) ROX reference dye is added to Syber green mix. Each sample is performed in duplicate.

Volume (µL)	Reagent
7.5	Syber green + ROX
0.6	10µM F/R primer mix
4.4	ddH_2O

Table 2.3 – Mixture of reagents necessary for one qRT-PCR reaction

qRT-PCR was performed using Mx3005P (Stratagene) according to the manufacturer's instructions. The reaction begins with enzyme activation at 95'C for 15 minutes, followed with 40 cycles consisting of 95ºC for 15 seconds, 60ºC for 30 seconds, and 72ºC for 30 seconds. Subsequently after the cycles, the process terminates with 95ºC for 1 minute, 58'C for 30 seconds, and 95 ºC for 30 seconds. Primers used are in the table 2.4.

The data was analysed using MxPro which calculates a Ct value for each reaction. This is the threshold cycle, the cycle number when the gene product had amplified sufficiently to yield a detectable fluorescence signal; a higher Ct value means there is less of the gene product. The threshold is set to 0.01. This Ct value is then normalised to a reference gene (*TBP*) Ct value to calculate an average relative expression. The standard error of the mean (SEM) is used for the error bars.

The dissociation curve tab measures fluorescence against temperature for each reaction. Each gene product has a specific melting temperature, so these curves can be used to gauge if the reactions are measuring the gene of interest i.e. a specific product, or non-specific DNA products.

Genes	Primer Sequence	
	Forward (5'-3')	**Reverse (3'-5')**
FABP3	TTT AAG TTG GGG GTG GAG TTC	ACA AGT GTG GTC TCT TGC CC
AMHR2	TAC TCA ACC ACA AGG CCC AG	GGT CTG CAT CCC AAC AGT CT
CCBE1	TCA CTG GTG ACA AGG TGC TG	CTT CCC TTT GGT CCT GGT G
FLCN	TCT CTC AGG CTG TGG GAG C	CCA GCA TGC GGA AAG AAG
AKR1C1	CCT AAA AGT AAA GCT TTA GAG GCC ACC	GAA AAT GAA TAA GGT AGA GGT CAA CAT AAT
AKR1C2	CCT AAA AGT AAA GCT CTA GAG GCC GT	GAA AAT GAA TAA GAT AGA GGT CAA CAT AG
AKR1C3	CTG ATT GCC CTG CGC TAC	TCC TCT GCA GTC AAC TGG AAC
CLU	AGC AGC TGA ACG AGC AGT TT	AGC TTC ACG ACC ACC TCA GT
MYCN	CCT CAG TAC CTC CGG AGA GGA	TTC TCC ACA GTG ACC ACG TCG
G9a	CAA CTT CCA GAG CGA CCA G	GTG AAC AAC CAC CTG GAG GT
BOK	CAA GAC CCT GGC AAC CTG	GCT GAC CAC ACA CTT GAG GA
TBP	AGC CAC GAA CCA CGG CAC TGA T	TAC ATG AGA GCC ATT ACG TCG T
ALK	CGA CCA TCA TGA CCG ACT ACA A	CCC GAA TGA GGG TGA TGT TTT
CASP8	CAG TCA CTT TGC CAG AGC CT	GCA TCT GTT TCC CCA TGT TTT

Table 2.4 – Sequences for primers used in qRT-PCR.

Preparation of Protein Lysates

Floating and attached cells were harvested for protein analysis. These were harvested by collecting the media from the treated wells and trypsinisation respectively. These cells were then pelleted and lysed with 100 to 200 µL RIPA buffer and Inhibitors (1x phosphatase (PhoStop™, Sigma Aldrich) and 1x protease inhibitor). These were then sonicated (Diagenode Bioruptor) at high frequency in 30 second bursts for two and a half minutes. Samples were submerged in ice cold water. If the samples were still 'gloopy', the samples would be re-sonicated. Next, the lysates are centrifuged at 4˚C for 15 mins at 13,000 rpm. The protein lysate is now in the supernatant. These samples can now be quantified and stored at-80˚C.

Protein quantification by BCA assay

Protein concentrations are determined using Bicinchoninic acid assay (BCA) with Micro BCA ™ protein assay kit (Thermo Fisher). A protein standard curve is made using bovine serum albumin (BSA) (2mg/ml) and is added in a range from 0 to 12µL. 5µL of ddH_2O is added to the wells in use and 2µL of protein lysate is then added. Each protein lysate is measured in duplicate. 100µL of A, B, C solution (10:9:1 ratio respectively) is then added to each well with protein lysate and the plate is incubated at 37˚C for 15 minutes. The plate is now read using SpectraMax 190 plate-reader (Molecular Devices) at 562 nm. These values can now be compared to the curve to determine the volume of lysate necessary for 20µg of protein.

Immunoblot analysis

SDS-Polyacrylamide gels were prepared as described in Table 2.5. The samples were prepared to contain the same concentration of protein, generally 20µg, 1/5th the total volume of 5x SDS loading buffer, with the remainder filled with ddH_2O. These samples are then heated at 95˚C for five minutes, spun briefly before loading in to the wells of the gel. The samples are then run alongside 5µL rainbow ladder protein marker (Precision Plus Protein™ Kaleidoscope™) for 1 hour at 160V in 1x Tris-glycine-SDS running buffer.

After the samples have reached the bottom of the gel, the gel is removed from the glass cassette, the stacking layer removed, and the gel washed in 1x transfer buffer for 5 minutes. At the same time, PVDF membrane (Millipore) is incubated for 5 minutes in methanol and then incubated in the tank full of 1x Transfer buffer.

To transfer the proteins to the membrane, two sponges and six filter papers were pre-soaked in 1x transfer buffer. Within the transfer cassette (Bio-Rad), a sponge, three pieces of paper, gel, PVDF membrane, three pieces of paper and sponge was placed on top of each other. This is termed a “sandwich” which at each layer of construction, bubbles are carefully pressed out by rolling a stripette across each layer. The protein transfer was conducted in the ice-cold 1x transfer buffer at 120 Volts for 1 hour 20 minutes.

After transfer, the membrane is now incubated in 5% milk PBST (w/v) for 1 hour whilst on a shaker. Next, the membrane is briefly washed with PBST a couple of times before being incubated in primary antibody at 4˚C overnight/ 2 hours at room temperature. Table 2.6 details all the primary antibodies used.

After incubation, the membrane is washed three times for four minutes each with PBST before being incubated in secondary antibody diluted 1:5000 in 5% milk PBST for 1 hour at room temperature on a shaker. After, the membrane is washed four times for five minutes in PBST before the protein is detected by chemiluminescence with ECL Prime western blotting detection reagent (Amersham Biosciences) (1mL A and B per blot). The ECL covers the membrane for five minutes before being placed in an autoradiograph cassette and the membranes are then exposed to light-sensitive x-ray films (Kodak Diagnostic Film). The exposed films are developed by the Compact X4 Film Processor (X-ograph Imaging Systems Ltd).

All immunoblots shown are representative of at least two biological and two technical replicates.

Running Gel	RG 10%	RG 15%
ddH_2O	7.3 mL	4.4 mL
Resolving buffer	4.4 mL	4.4 mL
30% acrylamide/ 1% bis	5.8 mL	8.7 mL
APS solution	200µL	200µL
TEMED	6µL	6µL

Stacking Gel	SG 4.5%
ddH_2O	5.9 mL
Stacking buffer	2.6 mL
30% acrylamide/ 1% bis	1.5mL
APS solution	200µL
TEMED	6µL

Table 2.5 – Ingredients for making the SDS polyacrylamide running and stacking gels.

Antibody	Molecular weight (kDa)	Dilution	Secondary	Supplier	Catalogue Number
G9a	170	1/1000	Rabbit	Abcam	ab185050
MYCN (B8.48)	64	1/2000	Mouse	Santa Cruz	SC-53993
β-Actin	42	1/40,000	-	Sigma	A3854
c-PARP	25	1/1000	Rabbit	Abcam	ab32064
BOK (D7V2N)	22	1/500	Rabbit	CST	86875
LC3B	16- 18	1/1000	Rabbit	Sigma	I7543
BAK	24	1/500	Mouse	BD	55638
BAX	23	1/1000	Rabbit	Santa Cruz	SC- 493

Table 2.6 – List of antibodies used for immunoblotting.
β-Actin does need a secondary because the primary antibody used is horseradish peroxidase (HRP) tagged which emit light.

Transfection of small interfering RNA

To deplete proteins of interest such as G9a and MYCN, short-interfering RNA (siRNA) were used to target these genes. On the day of the transfection, cells would be in their exponential growth phase (~60/70% confluent) and media would be replenished a few hours beforehand. For each siRNA transfection, two 1.5mL microcentrifuge tubes are labelled A and B. To tube A, OptiMem (Invitrogen) and 100µM siRNA are added, and to B OptiMem and Lipofectamine RNA iMAX (Invitrogen). The volumes are shown in table 2.7. Each tube is vortexed, briefly centrifuged and incubated at room temperature for 2 minutes. Then B is added to A and this is vortexed, briefly centrifuged and incubated at room temperature for 5 minutes. 100µL is then added slowly to cells that haven't adhered yet. The final concentration of siRNA used was 25nM. The sequences used are in table 2.8.

6 well plate			Total of each tube (µL)	Total of A + B added (µL)	Volume of Cells added to (mL)
Tube	Reagents	Volume (µL)			
A	100uM siRNA	0.75	50	100	3
	OptiMem	49.25			
B	RNA iMAX	2	50		
	OptiMem	48			

96 well plate			Total of each tube (µL)	Total of A + B added (µL)	Volume of Cells added to (µL)
Tube	Reagents	Volume (µL)			
A	100uM siRNA	0.025	10	20	80
	OptiMem	9.975			
B	RNA iMAX	0.2	10		
	OptiMem	9.8			

Table 2.7 – Volumes of reagents needed for siRNA transfections in 6 well plates and 96 well plates. The final volume of siRNA is 25nM.

Gene	siRNA	siRNA sequence (5'-3')
G9a	siG9a 2	GAA CAU CGA UCG CAA CAU CUU
G9a	siG9a new	GAA CAU CGA UCG CAA CAU C
MYCN	siMYCN 1	CCC GGA CGA AGA UGA CUU CUA
MYCN	siMYCN new	GAA CCC AGA CCU CGA GUU U
BOK	siBOK#1	CGA GAU CAU GGA CGC CUU U
Negative control	siNEG	UGG UUU ACA UGU UUU CUG A

Table 2.8 – siRNA sequences used for transfections.

2.4 – *In silico* methods

Kaplan Meier curves

Using the R2: Genomics Analysis and Visualisation Platform (https://hgserver1.amc.nl/cgi-bin/r2/main.cgi), the Kaplan Meier curves presented were generated under the Kaplan Scanner (overall) side panel for the gene of interest. This curve can then be refined by applying set parameter tracks available within the datasets used, for example filtering between MYCN status or high risk.

Semi-quantitative densitometry

Protein bands detected by immunoblotting were scanned at 600dpi and the subsequent semi-quantitative densitometry was performed using ImageJ. The values for the protein of interest were divided by the loading control (β-Actin) to determine a ratio which can be used to quantify the amount of protein.

2.5 – Buffer recipes

RIPA Buffer-

In 200mL ddH_2O, add 5mL 1M Tris-HCl (Severn Biotech) (2.5mM), 1.75g Sodium Chloride (150mM), 1mL 0.2M ETDA (Severn Biotech) (1mM), 0.4g SDS (0.2% w/v), 1mL NP40 (0.5% v/v), and 0.4g sodium deoxycholate (0.2% w/v). Adjust to pH 8. Prior to protein extraction add 1x Phosphatase inhibitor and 1x protease inhibitor to 10mL RIPA Buffer

10x Running buffer-

In 1L ddH_2O, add 30g Tris base, 144g glycine, and 10g SDS

10x Transfer buffer-

In 1L ddH_2O, add 30g Tris base and 144g glycine

1x Transfer buffer-

100mL 10x Transfer buffer, 200mL Methanol, 700 mL ddH_2O

Stripping Buffer-

In 1L ddH_2O, adjust to pH 2.0, add 1.8g glycine and 10g SDS

4x Resolving buffer-

1.5M Tris-HCl, 0.4% SDS (w/v), pH 8.8

Stacking buffer-

0.5M Tris-HCl, 0.4% SDS (w/v) pH 6.8

Ammonium persulphate solution-

In 1mL ddH_2O, add 0.5g APS (50% w/v)

PBST-

In 1L 1x PBS, add 1000µL (1mL) (0.01% v/v) Tween-20

BSA blocking buffer-

In 30mL PBST, add (5% w/v) BSA powder and 30µL (0.1% v/v) 10% Sodium Azide

Milk blocking buffer-

In 50mL PBST, add 2.5g (5% w/v) skim milk powder

MTT-

50 mg/mL MTT in PBS. Sonicate and filter.

SDS lysis buffer-

10% SDS (w/v) in 0.01M HCl

Chapter 3

Assessment of G9a as a targetable oncoprotein in neuroblastoma

3.1 Introduction

As discussed in more depth in chapter 1, Histone methyltransferase G9a is suggested to be an oncoprotein in various cancers, which is reviewed in depth by Casciello et al (116). Yet in the context of neuroblastoma, there is very little published; currently only three papers examine the impact of G9a small molecule inhibitor BIX-01294 on cell proliferation and cell death (259-261), yet the effect has not been well characterised despite the use of similar cell lines.

Expression of other histone methyltransferases have been suggested to correlate with poor prognosis. For example, high expression of histone modifier *EZH2* has recently been suggested to correlate with both poor prognosis and expression of poor prognostic indicator MYCN which helps to repress differentiation in *MYCN*-amplified neuroblastoma (292). Furthermore, arginine methyltransferase *PRMT5* expression has recently been suggested to correlate with *MYCN* expression in *MYCN*-amplified neuroblastoma (229). This suggests that MYCN protein can utilise these histone methyltransferases to help drive tumour progression, therefore profiling G9a mRNA and protein expression between high- and low-risk neuroblastoma based on *MYCN*-amplification status may help to elucidate a role between MYCN and G9a, which has not been shown before.

This chapter begins by determining the prognostic potential of high *G9a* expression in neuroblastoma alongside an immunoblot panel of endogenous protein in neuroblastoma cell lines to ascertain if there is also a correlation between MYCN and G9a protein expression. This chapter also aims to evaluate G9a as an oncoprotein in neuroblastoma by assessing the impact of G9a depletion by siRNA transfection on cell proliferation and cell death.

3.2 *G9a* mRNA expression is increased in poor prognostic and *MYCN*-amplified neuroblastoma

Neuroblastoma is the most common paediatric solid tumour with evidence to suggest the epigenome demonstrates an important role in neuroblastoma tumour proliferation (293-295). As mentioned previously, there is plenty of evidence to suggest that G9a expression level is associated with poor prognosis in multiple cancer lines, so it stands to reason that this epigenetic modifier would likely have a role in neuroblastoma too.

However, only one paper has been published in neuroblastoma looking at *G9a* expression and poor prognosis (261). Ke et al were the only group to assess the oncogenic potential of G9a by using the Genomic Analysis and Visual Platform R2 (http://r2.amc.nl), however they only used one dataset, Versteeg-88 (296). Here, they showed that increased G9a expression is strongly associated with a poor prognostic outcome in neuroblastoma, therefore suggest that G9a can be used as a prognostic marker (261).

In this study, the number of databases was expanded to corroborate these findings of G9a as a potential oncoprotein (Figure 3.1). Using three different neuroblastoma datasets from the R2 database, including the dataset used by Ke et al, the correlation between *G9a* mRNA expression and survival probability was gauged. The Versteeg-88 dataset is a tumour microarray of 88 neuroblastoma tumours, analysis of which displayed that tumours with high *G9a* expression (n=42) presented a low overall survival probability relative to tumours with low G9a (n=46), (Bonferroni $p=6.9e^{-3}$). Comparison of this data with the SEQC-498 dataset, RNA sequencing data from 498 neuroblastoma tumours, showed a comparable result of high *G9a* mRNA expression (n=62) leading to a significantly decreased overall survival probability (Bonferroni $p=4.1e^{-11}$). Finally, the third dataset, a 44k oligonucleotide array of 649 tumours-Kocak-649, again validated this hypothesis that *G9a* expression correlates with survival with high *G9a* expression (n=131) (Bonferroni $p=1.3e^{-7}$) (Figure 3.1A). Kocak-649 lacked survival information for 173 samples so the analysis was only performed on 476 tumour samples. The data from these databases all indicate that high *G9a* expression is worse for survival.

As stated in chapter 1, because *MYCN*-amplification is a standard marker for high-risk, poor prognosis neuroblastoma, it seemed logical to determine if *G9a* expression was still a potential poor prognostic indicator in tumours without *MYCN*-amplification similar to lung and bladder cancers (130, 143, 149). This refinement was not performed by Ke et al. Using the same datasets as before, the data was refined to only use the non-MNA tumours (Figure 3.1B). The SEQC- 498 and Kocak- 649 datasets suggested there was still a significant correlation between high *G9a* expression and low survival (Bonferroni p=0.014 and 0.038 respectively). However, the correlation suggested by the Versteeg- 88 dataset was not quite significant (Bonferroni p= 0.076) despite the Kaplan-Meier suggesting a significant relationship.

This was probably due to a reduced sample size relative to the other two datasets although the p values were not as low as they were previously. Overall, this data suggests that *G9a* expression is poor prognostic indicator independent of *MYCN*-amplification in neuroblastoma.

Despite two of the three datasets being significant for high G9a mRNA expression in non-*MYCN*-amplified tumours correlating with survival, there was a drastic difference in the Bonferroni p value between the datasets in Figure 3.1A and 3.1B. This suggests that *G9a* expression is potentially dictated by *MYCN*-amplification. Therefore, *G9a* expression was compared between *MYCN*-amplified and non-*MYCN*-amplified neuroblastoma tumours to examine this relationship in the same three datasets. Boxplots produced from the R2 platform using the datasets (Figure 3.2A) shows that there is a significant increase in *G9a* in *MYCN*-amplified tumours relative to non-*MYCN*-amplified tumours ($p=3.2e^{-3}$, $5.8e^{-21}$, $6.1e^{-18}$ respectively).

Moreover, using the SEQC-498 database, the boxplot of *G9a* expression in *MYCN*-amplified vs non-*MYCN*-amplified was further refined to only use high-risk tumours (Figure 3.2B). This suggested a significant increase in *G9a* expression in the high-risk *MYCN*-amplified relative to high-risk non-*MYCN*-amplified suggesting G9a is a viable risk factor and a potential therapeutic marker for poor prognosis. The other two databases did not have a risk factor filter which is why this analysis was only performed in the SEQC-498 database.

Because of the correlation at the RNA level, it was necessary to determine if this was true at the protein level too. A panel of protein lysates from five *MYCN*-amplified, three non-*MYCN*-amplified neuroblastoma, and two disease-free cell lines were immunoblotted for G9a and MYCN (Figure 3.2C). β-actin was used a loading control and MYCN protein was overexpressed in all the *MYCN*-amplified cell lines. There was higher expression of G9a protein the *MYCN*-amplified cell lines relative to the non-*MYCN*-amplified. This relationship was quantified using semi-quantitative densitometry of the immunoblots using image J (Figure 3.2D). Relative G9a was quantified to β-actin. Relative G9a levels were shown to be significantly higher in the *MYCN*-amplified cell lines relative to non-*MYCN*-amplified and disease-free cell lines (*** $p<0.001$). G9a was ubiquitously expressed in all the cell lines tested, however at lower levels in the non-MNA and disease-free. In addition, there are two bands shown

for G9a, the top is isoform A and the bottom is the shorter isoform B. The immunoblot suggests that there is generally more of A than B, yet there is no pattern in the amount of B between the cell lines.

Overall, examination of G9a and MYCN mRNA and protein in neuroblastoma cell lines strongly suggests that G9a is more highly expressed in *MYCN*-amplified cells.

3.3 G9a depletion in Kelly cells has a significant effect on cell growth

High G9a mRNA and protein expression in *MYCN*-amplified cell lines strongly suggests G9a has a role as a potential oncoprotein. Therefore, to assess the functional role of G9a in neuroblastoma, *MYCN*-amplified Kelly cells were transfected with two short interfering RNAs (siRNAs) targeting G9a histone methyltransferase.

Phenotypically, there was a significant difference between the non-target control and the two G9a depleted cells with there being drastically less cells in the treatments (Figure 3.3A) suggesting cell proliferation repression along with more detached and floating cells which is indicative of cell death. Furthermore, they were phenotypically distinct with the siG9a treated cells looking more rounded morphologically and dead, again suggesting cell death. The phenotypic effect of G9a depletion in neuroblastoma cells has not been published to date.

The floating and attached cells were harvested and immunoblotted for G9a to confirm the G9a knockdowns (Figure 3.3B). In addition, the presence of apoptotic cell death was suggested by the increase in cPARP in both siG9a treatments (Figure 3.3B). Since the phenotypic and cPARP changes are similar between the two transfections relative to the negative control, it can be safely assumed that this is not an off-target effect of the siRNA transfection.

The cells were monitored by live cell imaging system IncuCyte Zoom for percentage phase confluence to assess the phenotypic effects of G9a depletion. G9a depletion in Kelly cells resulted in a significant decrease ($n=3$, * $p<0.05$) in percentage phase object confluence relative to the non-target control siNEG from 36 hours with siG9a2 and 24 hours with siG9a new (Figure 3.3C).

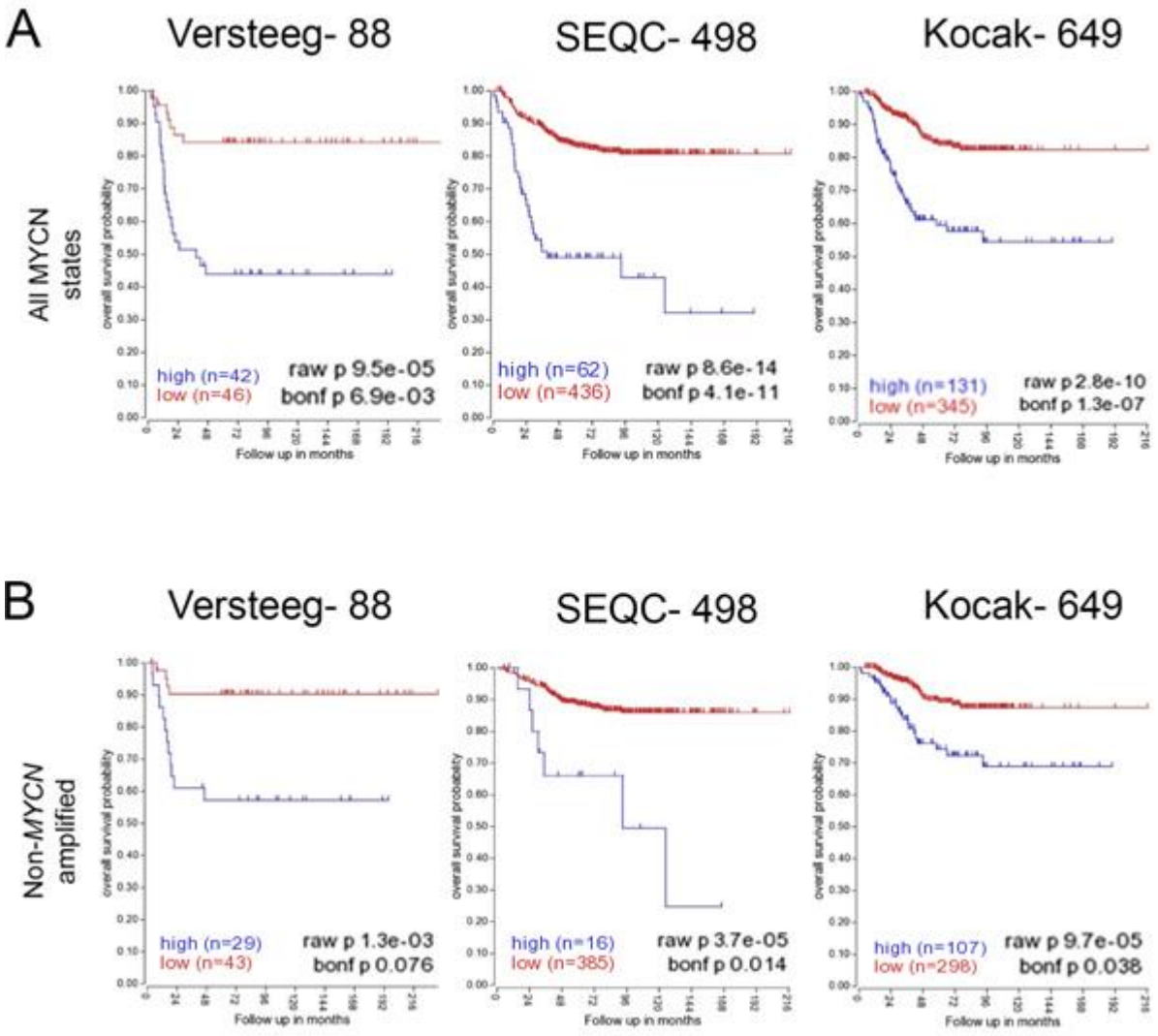

Figure 3.1 – High G9a mRNA expression correlates with poor prognosis in neuroblastoma

A *– Kaplan-Meier survival curves of neuroblastoma show a positive relationship between high G9a mRNA expression and poor prognosis. The blue and red lines represent high and low G9a mRNA expression respectively, whilst n represents the number of tumours in each category. This correlation was shown in three separate named tumour array datasets. Versteeg-88 analysis derives from microarray data analysing eighty eight human tumours (297). SEQC-498 is derived from RNA sequencing data of 498 neuroblastoma. Kocak-649 is generated using 44K oligonucleotide microarrays of neuroblastoma tumours and cell lines (298). In the Kocak-649 dataset, only 476 of the 649 neuroblastoma samples were analysed as only these had survival information available (222).* ***B*** *– Kaplan-Meier survival curve from the databases shown in A were refined to only include tumours with non MNA states. This showed that there is a positive relationship between high G9a mRNA expression and poor prognosis after poor prognostic indicator MYCN-amplification is taken out. The blue and red lines represent high and low G9a mRNA expression respectively, whilst n represents the number of tumours in each category.*

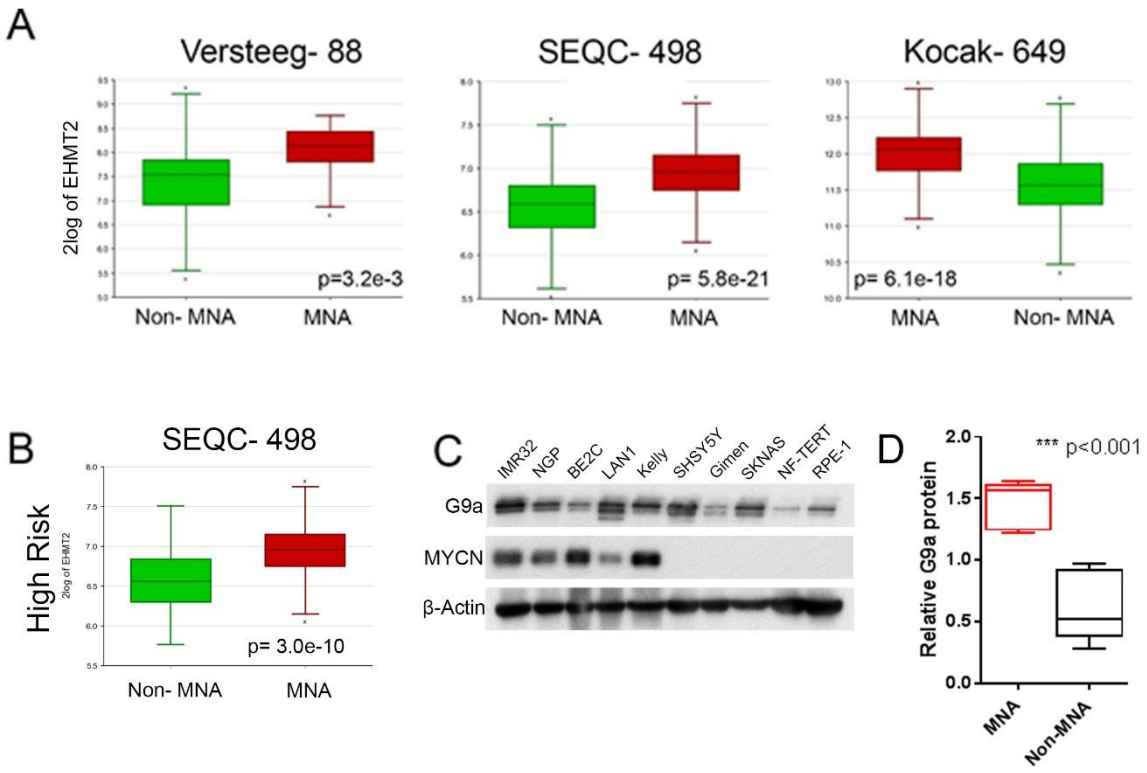

Figure 3.2 – High G9a protein expression correlates with MYCN protein
A *– Significantly higher G9a mRNA expression is observed in MNA neuroblastoma relative to non MNA. This correlation was shown in three separate named tumour array datasets previously mentioned in Figure 3.1. The red and green colours represent MNA and non MNA respectively, with the bracketed numbers representing the number of tumours. The p-values are calculated by one-way ANOVA (Analysis of Variance) on R2.* ***B*** *– Significantly higher G9a mRNA expression is observed in MNA neuroblastoma relative to non MNA in high-risk only neuroblastoma tumours. This filter was added in the SEQC- 498 database.* ***C*** *– Immunoblot of G9a protein expression in a panel of MYCN- and non-MYCN-amplified neuroblastoma cell lines. β-Actin is used as a loading control. Representative of two biological replicates.* ***D*** *– G9a expression is higher in MNA neuroblastoma when normalised to β-Actin. Box plot of relative G9a protein is generated from semi-quantitative densitometry of blots from* ***C****. G9a expression was normalised to β-Actin. Significance measured by unpaired T test (*** p<0.001).*

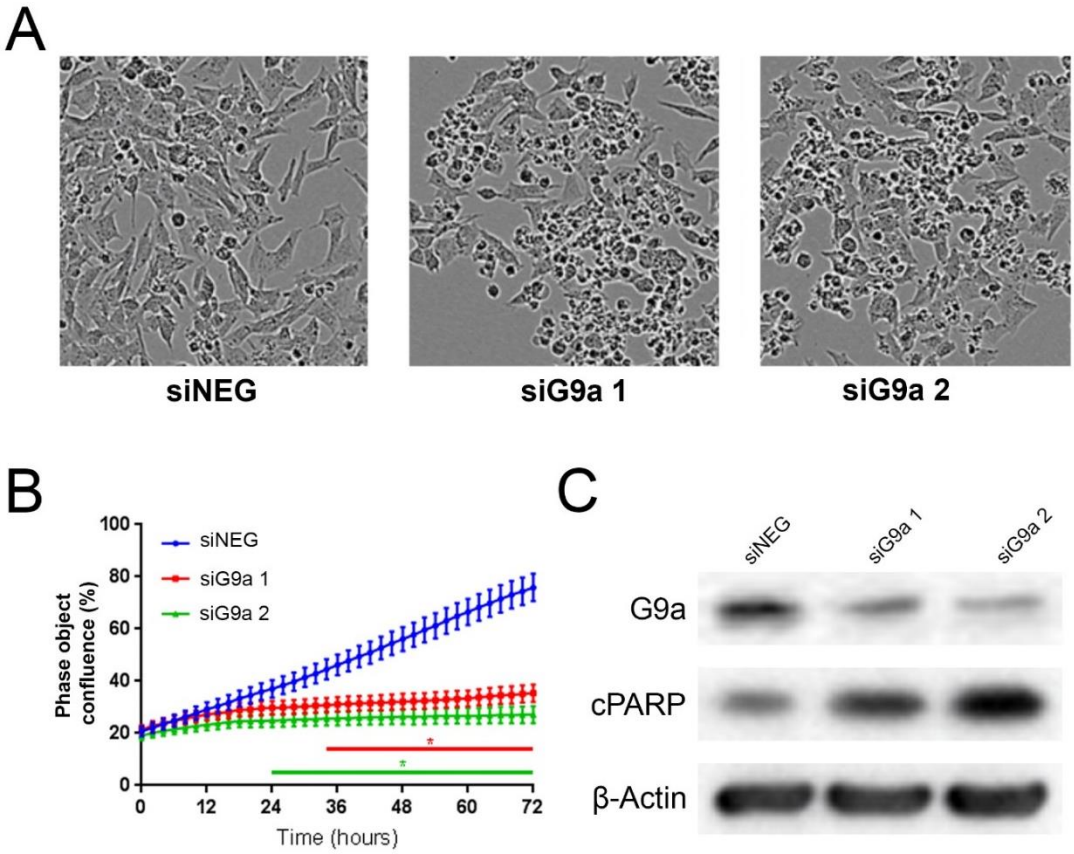

Figure 3.3 – G9a influences proliferation and survival in Kelly cells
A *– Photomicrographs at 10x objective magnification of Kelly cells after 72-hour knockdown of histone methyltransferase G9a via siRNA transfections.* ***B*** *– Graph depicting the percentage phase object confluence of the siG9a transfected Kelly cells relative to the negative control, siNEG. The asterisk and lines below the graph mark significant changes in phase object confluence for each G9a siRNA treatment relative to the negative control (n=3, * p<0.05). Error bars show the SEM.* ***C*** *– Immunoblot confirming the knockdowns from samples shown in A. These are the negative control, siNEG, and two different G9a siRNAs. cPARP is indicative of cell death. β-Actin was used as a loading control.*

3.4 G9a depletion leads to apoptotic cell death

The Kelly cells depleted of G9a in Figure 3.3 were phenotypically distinct relative to the negative control as they were rounded and there was a high quantity of floating cells indicative of apoptosis and cell death as well as an increase in cPARP relative to the negative control. This is all indicative of apoptotic cell death so to confirm this, a pan-caspase inhibitor, Q-VD-OPh (QVD), was added to G9a depleted Kelly cells in a 96-well format. These cells were also monitored by live cell imaging system IncuCyte Zoom for percentage phase confluence. A significant and similar decrease in phase object confluence was seen in the treatments with and without QVD after 28 hours ($p<0.05$) suggesting this decrease in proliferation is not due to apoptosis (Figure 3.4A).

The IncuCyte also measures red object count; visible cell death was present alongside the reduced proliferation, so DRAQ7, a red-fluorescence non-permeable DNA dye, was added to quantify the change in dead cells. The normalised object red count (Figure 3.4A) reveals that there is an increase in the volume of dead cells detected, significantly so after 44 hours, as shown by the green line, $p<0.05$. Apoptosis was then rescued by the addition of QVD as shown by the red object count for both siNEG and siG9a transfections being similar. They were both indifferent from their starting normalised red object count suggesting successful ablation of apoptosis. This inhibition was significantly different to QVD negative treatments after 22 hours, as shown by the black line, $p<0.05$.

Phenotypically, there were less floating and rounded cells observed in the siG9a treatments with the addition of QVD (Figure 3.4B), suggesting that the apoptosis is rescuable. However, the cells did not match the siNEG treatment with QVD further emphasising that G9a influences other cell process like proliferation.

When scaled up to a 12-well format, cells of the same treatment were harvested, and trypan blue inclusion assay performed to count the dead cells. There is an expected increase in cell death in the G9a depleted cells relative to the negative control in the QVD-negative treatments, over 1.5-fold increase ($n=2$, * $p<0.05$) (Figure 3.4C). Furthermore, in the presence of QVD, G9a depleted cells were rescued from cell death with over a 2-fold decrease in percentage cell death relative to the QVD negative control ($n=2$, * $p<0.05$). However, there was no significant difference in the level of basal death between the QVD positive and negative treatments despite a significant difference in the red object count data. This suggests that there may be a difference in basal cell death dependent on the total number of cells in a well at one time.

An immunoblot of the floating and adherent cell lysates (Figure 3.4D), not only confirmed an effective knockdown of G9a protein, but also there is no change in cPARP levels in the treatments with QVD added relative to the significant increase in cPARP with siG9a added and previously seen in Figure 3.3B. This is a further suggestion that this cell death is apoptotic.

All this data suggests that the death observed in G9a-depleted Kelly cells occurs through caspase-dependent apoptosis, which agrees with the conclusions drawn by Lu et al (260).

3.5 Apoptotic cell death associated with G9a depletion is preferential to MYCN-amplified neuroblastoma

Since G9a and MYCN mRNA and protein expression correlate, the effect on cell death and proliferation by depleting G9a in non MNA amplified cell lines needed to be examined to determine if this is an artefact of the MYCN status of neuroblastoma.

G9a was depleted in non MNA neuroblastoma cell lines Gimen. Using the trypan blue inclusion assay as mentioned previously with the Kelly cells, the live and dead cell counts were measured in Gimen cells treated with siRNA G9a new (here after denoted as siG9a) after 72 hours. There was no significant increase in the percentage cell death seen in the G9a depleted cells relative to the negative control ($n=4$, $p=0.23$) suggesting that G9a depletion has no death response in Gimen cells (Figure 3.5A). However, there was still a very significant decrease ($n=4$, *** $p<0.01$) in the number of live cells in the treated cells relative to the negative control. This can be used to assume that the growth rate inhibition effect exhibited by G9a depletion is still present despite the lack of apoptotic cell death in Figure 3.5A. This is further shown by immunoblotting the protein lysates from the treated cells (Figure 3.5B). An effective knockdown was confirmed, yet there was no increase in apoptosis indicator cPARP.

Other non-*MYCN*-amplified cells, SKNAS and SHSY5Y, were also depleted of G9a. The same lack of change in cPARP levels as seen in the Gimen cell line was also observed (Figure 3.6) despite effective G9a depletion suggesting that this apoptosis only occurs in *MYCN*-amplified cell lines.

Overall, this data suggests whilst G9a depletion seemingly has a universal effect on the inhibition of cell growth, whereas apoptotic death that is driven by the depletion of G9a in neuroblastoma is dependent on the *MYCN*-amplification status of the neuroblastoma as apoptosis is only observed in the MNA cell lines Kelly, LAN-1, and IMR32 and not in the non-MNA cell lines Gimen, SKNAS, and SHSY5Y.

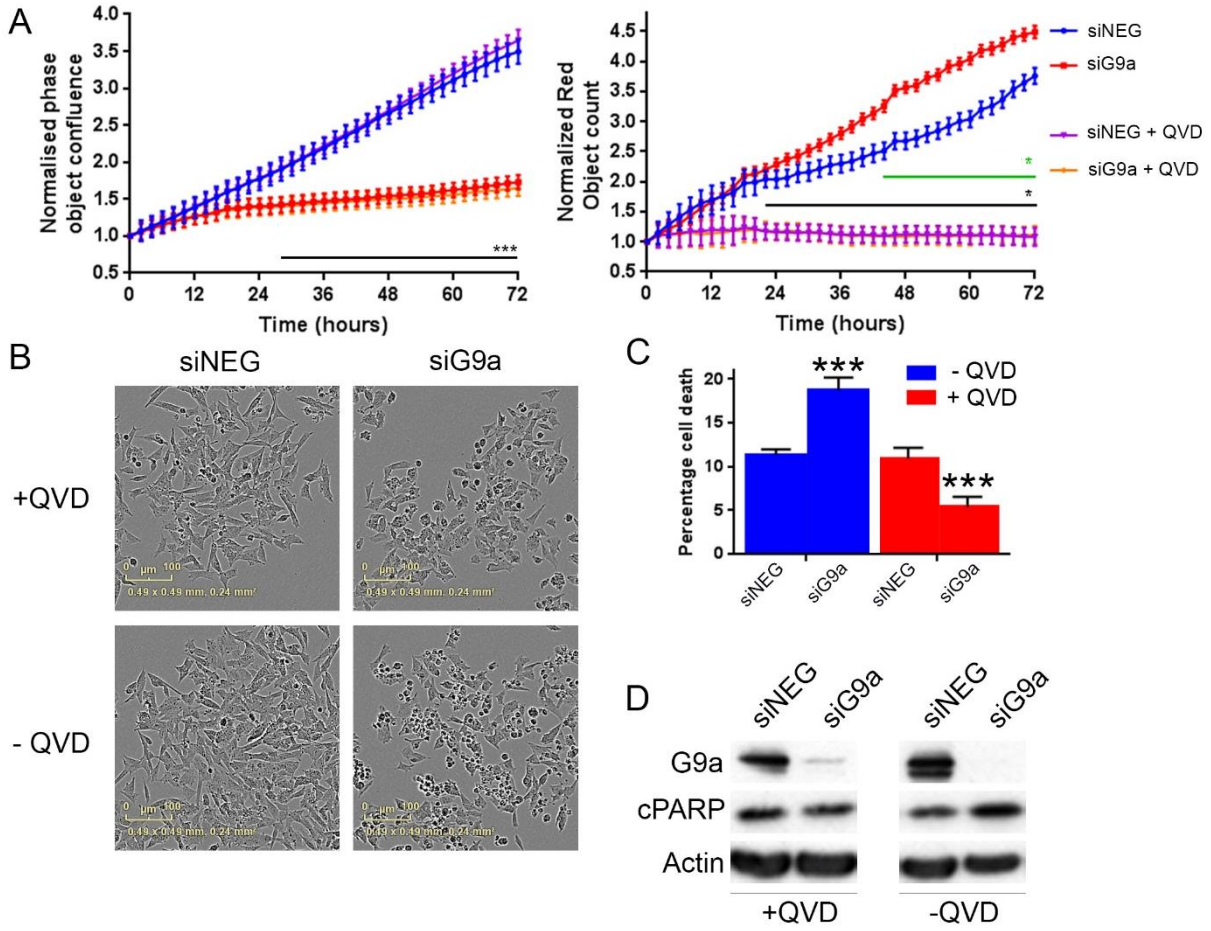

Figure 3.4 – Depletion of G9a leads to apoptosis. This can be rescued by the addition of apoptosis inhibitor QVD

A *– Graph depicts the normalised percentage phase object confluence as a proxy of cell growth. The cells were transfected with siRNA at 25nM and incubated for 72 hours. QVD was added at a concentration of 10μM. This shows that the decrease in cell growth associated with G9a depletion was not affected by QVD. The blackline underneath the graph shows significance (*** p<0.01) after 28 hours. Normalised red object counts shows that G9a depletion leads to apoptotic cell death due to a significant increase in the red object count, a proxy for cell death, after 44 hours (* p<0.05, n=2, green line) between siNEG and siG9a new. Also, the effect of apoptosis inhibitor QVD is significantly apparent after 22 hours (* p<0.05, n=2, black line) showing that the apoptosis is rescuable. Error bars show the SEM.* ***B*** *– Photomicrographs at 10x objective magnification of the treatments from A. These show the phenotype of apoptotic phenotype along with the rescuable apoptosis.* ***C*** *– Floating and adherent cells from* ***A*** *were harvested and counted for trypan blue inclusion assay. The graph depicts the percentage cell death of G9a depletion relative to the negative control, with and without QVD. The asterisks mark significant changes (p<0.01, n=2). There is a significant increase in cell death because of G9a depletion relative to the negative control, and the effect of QVD is further apparent due to the significant reduction in cell death caused by siG9a new with QVD relative to the negative control with QVD. Error bars show the SEM.* ***D*** *– Immunoblot to confirm apoptosis in cells without QVD treatment from A. β-Actin is used as loading control.*

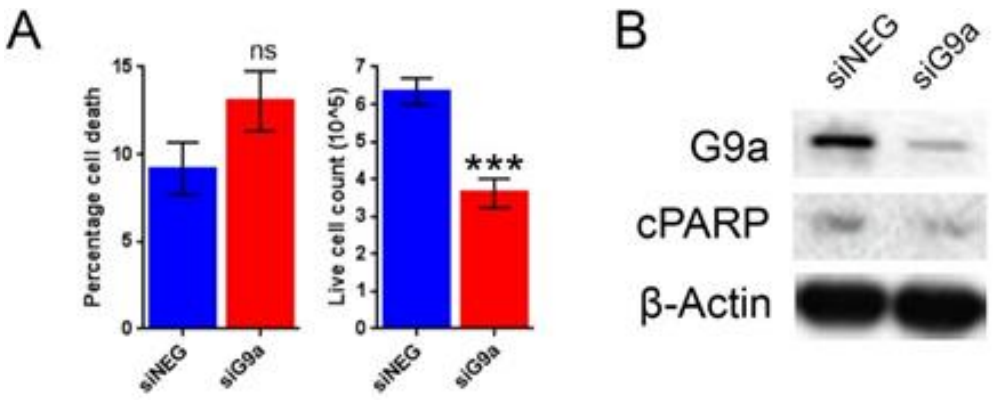

Figure 3.5 – Apoptotic cell death caused by G9a depletion does not occur in Gimen cells

A *– Floating and adherent cells from Gimen cells treated with negative control, siNEG, and siG9a new were harvested and counted by trypan blue inclusion assay. The left-hand graph shows the percentage cell death between the two treatments. The righthand graph shows the live cell count (10^5) of the Gimen cells harvested in A. The live cell count is used as a gauge for cell growth. Significant changes are measured the asterisks (*** p<0.01, n=4). Error bars show the SEM.* ***B –*** *Immunoblot of the treatments from A and of SKNAS and SHSY5Y cells transfected with negative control, siNEG, and siG9a new. It confirms the knockdowns of G9a, and that no apoptosis is occurring as shown by cPARP Cleaved PARP (cPARP) is indicative of apoptosis. β-Actin is used as loading control.*

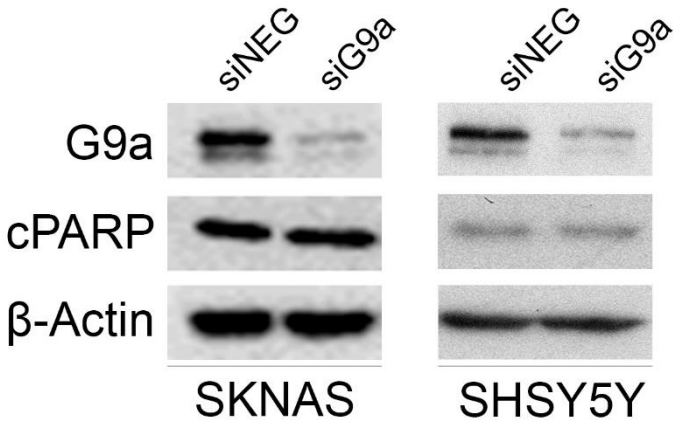

Figure 3.6 – Apoptotic cell death caused by G9a depletion does not occur in SKNAS or SHSY5Y cells

Immunoblot of floating and adherent cells from SKNAS and SHSY5Y cells treated with negative control siNEG and siG9a. cPARP is a marker for apoptosis and cell death. β-Actin is used as loading control.

To ascertain if apoptosis truly is dependent on the *MYCN*-amplification of the neuroblastoma, therefore G9a and MYCN are potentially synthetic lethal, G9a was depleted in SHEP-21N (S21N) cells. S21N cells are engineered from non-MNA SH-EP and contain a system that allows for the expression of *MYCN* in the absence of tetracycline (TET) (299). This enables the effect of G9a depletion to be determined in two cell lines that only differ in their *MYCN*-amplification state determining if this is a *MYCN*-amplified neuroblastoma trait.

G9a depleted S21N cells with and without TET were harvested and trypan blue inclusion assay was performed to determine if the G9a depletion-associated apoptosis is directly determined by the *MYCN*-amplification state of neuroblastoma (Figure 3.7A). In the S21N with TET (*MYCN* expression off), there was no difference in the percentage cell death between the negative control and the cells depleted of G9a. However, in the S21N without TET (*MYCN* expression on), there is a very significant increase in cell death (n=3, *** $p<0.01$,) between the two treatments. This apoptotic cell death was confirmed by immunoblotting the treated cells for cPARP (Figure 3.7B). There was no change in cPARP between the MYCN off S21N cells yet there was an increase in the cPARP levels in the MYCN on S21N cells further solidifying that G9a depletion-induced apoptosis MYCN dependent.

Moreover, in S21N cells with MYCN on, MYCN protein completely disappeared when G9a was depleted (Figure 3.7B). The extent of MYCN protein depletion is surprising as this link between G9a inhibition and MYCN has only been suggested once (260); the effect on MYCN protein after G9a depletion has not been shown before. This adds further evidence to G9a and MYCN being positively linked.

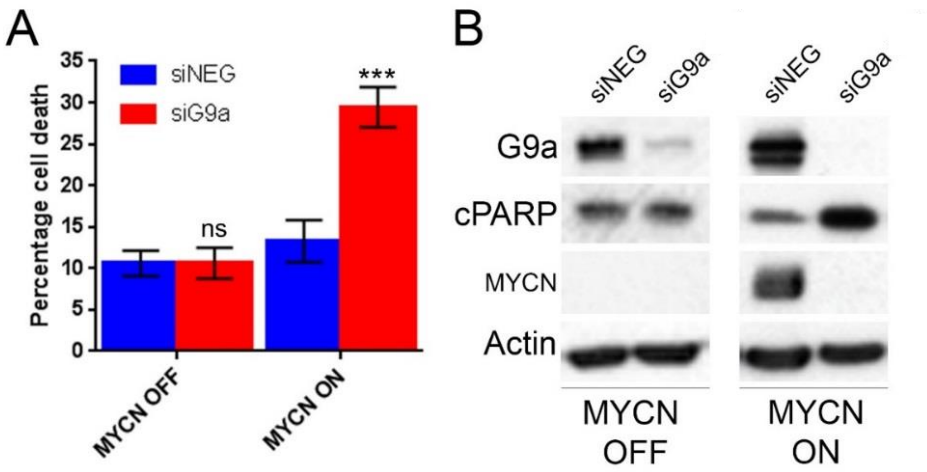

Figure 3.7 – G9a knockdown preferentially kills *MYCN*-amplified neuroblastoma cells
A *– The graph shows the percentage cell death of S21N cells in the presence and absence of tetracycline to alter their MYCN expression. These cells were transfected with siG9a new to deplete G9a and cell death was measured 72 hours later after trypan blue inclusion assay. There is no difference in cell death in the S21N with tetracycline (MYCN OFF) but a significant increase in those without tetracycline (MYCN ON) (*** p<0.01, n=3). Error bars show the SEM.*
B *– Immunoblot of cell lysates from A. This confirms the increase in cPARP protein because of G9a depletion only in the MYCN-amplified S21N cells. β-Actin is used as the loading control.*

3.6 Discussion

The aim of this chapter was to assess G9a as a potential oncoprotein in neuroblastoma by expression and function analysis; the results suggest that *G9a* expression correlates with *MYCN*-amplification. Depletion of G9a exhibits a profound inhibition in proliferation in tested neuroblastoma cell lines; this is not cell death dependent. Furthermore, effective G9a depletion in tested *MYCN*-amplified cell lines leads to an increase in apoptotic cell death which is not exhibited in tested non-*MYCN*-amplified cell lines suggesting a potential synthetic lethal relationship between G9a and MYCN.

In both *MYCN*- and non-*MYCN*-amplified neuroblastoma cell lines with G9a depleted, there is a significant decrease in the proliferation. Real-time phase object confluence data recorded by the IncuCyte showed a significant plateauing of cell growth in *MYCN*-amplified Kelly cells from 24-to-36 hours after successful siRNA transfection over a 72-hour time course. Furthermore, Gimen cells with wild type G9a had a significantly greater number of live cells, a proxy for proliferation rate, relative to those cells with G9a depleted after 72-hour knockdowns. This is similar to results shown in gastric carcinoma cells MGC-803 with G9a depletion leading to decreased cell proliferation (147). These cells are also non-*MYCN*-amplified as MYCN is not a risk factor in gastric

carcinoma. This all suggests that G9a is an oncogene involved in cell proliferation in neuroblastoma independent of high-risk factor MYCN.

Depletion of G9a was also shown to induce apoptosis in *MYCN*-amplified neuroblastoma cell lines tested suggesting a potential synthetic lethal relationship. Depletion of G9a in Kelly cells led to a consistent increase in apoptosis indicator cPARP. This was not seen in the three non-*MYCN*-amplified neuroblastoma Gimen, SHSY5Y, and SKNAS when G9a was depleted. G9a knockdown in *MYCN*-inducible S21N cells further suggests this synthetic lethal relationship as apoptosis following G9a depletion is dependent on the presence of MYCN. This link is also addressed in the next chapter when the current small molecule inhibitors of G9a are assessed in multiple cell lines. G9a depletion-associated apoptosis has been suggested in other cancers such as gastric carcinoma (147), colorectal cancer (154), non-small-cell lung cancer (300), and osteosarcoma cancer cells (301). These are not *MYCN*-amplified cell lines however, which suggests a novel relationship between MYCN and G9a in *MYCN*-amplified neuroblastoma cell lines. The data presented in this chapter suggests a role for G9a in repressing apoptosis in neuroblastoma. There is an increase in apoptosis following G9a depletion which is rescued following use of potent pan-caspase inhibitor QVD. This shows that this apoptosis is caspase-dependent.

This synthetic lethal relationship has not been tested before in studies regarding neuroblastoma as apoptotic cell death has only been suggested by Lu et al. Here they treated *MYCN*-amplified LA1-55n cells with by small molecule inhibitor BIX-01294 and evaluated the effect on caspase 3 and caspase 8 activities (260). Therefore, although BIX-01294 mediated G9a inhibition has been shown in both MYCN states, a comparison between the two, and subsequent suggestion of a lack of apoptosis in the non-*MYCN*-amplified, has not been shown before.

An unexpected result from this chapter was the complete downregulation of MYCN protein in the S21N cells with *MYCN* ON after G9a depletion (Figure 3.6 B). G9a and MYCN regulation has only been shown once and very fleetingly in published literature. Lu et al suggests that LA1-55n cells treated with 5µg/ml (8.33µM) BIX-01294 for 24 and 48 hours show a significant change in *MYCN* mRNA expression. Moreover, LA1-55n cells were treated with 1, 2.5, and 5µg/ml (1.67, 4.17, and 8.33 µM respectively) for 24 hours show a reduction in MYCN protein in a dose dependent manner (260).

There are many issues with these results however. As mentioned previously, BIX-01294 has been shown to toxic above concentrations of 4.1μM (166), therefore the results from treatments using concentrations ≥2.5μg/ml are most likely an artefact of off-target toxicity. Therefore, the only reliable result shown is the immunoblot of MYCN protein change after 1μg/ml which is not significant.

They also do not show if MYCN decrease is mirrored in G9a depleted cells which is why this was assessed first. Furthermore, in the MYCN protein immunoblot, β-actin control looks as if it decreases alongside the MYCN suggesting that this could be a reason for the MYCN decrease. Therefore, there are issues with the result described by Lu et al which are addressed in the data shown in this chapter.

MYCN has been shown to be regulated by other epigenetic and post-translational modifiers such as PRMT5 (229) and Aurora kinase A (253), therefore G9a could also directly methylate MYCN like it does other non-histone targets or indirectly via a complex, which may lead to a destabilisation effect at the protein level which may suggest why the G9a depletion in the MYCN induced S21N cells led to MYCN depletion. The relationship between G9a and MYCN is further explored in Chapter 5 when G9a inhibition and MYCN protein and mRNA expression are evaluated in more detail.

To conclude, this chapter suggests that G9a is an oncogene in neuroblastoma, and is primarily involved in driving cell proliferation, but with the assistance of *MYCN*-amplification, G9a can also act as a survival factor to inhibit apoptotic cell death, thus share a synthetic lethal relationship. This chapter is also the first instance of a synthetic lethal relationship being suggested between G9a and MYCN in MYCN-overexpressing cells.

Chapter 4

G9a small molecule inhibitor UNC0638 induces apoptosis in *MYCN*-amplified neuroblastoma

4.1 Introduction

As shown in chapter 3, G9a is an oncoprotein in neuroblastoma whose depletion leads to decreased cell proliferation and an increase in apoptotic cell death suggesting G9a acts as a key survival factor. This suggests that G9a represents an important target for novel therapeutics, especially in high-risk poor prognostic *MYCN*-amplified neuroblastoma, therefore the need to determine the efficacy of current small molecule inhibitors specific to G9a is paramount. None of the G9a and neuroblastoma papers mentioned in chapter 1 assessed the effect of *MYCN*-amplification on G9a inhibition as the cell lines used were not categorised in to *MYCN*-amplified and non-*MYCN* amplified. It therefore seemed that this should be assessed in this chapter given the results thus far relating to *MYCN*-amplification and apoptotic cell death.

Most studies using G9a small molecule inhibitors utilise BIX-01294 despite it being the eldest generation G9a small molecule inhibitor available (75), which is most likely because of the potency. As mentioned previously BIX-01294 has been suggested to be toxic at concentrations above 4.1μM, therefore these studies are potentially unreliable. For example, Woo et al has recently suggested that BIX-01294 sensitises renal cancer cells to TRAIL-induced apoptosis (302), however the concentrations of BIX-01294 Woo et al use is above this 4.1μM threshold (10μM) suggesting this sensitising effect seen may actually be an effect of off-target toxicity.

To date there has been no study comparing small molecule G9a inhibitors, mentioned in chapter 1, to test their effectiveness in reducing cell viability in any cell line, let alone neuroblastoma. The previous chapter of this thesis demonstrated G9a as an oncoprotein in neuroblastoma and that depletion of G9a in *MYCN*-amplified neuroblastoma triggered caspase-dependent apoptotic cell death to occur. This highlights the potential for G9a inhibition as a therapeutic strategy in poor prognostic high-risk neuroblastoma. In this chapter, the aim is to evaluate the sensitivity of neuroblastoma cell lines to G9a small molecule inhibitors.

4.2 Assessing the potency of G9a small molecule inhibitors Kelly neuroblastoma cells

The small molecule inhibitors available at the start of this project were UNC0638, UNC0642, UNC0646, and A366. The potency of these compounds was evaluated in

this section for their potential as therapeutic agents for neuroblastoma, specifically looking at the efficacy in high-risk MYCN-overexpressing neuroblastoma.

The four compounds were tested by MTT based cell proliferation assay to determine the potency of these inhibitors in Kelly neuroblastoma cell line (Figure 4.1A). The potency was measured by determining an IC_{50} for each compound, the concentration of a drug required for 50% inhibition *in vitro.* UNC0638 and UNC0642 were more potent ($p<0.05$, n=3) than the other inhibitors as they were the only inhibitors to have an IC_{50} below 10µM. All the inhibitors exhibited a similar response up to 1.25µM, but Kelly cells are more sensitive to small molecule inhibitors UNC0638 and UNC0642 from 2.5µM onwards. There was over a two-fold difference between the IC_{50} values of UNC0638 and UNC0642, with UNC0638 having a very significantly lower IC_{50} ($p<0.01$, n=3), and the same difference again between UNC0642 and UNC0646. A366 did not register an IC_{50} at the highest tested concentration of 20 µM (Figure 4.1B).

Therefore, the two inhibitors UNC0638 and UNC0642 would be candidates for a small molecule inhibition screen on a wider panel of neuroblastoma and disease-free cell lines.

A

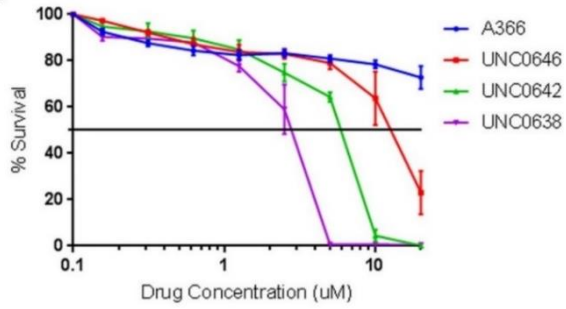

B

G9a Inhibitor	IC50 (uM) ±SEM
A366	>20
UNC0638	2.8± 0.2
UNC0642	5.9± 0.1
UNC0646	12.7± 2.4

Figure 4.1 – Compounds UNC0638 and UNC0642 are more effective at reducing cell viability in Kelly cells after 72 hours

***A** – Neuroblastoma Kelly were screened by MTT based cell proliferation assay to determine sensitivity to small molecule inhibitors A366, UNC0638, UNC0642, and UNC0646. These were treated in a serial dilution from 20 µM for 72 hours, n=3. 0.1µM is the labelled proxy for 0µM due to the log scale on the x-axis. Error bars show the SEM. **B** – Table of MTT assay based IC_{50} (µM) values determined for the Kelly treatments from **A.** Values are means ± standard error of the mean (SEM) of three independent experiments. (IC_{50} (µM): Half maximal inhibitory concentration).*

4.3 G9a small molecule inhibitors preferentially inhibits cell growth in *MYCN*-amplified neuroblastoma cell lines

Having previously demonstrated the activity of UNC0638 and UNC0642 in Kelly cells, these small molecule inhibitors were next tested in a wider panel of neuroblastoma cell lines. Eight neuroblastoma cell lines- five *MYCN*-amplified and three non-*MYCN*-amplified and two disease-free cell lines, RPE-1 and NF-TERT, were tested and their respective IC_{50}'s assessed similar to that described by Kollareddy et al (303). Therefore, the efficacy of UNC0638 and UNC0642 modulated inhibition needed to be established by determining the IC_{50} values.

All the neuroblastoma cell lines tested had a reduced viability upon treatment with UNC0638 (Figure 4.2A) and UNC0642 (Figure 4.2B). The small molecule inhibitors had no apparent effect on the disease-free cell lines with a percentage survival of roughly 100% at the highest concentration tested suggesting the drugs would not harm non-cancerous cells.

There was also an obvious genotype segregation attributable to *MYCN*-amplification as the five *MYCN*-amplified neuroblastoma cell lines (Kelly, NGP, LAN-1, BE(2)C, IMR32) were significantly more sensitive than the three non-*MYCN*-amplified (SHSY5Y, SKNAS, Gimen) when treated with UNC0638 ($p=0.0028$), and UNC0642 ($p=0.0006$). The disease-free cell lines were not added to this analysis. This is emphasised by graphs that show the average percentage survival based on all MNA and non-MNA cell lines treated with UNC0638 and UNC0642 inhibitors (Figure 4.2C and D). A clear trend is shown that MNA cell lines are more sensitive to G9a small molecule inhibitors than non-MNA.

The IC_{50}'s ranged from 2.8 to 16.5μM in the MNA cell lines treated with UNC0638 and 5.9 to 19.7μM with UNC0642 (Figure 4.2E). The non-MNA were all consistently over 20μM. The IC_{50} values are visualised (Figure 4.2F), with a suggested significant trend towards *MYCN*-amplification and a sensitivity towards G9a inhibition. Furthermore, this chart suggests that in UNC0642, there is a greater difference in the concentration of drug required to illicit an IC_{50} value between the two genotypes. Although only three non-*MYCN*-amplified cell lines were tested, this data highlights the exciting efficacy that G9a small molecule inhibitors have in therapeutically treating high-risk MNA neuroblastoma.

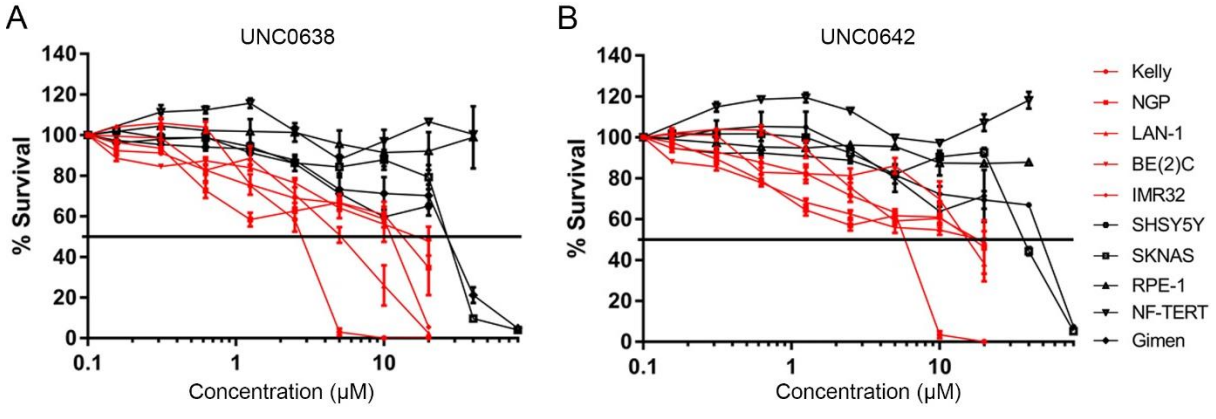

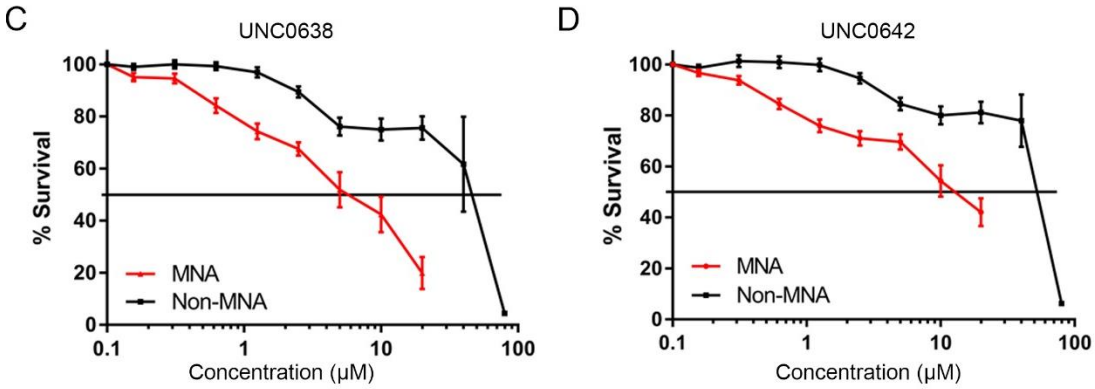

E

Cell line	UNC0638 ± SEM	UNC0642 ± SEM
Kelly	2.8 ± 0.2	5.9 ± 0.1
NGP	13.3 ± 3.7	16.4 ± 1.2
LAN-1	5.2 ± 1.0	16.5 ± 3.6
BE(2)C	16.5 ± 4.2	19.7 ± 4.0
IMR32	11.2 ± 0.2	18.0 ± 0.9
SHSY5Y	33.7 ± 0.6	52.8 ± 1.0
SKNAS	24.1 ± 0.3	48.3 ± 0.3
Gimen	29.1 ± 1.1	36.9 ± 1.3
RPE-1	> 20	> 20
NF-TERT	> 20	> 20

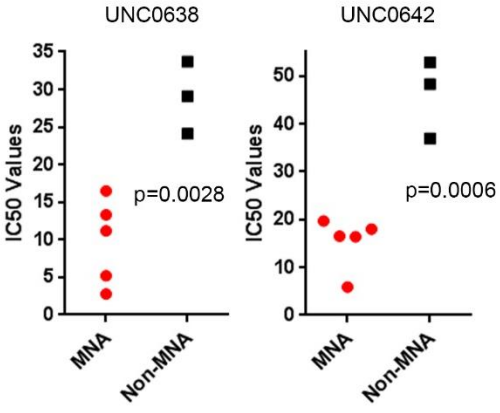

Figure 4.2 – Small molecular inhibitors UNC0638 and UNC0642 inhibition of neuroblastoma cells

A *– Eight neuroblastoma cell lines, five MYCN-amplified (red lines), three non-MYCN-amplified and two non-cancerous cell lines (black) were screened by MTT based cell proliferation assay to determine sensitivity to G9a inhibitors UNC0638 and 0.1 μM is a proxy for 0 μM due to the log scale on the x axis. MYCN-amplified neuroblastoma cell lines are more sensitive than the non-MYCN-amplified. Error bars show SEM.* ***B*** *– Same as A but using small molecule inhibitor UNC0642.* ***C*** *and* ***D*** *– Average values for all of the MNA and non-MNA cell line treatments from* ***A*** *and* ***B****. UNC0638 (****C****) and UNC0642 (****D****). Error bars show SEM.* ***E*** *– Table of MTT assay based* IC_{50} *(μM) values determined for the cell lines from* ***A*** *and* ***B****. Values are means ± SEM of three independent experiments. (*IC_{50} *(μM): Half maximal inhibitory concentration). Red colour is indicating MYCN-amplification.* ***F*** *– MTT assay based* IC_{50} *(μM) values for UNC0638 and UNC0642 from* ***A*** *and* ***B*** *are visualised as a scatter graph between MYCN- (MNA) and non-MYCN- amplified (Non- MNA) cell lines. Error bars show the SEM.*

4.4 *MYCN*-amplified S21N neuroblastoma is more sensitive to UNC0638 G9a small molecule inhibitor

Next, these drugs were evaluated in SHEP-21N cells to further assess the effect MYCN has on G9a small molecule inhibitor sensitivity.

The cells with the active *MYCN* state, MYCN ON, were significantly more sensitive to both UNC0638 and UNC0642 ($p<0.01$, $n=3$) than the MYCN OFF SHEP-21N cells (Figure 4.3A-B). The IC_{50} values for MYCN OFF (29.6µM and 34.8µM) were over 2.5-fold more than those for MYCN ON (8.9µM and 13.2µM) for UNC0638 AND UNC0642 respectively (Figure 4.3C).

This further supports that small molecule inhibitors of oncoprotein G9a has a therapeutic use in high-risk *MYCN*-amplified neuroblastoma because of a synthetic lethal relationship between G9a and MYCN.

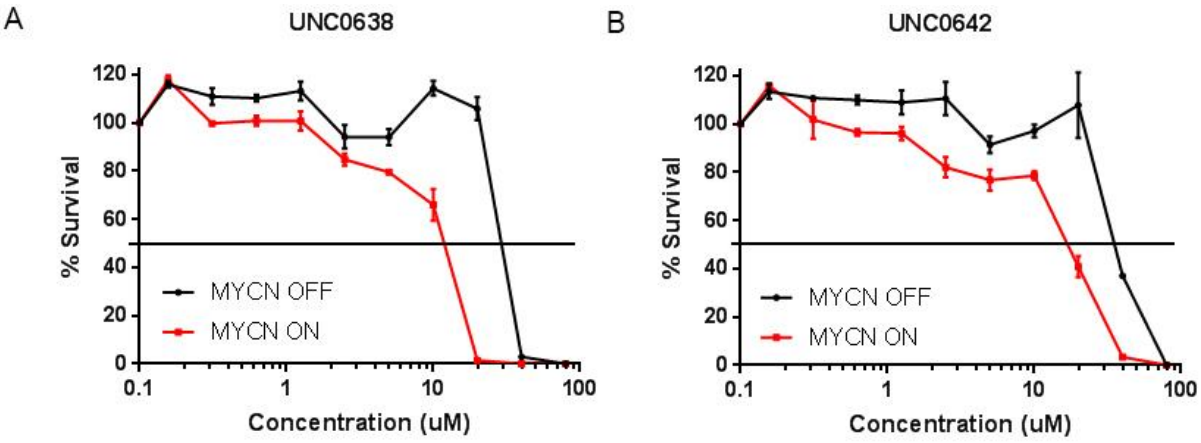

C

Cell line		Drug Concentration (µM)	
		UNC0638 ± SEM	UNC0642 ± SEM
S21N	MYCN OFF	29.6± 1.2	34.8± 0.5
	MYCN ON	8.9± 1.3	13.2± 2.1

Figure 4.3 – Small molecular inhibitors UNC0638 and UNC0642 inhibits cell growth preferentially in *MYCN*-amplified neuroblastoma cells
A *– Screening of MYCN-inducible cell line S21N with and without tetracycline using drug UNC0638. MYCN-amplified (MYCN ON) cell lines (red) are more sensitive than non-MYCN-amplified (MYCN OFF) cell lines (black). All MTT assays were carried out in three independent biological replicates each having three technical replicates (n=3, mean ± SEM) 0.1 µM is a proxy for 0 µM due to the log scale on the x axis. Error bars show the SEM.* ***B*** *– Screening of MYCN-inducible cell line S21N with and without tetracycline using drug UNC0642. Error bars show the SEM.* ***C*** *– Table showing the MTT assay based IC_{50} (µM) values for MYCN-amplified and non-MYCN-amplified S21N neuroblastoma. This is determined using an average of the IC_{50} (µM) values from three biological repeats.*

4.5 UNC0638 effectively represses proliferation in neuroblastoma

Since there is no plan to do *in vivo* work, UNC0638 was selected for further study as it was more potent than its UNC0642 counterpart so the poor PK properties of UNC0638 will not hinder this study.

To ascertain if the effects of G9a inhibition are akin to the proliferation repression seen from G9a depletion in neuroblastoma in chapter 3, neuroblastoma cells were treated with UNC0638 over 66 hours. Kelly cells were initially treated as these were the most sensitive cell line in the UNC0638 treatment screening (Figure 4.2C). Kelly cells were treated with one and two times the IC_{50} value discovered for UNC0638, 2.5µM and 5µM respectively.

Phenotypically, the treated Kelly cells look akin to the G9a depleted cells with more rounded and dead cells (Figure 4.4A). This appears to be concentration dependent as there are more dead cells at the higher concentration. Moreover, there are less cells in the two treated cells relative to the DMSO control suggesting a reduction in cell proliferation as observed previously. This is confirmed by the live cell imaging system IncuCyte Zoom which measured the percentage phase confluence of these cells (Figure 4.4B). This shows a significant reduction in the normalised phase confluence in the two treated cell lines in a dose dependent manner, with 2.5 µM significantly (*$p \leq 0.05$) different after 32 hours, and 5 µM significantly (*$p \leq 0.05$) and very significantly (***$p \leq 0.01$) different from 14 hours and 24 hours respectively. *MYCN*-amplified IMR32 cells were also treated with 5µM UNC0638 for 72 hours, to see if this effect was seen in other *MYCN*-amplified cell lines. These cells also reduced in proliferation with less cells seen phenotypically (Figure 4.5A). Again, they are also more rounded indicative of cell death as well as the neurites being shorter and less defined. In addition, the normalised phase confluence graph confirms a very significant ($p \leq 0.01$) reduction in cell growth after 24 hours (Figure 4.5B).

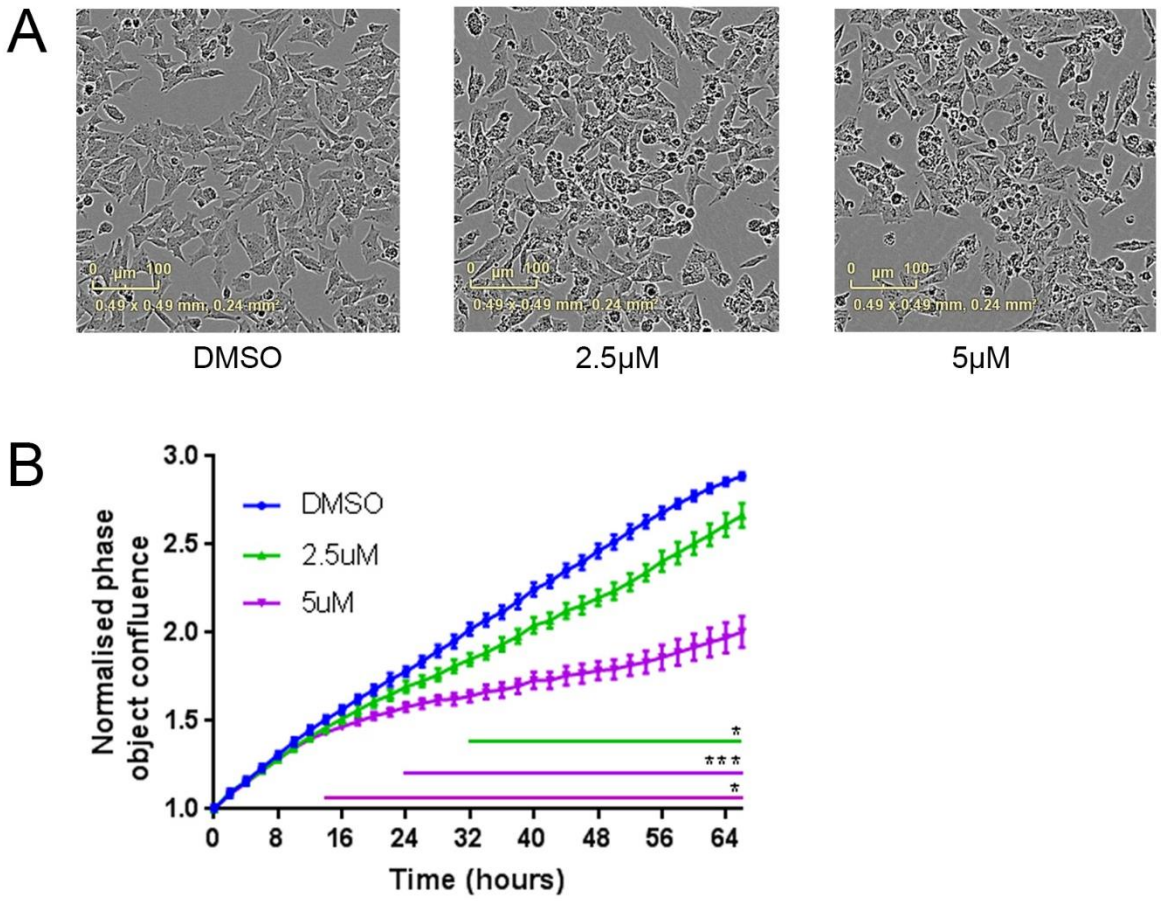

Figure 4.4 – G9a inhibitor UNC0638 inhibits proliferation in Kelly
A *– Photomicrographs at 10x objective magnification of Kelly cells after 66-hour treatment with negative control DMSO, 2.5µM, and 5µM G9a small molecule inhibitor UNC0638.* ***B*** *– Graph depicting normalised phase object confluence of the UNC0638 treated Kelly cells from* ***A****, relative to the DMSO control. Significance was evaluated at each time point by using T tests, * (p<0.05) and *** (p<0.01). The colours refer to the colours of the treatments. Error bars show the SEM.*

As G9a knockdowns in tested non-*MYCN*-amplified cell lines suggested a decrease in cell proliferation, Gimen and SHSY5Y cells were treated with 10µM UNC0638 for 72 hours to assess if this still occurred. When the Gimen treatments were harvested, trypan blue inclusion assay was performed to count the live cells. This live cell count was used as a proxy for cell proliferation as if there were more cells it would suggest that they are proliferating at a greater rate. The Gimen cells showed a significant reduction (* p<0.05, n=2) in live cell count after UNC0638 treatment, with over a 1.5-fold reduction (Figure 4.6A).

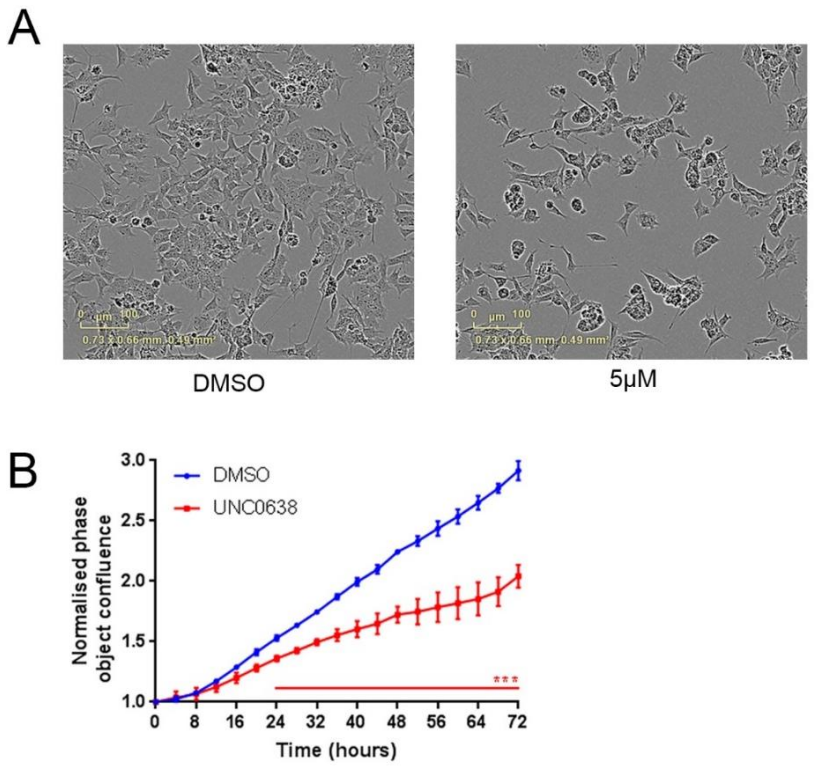

Figure 4.5 – G9a inhibitor UNC0638 inhibits proliferation in IMR32 cells
A *– Photomicrographs at 10x objective magnification of IMR32 cells after 72-hour treatment with negative control DMSO and 5μM G9a small molecule inhibitor UNC0638.* ***B*** *– Graph depicting normalised phase object confluence of the UNC0638 treated IMR32 cells from* ***A****, relative to the DMSO control. Significance was evaluated at each time point by using T tests *** (p<0.01). Error bars show the SEM.*

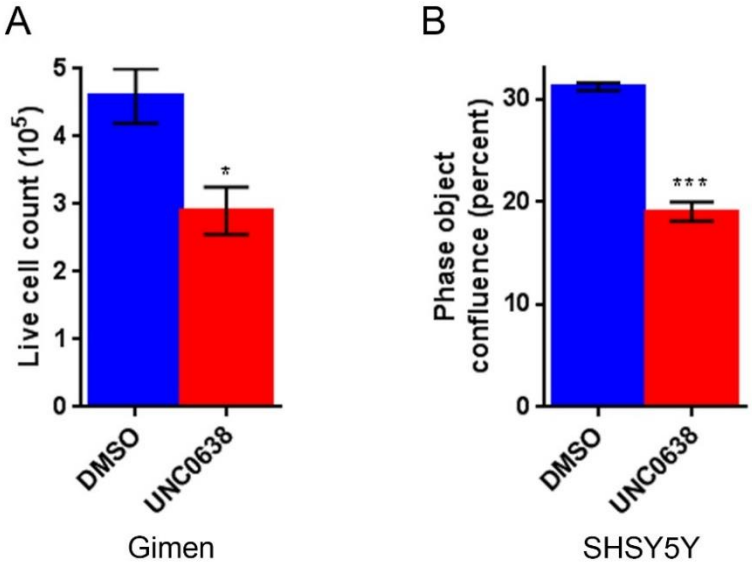

Figure 4.6 – UNC0638 inhibits proliferation in Gimen and SHSY5Y cells
A *– Floating and adherent cells from Gimen cells treated with negative control, DMSO and 10μM UNC0638 were harvested and counted by trypan blue inclusion assay. The number of live cells were then counted. This is used as a proxy for cell growth at the 72-hour end point. Significant changes are indicated by asterisks (* p<0.05, n=2).* ***B*** *– SHSY5Y treated cells were measured for percentage phase object confluence in the live cell imaging system IncuCyte Zoom at the 72-hour end point. Significant changes are indicated by asterisks (*** p<0.01, n=3). Error bars show the SEM.*

SHSY5Y cells were recorded by the IncuCyte Zoom after the 72-hour treatment to get a snapshot of the percent phase object confluence at the 72-hour end point. Again, this is used as a proxy for cell proliferation. There was over a third difference in the reduction in percentage phase object confluence after treatment, which was very significant (*** $p<0.01$, $n=3$) (Figure 4.6B). The percentage cell death from these trypan blue inclusion assays are shown further on in Figure 4.8.

All together this suggests that G9a inhibition by small molecule inhibitor UNC0638 elicits a reduction in cell proliferation in both genotypes of *MYCN*-amplified neuroblastoma cell lines, similar to that seen with G9a depletion.

4.6 UNC0638 induces apoptosis in *MYCN*-amplified neuroblastoma

As there was apoptosis in only the *MYCN*-amplified neuroblastoma cell lines depleted of G9a, and since there is a similar effect on proliferation reduction between G9a depletion and UNC0638 small molecule inhibition, it is necessary to determine if this is also the case with cell death. An extensive cell panel assessing potential apoptotic cell death from G9a small molecule inhibitors has not been performed before. UNC0638 was added to eight neuroblastoma cell lines to evaluate the apoptosis inducing potential of G9a inhibition.

Since the photomicrographs from figure 4.4 A and C showed an increase in rounded and floating cells indicative of cell death in the treated cells relative to the DMSO control, DRAQ7 was added to Kelly from figure 4.4 A and SKNAS treatments to visualise and quantify the amount of cell death.

In the Kelly cells treated with 2.5µM UNC0638, over the 66-hour treatment, there was an increase in the normalised red object count relative to the DMSO control. This was significant ($p<0.05$, $n=3$) from 18 hours after treatment was added and very significant ($p<0.005$, $n=3$) from 24 to 58 hours (Figure 4.7A). The reduction in significance during the final eight hours can be attributed to the cells being seeded too high so there were prematurely becoming confluent so there was probably an increase in cell death attributed to this. The floating and attached cells were harvested and immunoblotted for apoptosis indicator cPARP. The increase in apoptotic cell death was confirmed as there was a marked increase in cPARP between the treatment and the DMSO control (Figure 4.6B).

The SKNAS cells however showed no significant change in the normalised red count after 73.5 hours of treatment with 10µM UNC0638 (Figure 4.7C). It did suggest there was more basal cell death in the SKNAS cells though as both the DMSO and UNC0638 treatments were higher than in the Kelly cells. This was not G9a inhibition associated apoptosis however as an immunoblot of the harvest cell lysates showed no change in cPARP in the treatment relative to the control (Figure 4.7D).

Next, IMR32, Gimen, and SHSY5Y cells were treated with 5µM, 10µM, and 10µM UNC0638 respectively for 72 hours. These treatments were then harvested, and trypan blue inclusion assay was performed to determine a percentage cell death count. The IMR32 cells showed a significant increase ($p<0.05$, $n=3$) in percentage cell death with the UNC0638 treatment (Figure 4.8A). This was confirmed to be apoptosis after immunoblotting for cPARP, which increased after treatment.

There were no significant changes (ns) in the percentage cell death in Gimen, (Figure 4.8B) and SHSY5Y (Figure 4.8C) neuroblastoma when treated with UNC0638 relative to the DMSO control. There was also no change in cPARP protein in immunoblots of the harvest lysate indicating no apoptotic cell death.

Immunoblots of lysates from harvested LAN-1, BE2C, and NGP neuroblastoma cell lines all treated with 10µM UNC0638 revealed that there was no change in cPARP in the LAN-1 and BE2C cells (Figure 4.8D) despite being *MYCN*-amplified. NGP however did increase in cPARP. This suggests that, in LAN-1 and BE2C at least, there may be an extra layer of regulation on apoptosis that is not present in the other *MYCN*-amplified cell lines tested.

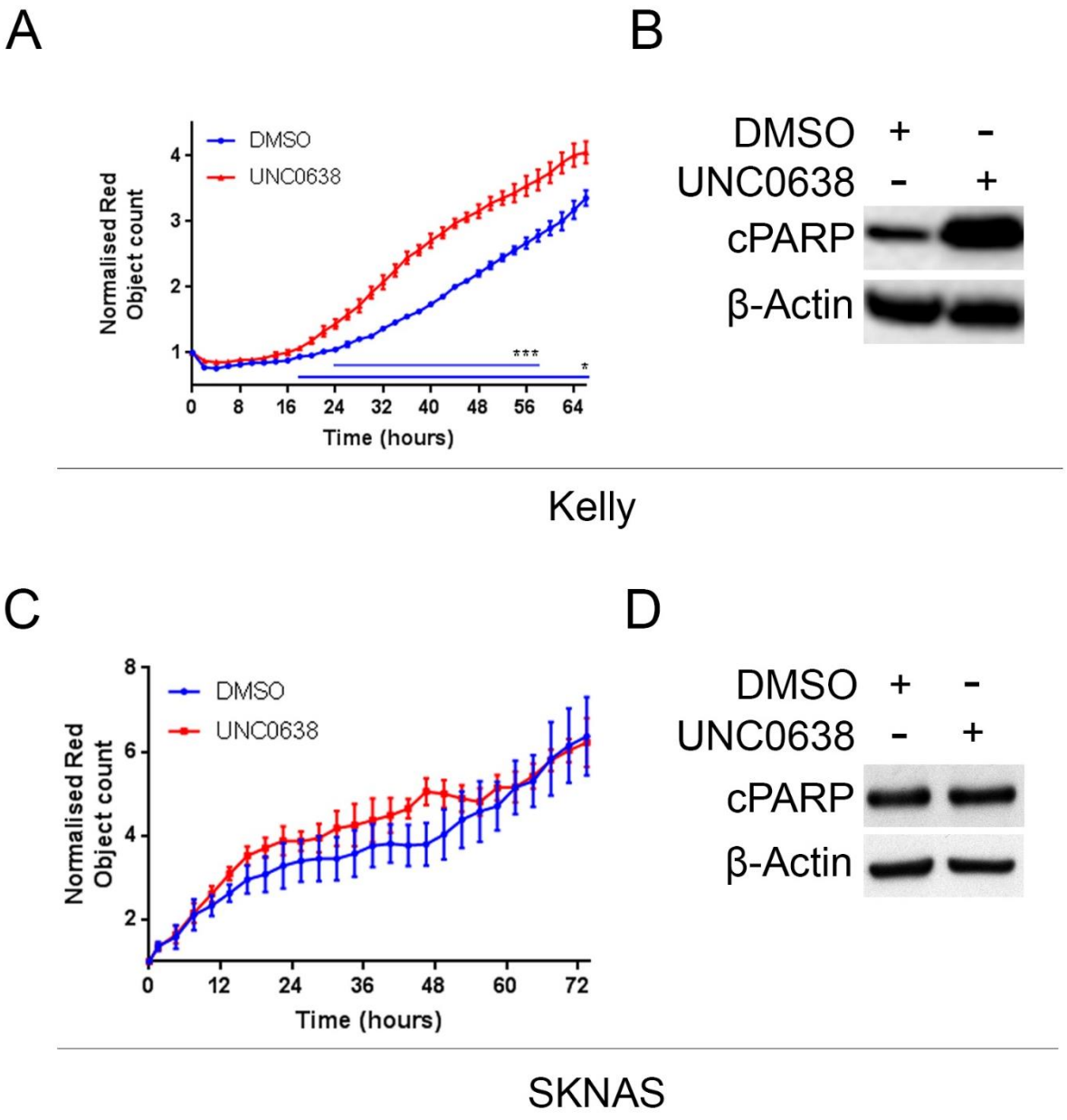

Figure 4.7 – UNC0638 induces apoptosis in Kelly cells but not in SKNAS

A- *Normalised red object count shows that G9a inhibition in Kelly cells using 2.5μM UNC0638 leads to apoptotic cell death due to a significant increase in the red object count, a proxy for cell death, after 18 hours (* p<0.05, *** p<0.01 n=2) between DMSO and UNC0638. Error bars show the SEM.* ***B*** *– Immunoblot of floating and adherent cells of treatments from* ***A****. cPARP is a marker for apoptosis and cell death. β-Actin is used as loading control.* ***C*** *– Normalised red object counts show G9a inhibition in SKNAS cells using 10μM UNC0638 does induce apoptotic cell death. Error bars show the SEM.* ***D*** *– Immunoblot of floating and adherent cells of treatments from* ***C****. cPARP is a marker for apoptosis and cell death. β-Actin is used as loading control.*

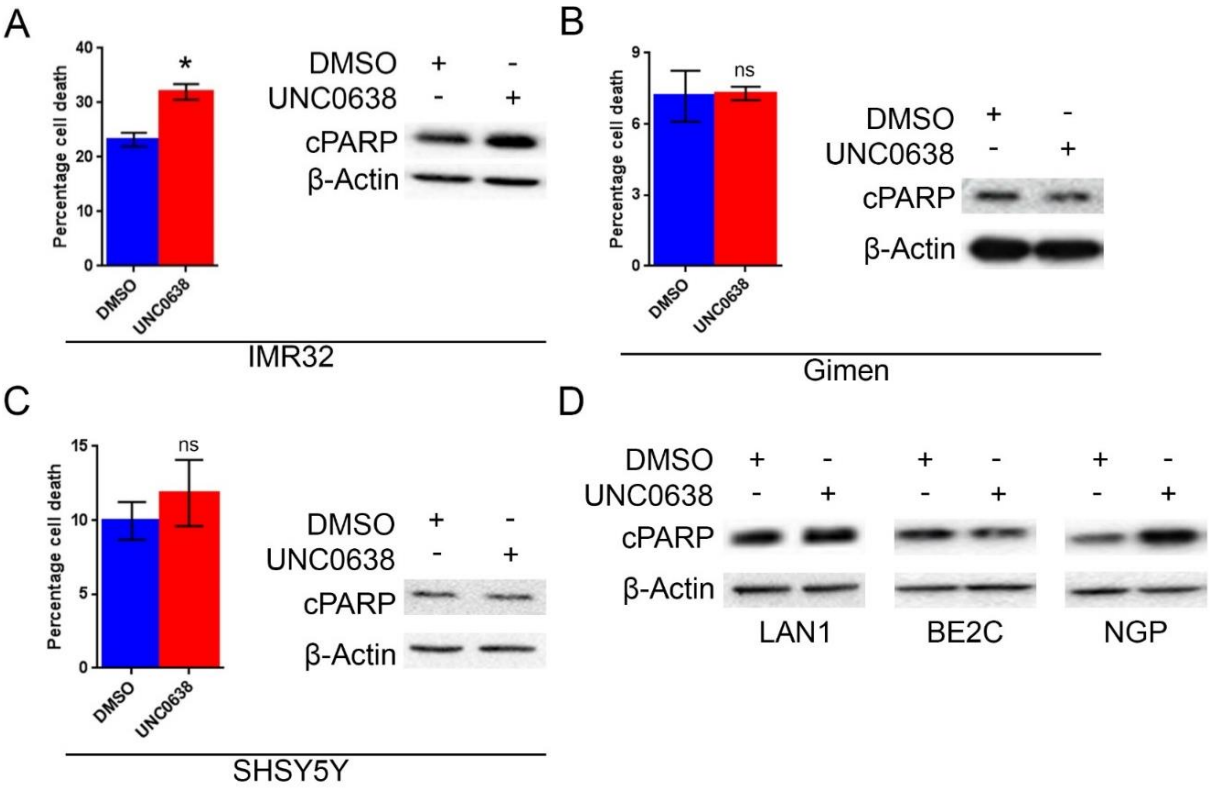

Figure 4.8 – Apoptotic cell death differs between *MYCN*-amplified genotypes
A *– Trypan blue inclusion assay of floating and adherent MYCN-amplified IMR32 cells 72 hours after DMSO and 5μM UNC0638 treatments. This is used to measure the percentage cell death between the two treatments. Asterisk denotes significance (p<0.05, n=3). Error bars show the SEM. Immunoblot of floating and adherent cells of treatments. cPARP is a marker for apoptosis and cell death. β-Actin is used as loading control.* ***B*** *– Trypan blue inclusion assay of floating and adherent non-MYCN-amplified Gimen cells 72 hours after DMSO and 10μM UNC0638 treatments. This is used to measure the percentage cell death between the two treatments. Ns denotes no significance (p>0.05, n=3). Error bars show the SEM. Immunoblot of floating and adherent cells of treatments. cPARP is a marker for apoptosis and cell death. β-Actin is used as loading control.* ***C*** *– Trypan blue inclusion assay of floating and adherent non-MYCN-amplified SHSY5Y cells 72 hours after DMSO and 10μM UNC0638 treatments. This is used to measure the percentage cell death between the two treatments. Ns denotes no significance (p>0.05, n=3). Error bars show the SEM. Immunoblot of floating and adherent cells of treatments. cPARP is a marker for apoptosis and cell death. β-Actin is used as loading control.* ***D*** *– Immunoblot of floating and adherent cells of MYCN-amplified LAN-1, BE2C, and NGP treatments. cPARP is a marker for apoptosis and cell death. β-Actin is used as loading control.*

4.7 G9a inhibition in S21N cells shows evidence of a synthetic lethal relationship between G9a and MYCN

As there was some discrepancy as to whether G9a inhibition leads to apoptosis in *MYCN*-amplified neuroblastoma (Figure 4.8D) G9a inhibitor UNC0638 was tested in MYCN inducible S21N cell line. Cell proliferation was significantly (*** $p \leq 0.01$) reduced in both MYCN ON and OFF variants, (Figure 4.9A), after 46 hours of 5μM UNC0638 treatment. When looking at the end timepoint specifically, the difference in the normalised object confluence is stark, (Figure 4.9B). Whilst the MYCN OFF version is still significantly (*** $p<0.05$, $n=3$) reduced in proliferation, the MYCN ON version has nearly halved. This suggests that G9a inhibition related reduction in cell proliferation is much more prominent in MYCN-amplified cell lines which fits with the trend shown throughout this chapter.

DRAQ7 was also added to these treatments to assess apoptotic cell death in these MYCN variants. This output was measured by the IncuCyte imaging system as red object count. There was no significant change in the normalised red object count in the MYCN OFF S21N cells, yet there was a drastically significant increase in cell death after 22 hours in the MYCN ON variant (*** $p<0.01$) (Figure 4.9C). This shows that whilst there is no cell death in the MYCN OFF cells, there is apoptosis in the MYCN ON cells suggesting a synthetic lethal relationship between MYCN and G9a. This is confirmed by immunoblot of these samples (Figure 4.9D) which shows an increase in cPARP in the cells treated with UNC0638 with MYCN ON, but not in cells with MYCN OFF. As with the S21N cells depleted of G9a (Figure 3.7B) there is also a decrease in MYCN protein in the MYCN ON cells when treated with UNC0638 which suggests that G9a histone methyltransferase activity may regulate MYCN protein at a post-translational level.

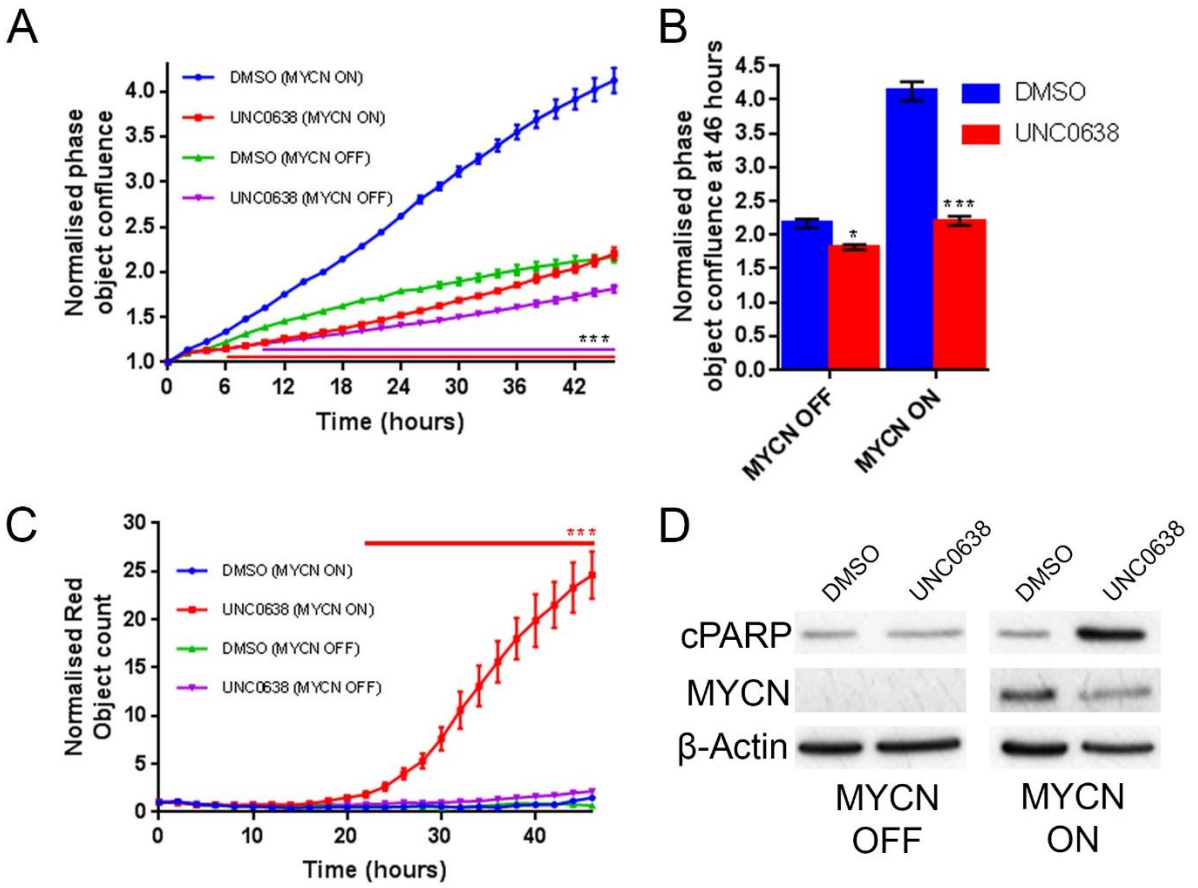

Figure 4.9 – G9a inhibition preferentially kills *MYCN*-amplified S21N neuroblastoma cells

A *– Graph depicting normalised phase object confluence of the S21N cells with MYCN ON and MYCN OFF treated with DMSO and 2.5μM UNC0638 for 46 hours. Significance was evaluated at each time point by using T tests *** (p<0.01). Red (MYCN ON) and purple (MYCN OFF) lines are relative the respective DMSO treatments. Error bars show the SEM.* ***B*** *– Chart of normalised phase object confluence at the end time point of 46 hours of the cells from* ***A****. Asterisks denote significance (n= 3, * p<0.05, *** p<0.01). Error bars show the SEM.* ***C*** *– Normalised red object counts for the treatments from* ***A****. Significance was evaluated at each time point by using T tests *** (p<0.01). Error bars show the SEM.* ***D*** *– Immunoblot of S21N cells with MYCN OFF and MYCN ON from* ***A*** *probing for cPARP and MYCN. β-Actin is used as a loading control.*

4.8 Discussion

In this chapter, a panel of four current small molecule inhibitors of G9a were tested for potency in a variety of neuroblastoma cell lines. Here it is shown that, despite all being labelled as potent and selective inhibitors, there is a difference in effectiveness between the drugs on the same neuroblastoma cell line.

This chapter also shows that G9a inhibition by UNC0638 induces apoptotic cell death, but only in MYCN-amplified neuroblastoma. This goes someway to corroborating current literature in neuroblastoma as only one paper thus far shows G9a inhibition via BIX-01294 leads to apoptotic cell death in neuroblastoma through an increase in caspase 8/caspase 3 activity (260). However, Lu et al only look at one cell line, LA1-55n which is derived from LA1-5s (a clonal subline of LAN-1) so is *MYCN*-amplified. This suggests that very little has been evaluated on G9a mediated apoptosis in neuroblastoma.

G9a in the context of synthetic lethality has not been well characterised with only one study shown to utilise G9a inhibitors as a therapeutic agent in this manner. It has been suggested that immortalised breast luminal epithelial cell line MCF10A with an extended C-terminus frameshift mutant of transcription factor GATA3 (GATA3-ext) are more sensitive to G9a inhibition associated apoptosis via BIX-01294 and UNC0638 than cells with wild type GATA3 (304). Mair et al don't elaborate on a mechanism for this however. The data shown in this study suggests another novel synthetic lethal relationship for G9a between it and MYCN. This exciting development shows new and novel research for high-risk neuroblastoma therapeutics.

G9a inhibitors have been shown to induce apoptosis in other cancer cell lines too. There has been shown to be an increase in caspase activation and cPARP 24 hours after BIX-01294 treatment in human bladder cancer (305). Cui et al argues that BIX-01294 treatment activates endoplasmic reticulum (ER) stress which has already been shown to induce apoptosis after long-term stress (306). This ER stress could also be an off-target effect of the BIX-01294 drug, however the identification of early responding genes after G9a depletion in bladder carcinoma and lung adenocarcinoma suggests a more reliable dataset. Furthermore, microarray analysis of was used to identify downstream targets of G9a. A known positive regulator of apoptosis in cancer cells, E3 ubiquitin ligase *SIAH1*, was found to be upregulated following G9a depletion

(149, 307). Cho et al show in multiple lung adenocarcinoma, lung squamous cell carcinoma, small cell lung cancer, and bladder cancer cell lines that G9a binds to the promoter region of *SIAH1* and represses it through H3K9 di-methylation thus helping to repress apoptosis.

G9a can also mediate tumour metastasis with G9a expression shown to correlate with the invasive potential of lung adenocarcinoma; increased expression typifies increased invasiveness (143). Furthermore, results from Chen et al show the histone methyltransferase activity of G9a is necessary for the invasive phenotype of lung cancer cells. G9a directly downregulates epithelial cell adhesion molecules (Ep-CAM) by recruiting a complex of repressor proteins to the *Ep-CAM* promoter (143). G9a knockdown was able to demethylate the promoter and increase *Ep-CAM* expression. They did not use any small molecule inhibitors of G9a in this study, but abolition of G9a's catalytic activity impedes invasiveness suggesting small molecule inhibitors could also upregulate *Ep-CAM* expression to reduce this invasive phenotype.

An issue with these inhibitors are that they inhibit the SET domains of both G9a and GLP since they share approximately 80% sequence identity (75, 165), therefore it is difficult to determine if there is a response to inhibiting one of these proteins separately since they possess distinct physiological and pathophysiological functions (308). Whilst GLP and G9a have similar non-histone targets such as reptin (132) and sirtuin 1 (309), they also have different non-methylation targets and can recognise different substrates through their ankyrin repeat domains. For example, GLP ankyrin repeats act as an effector domain for K310 mono-methylated transcription factor RelA to repress NF-κB signalling by binding at target genes to generate a silent chromatin state (310). G9a is shown to not recognise this site. Recently, a GLP specific compound MS012 has been manufactured that has over a 140-fold selectivity for GLP over G9a (311). Alongside GLP depletion, this inhibitor could be used to further define the differing spheres of influence G9a and GLP have over targets and gene regulation.

This all suggests the importance of G9a in being able to regulate cellular processes like apoptosis in multiple cancer cell lines and therefore suggests why G9a should be a therapeutic target.

Chapter 5

G9a regulates novel targets including BOK and MYCN protein

5.1 Introduction

As a lysine methyltransferase, G9a has been associated with various cellular processes. These involve differentiation (119), proliferation (312, 313), and senescence (314). As discussed previously, G9a can act as a transcriptional regulator. G9a deposits methylation marks to target lysine residues which results in mono-/di-methylation marks on H3K9 (113). These deposited marks are associated with active and repressed gene transcription respectively. G9a also regulates gene expression through methylation of non-histone targets; G9a automethylates its N-terminus to recruit binding partner HP1. This either activates gene transcription such as a subset of glucocorticoid genes (315), or represses gene transcription by HP1 recruitment of other transcriptional repressors like HDAC1 and DNMT1 (129). G9a also methylates transcription factor C/EBP β to repress myeloid gene activation (139). This all suggests that G9a can switch between being a transcriptional activator or a repressor depending on either its methylation target; histone and non-histone, and the degree of methylation, or its binding partner via the ankyrin repeat domain.

MYCN is a transcription factor that has many target genes related to many functions within the cell such as cell cycle and apoptosis. These targets are either be expressed or repressed by MYCN activity. *MYCN*-amplification occurs in about 50% high-risk poor prognosis neuroblastoma (211), and high MYCN protein is also closely associated with poor prognosis (297). *MYCN*-amplification has been suggested to correlate with cells failing to arrest correctly in G1 phase (316), due to the upregulation of MYCN target cyclin D2 (317). This suggests that *MYCN*-amplification is causing an increase in the MYCN upregulated targets and a decrease in repressed targets to help drive tumourigenesis. Therefore, being able to manipulate MYCN protein stability would help to reverse this.

MYCN protein stability can be regulated by various post-translational modifications. For example, a cascade of phosphorylation events at specific residues consequently leads to the ubiquitination and proteasomal degradation of MYCN protein (227). Moreover, it has been suggested that di-methylation by arginine methyltransferase PRMT5 can increase MYCN protein stability (229). These both suggest how post-translational modifications can affect MYCN stability to either increase or decrease MYCN protein levels.

Previous unpublished RNA sequencing (RNAseq) data from Dr. Malik and Dr. Szemes assessed the impact on gene expression between resistant non-*MYCN*-amplified SKNAS cells and sensitive *MYCN*-amplified LAN-1 cells treated with BIX-01294. These identified changes in gene expression between the *MYCN*-amplification statuses, as well genes that were being up- and downregulated by G9a. Some of these genes have not been associated with G9a regulation before and thus will be explored within this chapter.

In addition, in this chapter, it is shown that G9a can regulate MYCN oncoprotein in *MYCN*-amplified neuroblastoma and can therefore repress and re-express downstream MYCN targets. One of these targets is suggested to be little known pro-apoptotic factor BOK which is suggested here to have a key role in regulating apoptosis in G9a inhibited MYCN-amplified neuroblastoma. This therefore emphasises the importance of G9a as a novel target in high-risk neuroblastoma therapeutics.

5.2 Discovery of novel repressed G9a targets

A selection of genes from the RNAseq data set which had the highest fold change in expression are shown in Figure 5.1A. These suggest that whilst they are all upregulated in LAN-1 cells, *AMHR2* (anti-Mullerian hormone receptor II) and *BOK* (BCL-2 related ovarian killer) show no change and downregulation respectively in the resistant SKNAS cells suggesting that MYCN may help to regulate these genes. These genes have not been shown to be regulated by G9a in published literature to date. Furthermore, using the SEQC-498 database from the Genomic Analysis and Visual Platform R2, Kaplan-Meier curves show that high expression of these genes are markers for good prognosis (p values indicated in figure 5.3A).

Since BIX-01294 is not a reliable small molecular inhibitor, these genes were re-probed in neuroblastoma cell lines, two sensitive cell lines Kelly and LAN-1, and two resistant SKNAS and GIMEN, treated with UNC0638 for 24 hours (Figure 5.1B) to determine if these are true G9a repressed targets as suggested by the RNAseq data. First *FABP3*, *BOK*, and *AMHR2* were assessed (Figure 5.1 B-D). *FABP3* (Fatty acid binding proteins 3) is upregulated in all cell lines with *MYCN*-amplified Kelly and LAN-1 having a drastically increased relative change, around 60-fold, comparative to the non-*MYCN*-amplified despite similar basal levels. *BOK* was very significantly

upregulated in Kelly and LAN-1 cells, whereas in SKNAS and Gimen cells there is no significant fold change. *AMHR2* was significantly upregulated in with *MYCN*-amplified cell lines Kelly and LAN-1, with around a 10-fold increase in Kelly. There was no significant change in the non-*MYCN*-amplified cells.

Aldo-keto reductase family *AKR1C1*, *AKR1C2*, and *AKR1C3* were all significantly upregulated in Kelly, LAN-1, and SKNAS cells but there was no increase in Gimen cells (Figure 5.1 E-G). *FLCN* (folliculin) is very significantly up regulated in Kelly, LAN-1, but there is no significant change in SKNAS cells and a significant downregulation in Gimen cells (Figure 5.1 F). *CCBE1* (Collagen and calcium-binding epidermal growth factor domains 1) is very significantly increased in all four cell lines suggesting it as a repressed target of G9a histone methyltransferase domain (Figure 5.1 I).

This data suggests that *CCBE1* and *FABP3* are genes normally repressed by G9a histone methyltransferase activity in neuroblastoma, with *FABP3* strongly increased in *MYCN*-amplified cell lines. The AKR1C1-3 family of genes were upregulated in three of the four cell lines with no change in Gimen cells suggesting these cells have an additional layer of regulation. *BOK, FLCN* and *AMHR2* relative expression is significantly increased in *MYCN*-amplified Kelly and LAN-1 and there is no change in the non-MYCN-amplified SKNAS and Gimen suggesting these changes on MYCN dependent.

A

RNA Seq data	Fold change in gene expression following BIX treatment (log2)		Expression for good prognosis	SEQC- 498 p value	
G9a gene targets	LAN1	SKNAS		Raw	Bonferroni
AMHR2	10.02	1.02	High	2.20E-08	1.10E-05
FABP3	12.76	3.45	High	1.00E-24	5.00E-22
CCBE1	3.22	2.26	High	3.70E-33	1.80E-30
FLCN	1.67	1.74	High	1.10E-25	5.20E-23
CLU	1.72	1.62	High	3.70E-17	1.80E-14
AKR1C1	2.61	4.26	High	1.50E-28	7.30E-26
AKR1C2	3.88	9.74	High	1.90E-23	9.10E-21
AKR1C3	5.13	2.03	High	7.80E-10	3.80E-07
BOK	2.53	0.75	High	1.40E-21	6.80E-19

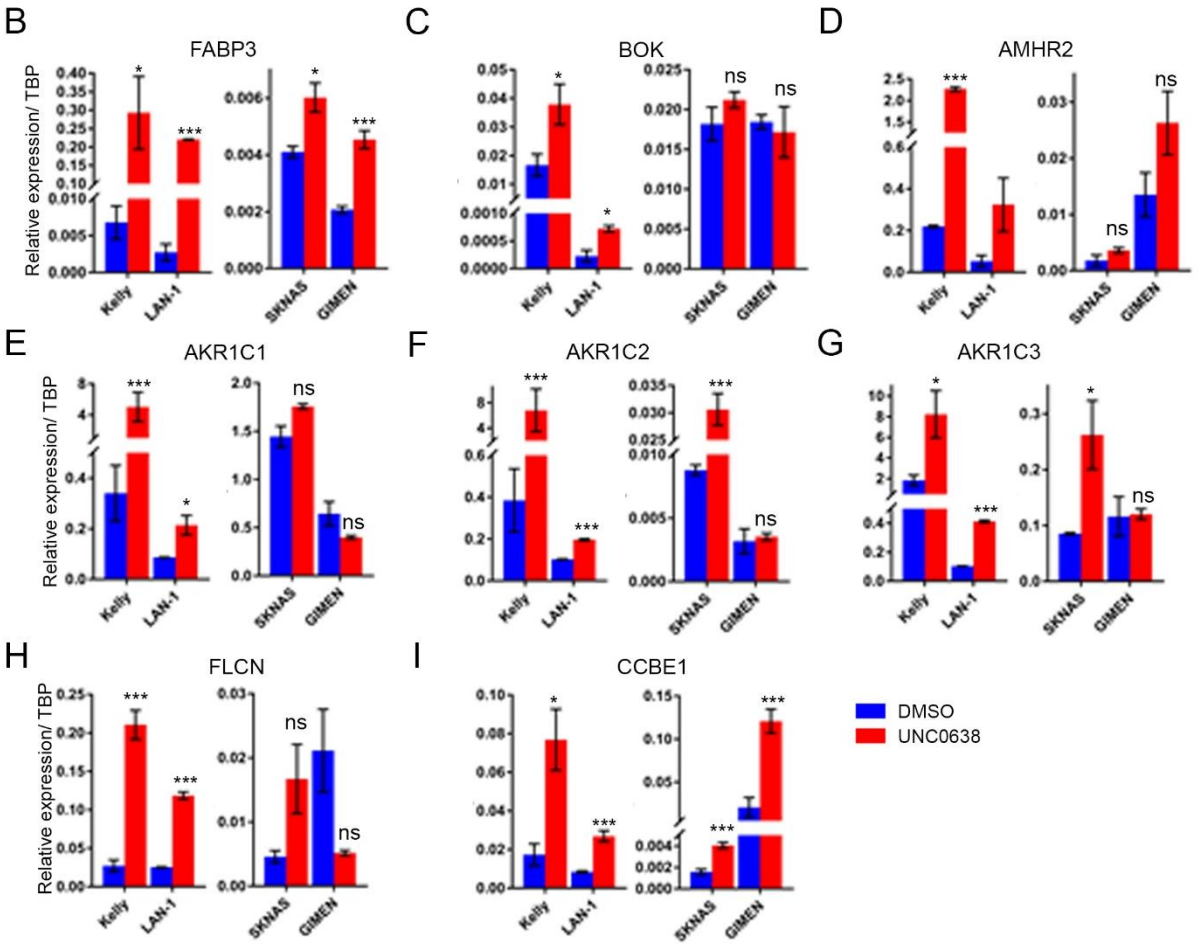

Figure 5.1 – G9a inhibition regulates novel gene targets

A *– Table showing eight genes that were of interest following RNA sequencing data from LAN-1 and SKNAS neuroblastoma cells treated with BIX-01294 previously produced by members of the laboratory. This assesses the fold change in gene expression (log_2), if high expression is good for prognosis, and the respective p values from the SEQC-498 database; both raw and Bonferroni.* ***B-I*** *– qRT-PCR of these eight genes (names labelled above each chart) in Kelly, LAN-1, SKNAS, and Gimen neuroblastoma cells treated with 5μM (Kelly) and 10μM (LAN-1, SKNAS, Gimen) for 24 hours cells. Expression is relative to TBP. Significance is measured by unpaired T test relative to DMSO control (ns p>0.05, * p<0.05, *** p<0.01, n=3). Error bars show the SEM.*

5.3 Separate MYCN and G9a depletion increases *BOK* expression

From these genes of interest, *BOK* was evaluated in further detail as it is a pro-apoptotic factor, and its increase in expression solely in *MYCN*-amplified Kelly and LAN-1 may suggest why apoptotic cell death has solely occurred in *MYCN*-amplified cell lines thus far.

To assess if BOK is regulated by G9a and MYCN, both G9a and MYCN were individually depleted in Kelly cells. Immunoblot of these transfections show effective knockdowns (Figure 5.2A), with both leading to an increase in BOK protein alongside an increase in cPARP. MYCN has been shown to regulate apoptosis by repressing pro-apoptotic genes such as p53 and CASP8 to help the cancer survive (184, 232, 233) so the increase in cPARP makes sense. Furthermore, there is a consistent and significant increase in relative fold expression of *BOK* of around 1.5 times in effective G9a and MYCN knockdowns, Figure 5.2B and C respectively.

Next, G9a was depleted in non-*MYCN*-amplified SKNAS as it was hypothesised that there would be no change in BOK protein since A) there was no change in *BOK* transcript after UNC0638 treatment (Figure 5.1B), and B) there was no cPARP increase in SKNAS cells previously depleted of G9a, (Figure 3.6). Immunoblot of SKNAS cells treated with siG9a showed no change in BOK or cPARP after effective knockdown (Figure 5.3A). Furthermore, there is no significant change in relative fold *BOK* expression after effective G9a knockdown (Figure 5.3B).

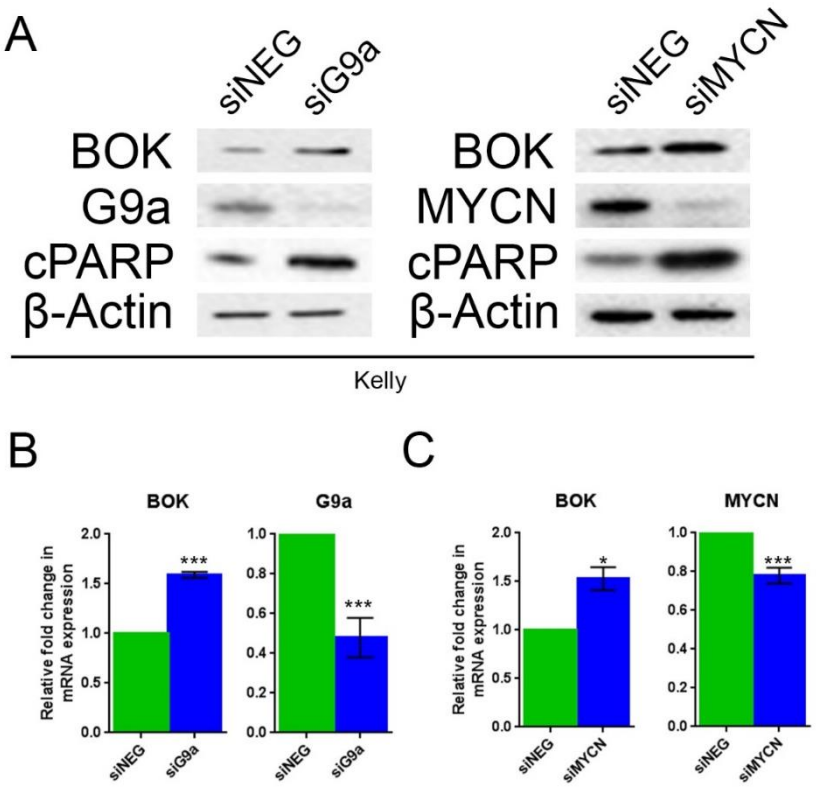

Figure 5.2 – G9a and MYCN depletion increase BOK expression
A *– Kelly cells depleted of G9a and MYCN. Immunoblot shows effective depletion of G9a and MYCN, alongside increase in cPARP and BOK in both transfections. β-Actin is used as a loading control.* ***B*** *– qRT-PCR of BOK and G9a genes in Kelly transfected with siG9a. Fold change is relative to TBP. Significance is measured by unpaired T test (*** p<0.01, n=3).*
C *– qRT-PCR of BOK and MYCN genes in Kelly transfected with siMYCN. Fold change is relative to TBP. Significance is measured by unpaired T test (* p<0.05, *** p<0.01, n=3). Error bars show the SEM.*

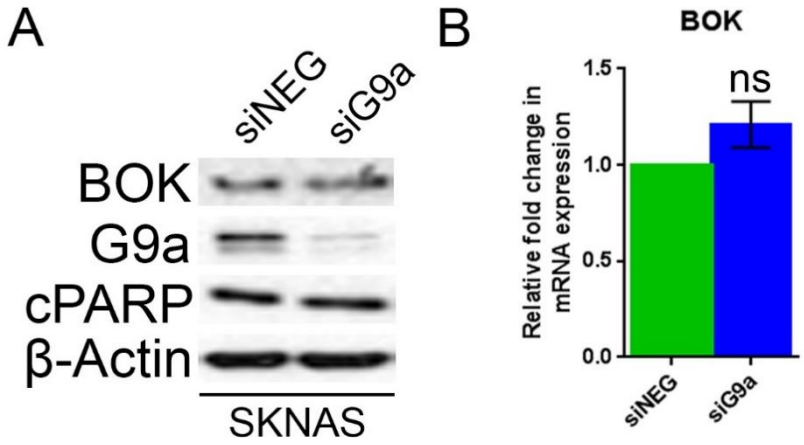

Figure 5.3 – G9a depletion does not change BOK expression in SKNAS
A *– SKNAS cells depleted of G9a. Immunoblot shows effective depletion of G9a increase in cPARP and BOK in both transfections. β-Actin is used as a loading control.* ***B*** *– qRT-PCR of BOK and G9a genes in Kelly transfected with siG9a. Fold change is relative to TBP. Significance is measured by unpaired T test (ns p>0.05, n=3). Error bars show the SEM.*

5.4 G9a inhibition increases BOK protein in tested *MYCN*-amplified cell lines

Next, it was assessed if treatment with UNC0638 would illicit the same increase in BOK protein as previously shown with *BOK* mRNA. *MYCN*-amplified Kelly and IMR32 cells and non-*MYCN*-amplified SKNAS and Gimen cells were treated with UNC0638 for 72 hours.

Immunoblotting of floating and adherent treated cells shows an increase in BOK protein in both Kelly and IMR32 cells following G9a inhibition, but not in the SKNAS and Gimen cells. This is mirrored by the changes or lack thereof in cPARP in the respective cell lines. BOK also seemingly decreases in SKNAS cells which is reflected in the decrease in cPARP (Figure 5.4) suggesting that BOK is an independent apoptotic regulator.

BOK has also been suggested to play a role in regulating macro-autophagy (autophagy) as increased *BOK* expression following oxidative stress has been shown to induce autophagy directly, as well as indirectly by a mechanism that involves BOK sequestration of MCL-1 to free Beclin-1 and thus induce autophagy (318). This suggests that BOK has a role in both type I (apoptosis) and II (autophagy) programmed cell death. Therefore, LC3B, an indicator of autophagy, was also probed for.

Kelly cells, which has easily inducible apoptosis, and LAN-1 cells, with seemingly methylated BOK, were tested after UNC0638 treatments; if there is still autophagy in LAN-1 cells with no BOK expression then this would suggest that BOK is not involved in autophagy following G9a inhibition. Cells were treated for 24 and 72 hours with UNC0638 (Figure 5.5). In Kelly cells, there is a consistent increase in BOK, cPARP, and LC3B. However, the LAN-1 cells show no BOK and as a result there is no change in cPARP. However, there is an increase in LC3B which suggests that whilst G9a inhibition seemingly induces both apoptotic and autophagy, BOK is not involved in the induction of the latter.

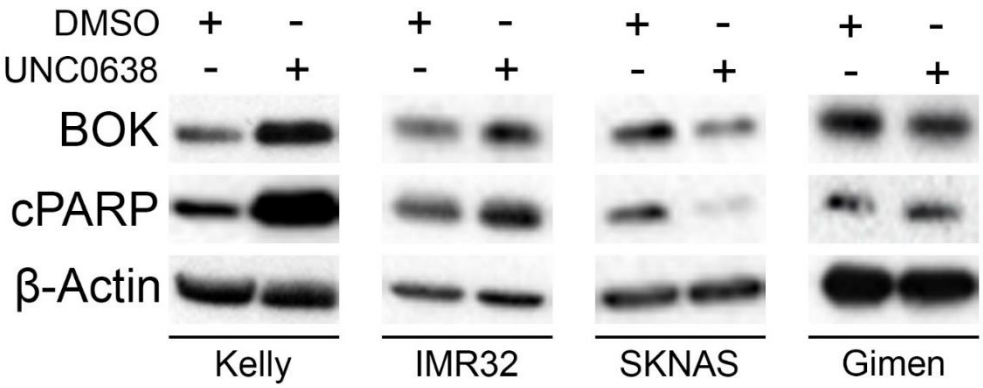

Figure 5.4 – BOK protein increases in *MYCN*-amplified neuroblastoma
Immunoblots for BOK and cPARP protein expression in a panel of MYCN- and non-MYCN-amplified neuroblastoma cell lines treated with UNC0638 for 72 hours. Kelly was treated with 5μM and IMR32, SKNAS, and Gimen treated with 10μM. β-Actin is used as a loading control.

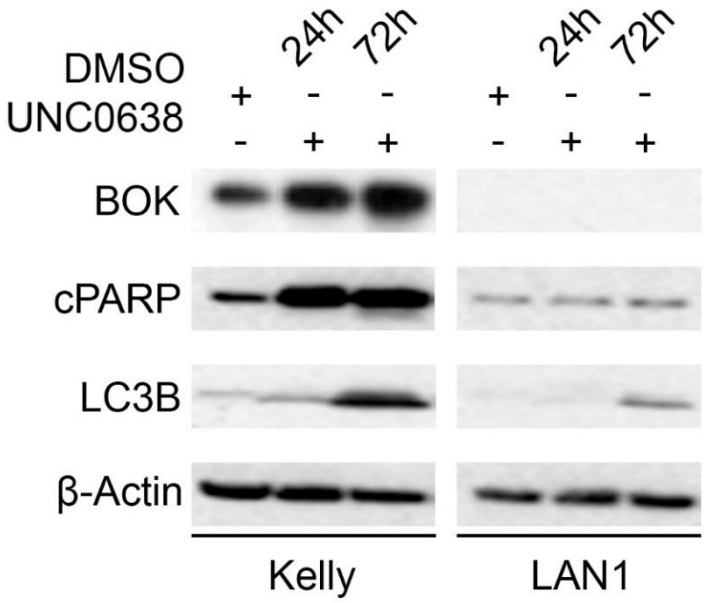

Figure 5.5 – BOK protein induction correlates with apoptosis and not autophagy
Immunoblots for BOK, cPARP, and LC3B protein expression in Kelly and LAN-1 neuroblastoma cell lines. Kelly was treated with 5μM and LAN-1 with 10μM UNC0638 and harvested at 24 hours and 72 hours. β-Actin is used as a loading control.

5.5 BOK mRNA and protein expression is decreased in poor prognostic and *MYCN*-amplified neuroblastoma

High expression of pro-apoptotic BCL-2 family *BAK* has been shown correlate with favourable prognosis in lung cancer (319) and colorectal cancer (320). As BOK is also a pro-apoptotic BCL-2 family member, this would imply that it would act similar in a similar manner with regards to prognosis. Carberry et al show that BOK protein can be used as a prognostic marker as stage II and III colorectal cancer patients possess decreased BOK protein relative to normal tissue suggesting BOK as a good prognostic marker (320). However, they also suggest that *BOK* mRNA does not correlate with prognosis, and that increased BOK protein levels actually associated with earlier disease recurrence and reduced overall survival (320), suggesting BOK is actually poor prognostic. Therefore, *BOK* expression and prognosis was assessed in neuroblastoma using the three different neuroblastoma datasets from the Genomic Analysis and Visual Platform R2 (http://r2.amc.nl) similar to chapter 3.2.

BOK was assessed to determine if high expression was considered a good or a bad prognostic indicator in neuroblastoma. *BOK* mRNA was expression was mapped to the outcome of each patient (Figure 5.6A). All three databases indicated that high *BOK* mRNA expression correlated with a significant increase in overall survival probability. Versteeg- 88 showed 58/80 patient tumour samples tested presented a high overall survival probability relative to tumours with low *BOK* expression (Bonferroni $p=5.7e^{-5}$). SEQC- 498 had a comparable result with 351/498 being in the high expression (Bonferroni $p= 6.8e^{-19}$) and Kocak- 649 had 408/476 (173 samples omitted as they lacked survival information) in the high expression, high outcome bracket (Bonferroni $p= 5.0e^{-21}$). These are all highly significant with the overall survival probability not below 0.8 (80%) in the high *BOK* expression across the patients across the three databases. This data indicates that *BOK* is correlated with outcome and that high *BOK* expression is favourable, which goes against what Carberry et al have presented (320). When *BOK* expression was limited to patients with non-*MYCN*-amplification only, this still shows a significantly favourable outcome with high *BOK* expression (Bonferroni $p= 0.049$, $1.4e^{-5}$, $2.5e^{-7}$ respectively) (Figure 5.8B).

Overall, this data suggests that high *BOK* expression correlates with good a prognostic outcome.

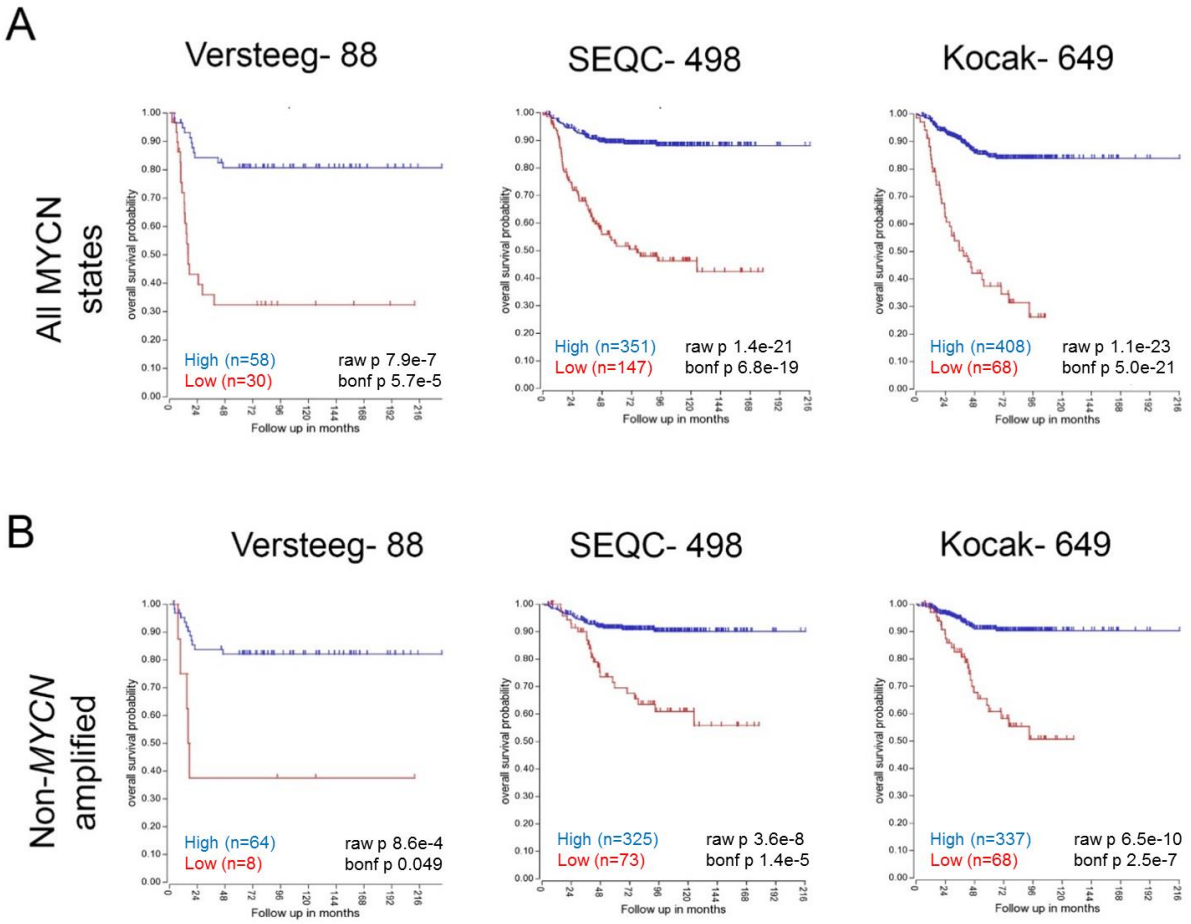

Figure 5.6 – High *BOK* mRNA expression correlates with good prognosis in neuroblastoma

A *– Kaplan-Meier survival curves of neuroblastoma show a positive relationship between high BOK mRNA expression and good prognosis. The blue and red lines represent high and low BOK mRNA expression respectively, whilst n represents the number of tumours in each category. This correlation was shown in three separate named tumour array datasets. Versteeg-88 analysis derives from microarray data analysing eighty eight human tumours (297). SEQC- 498 is derived from RNA sequencing data of 498 neuroblastoma (321). Kocak-649 is generated using 44K oligonucleotide microarrays of neuroblastoma tumours and cell lines. In the Kocak-649 dataset, only 476 of the 649 neuroblastoma samples were analysed as only these had survival information available (222).* ***B*** *– Kaplan-Meier survival curve from the databases shown in A were refined to only include tumours with non MNA states. This showed that there is a positive relationship between high BOK mRNA expression and good prognosis after poor prognostic indicator MYCN-amplification is taken out. The blue and red lines represent high and low BOK mRNA expression respectively, whilst n represents the number of tumours in each category.*

Next, *BOK* expression was compared between *MNA* and non-MNA neuroblastoma tumours to examine the relationship in the same three datasets. Boxplots produced from the R2 platform using the datasets (Figure 5.7A) shows that there is a consistent significant decrease in *BOK* mRNA in MNA tumours relative to non-MNA tumours ($p=8.4e^{-5}$, $4.4e^{-52}$, $2.8e^{-49}$ respectively).

Because of the correlation at the RNA level, it was necessary to determine if this was true at the protein level too. A panel of protein lysates from five MNA, three non-MNA neuroblastoma, and two disease-free cell lines were immunoblotted for BOK and MYCN (Figure 5.7B). β-actin was used a loading control. MYCN protein was overexpressed in all the MNA cell lines. There was a lower expression of BOK protein in these cell lines relative to the non-MNA. This relationship was quantified using semi-quantitative densitometry of the immunoblots using image J (Figure 5.7C). Relative BOK was quantified to β-actin. Relative BOK levels were shown to be significantly lower in the *MYCN*-amplified cell lines relative to non-MNA and disease-free cell lines (* $p<0.05$). BOK was ubiquitously expressed in all the non-MNA cell lines tested unlike in the MNA cell lines where there is no BOK protein in cell lines LAN-1 and BE2C cell lines. *BOK* gene has been shown to be methylated in colorectal cancer (320), so BOK may be methylated in these two cell lines. This would suggest why no apoptosis was seen in these two cell lines when treated with UNC0638 as there was no induction of BOK.

Overall, examination of BOK and MYCN mRNA and protein in neuroblastoma cell lines suggests that BOK is more highly expressed in non-MNA cells suggesting that MYCN may repress BOK expression.

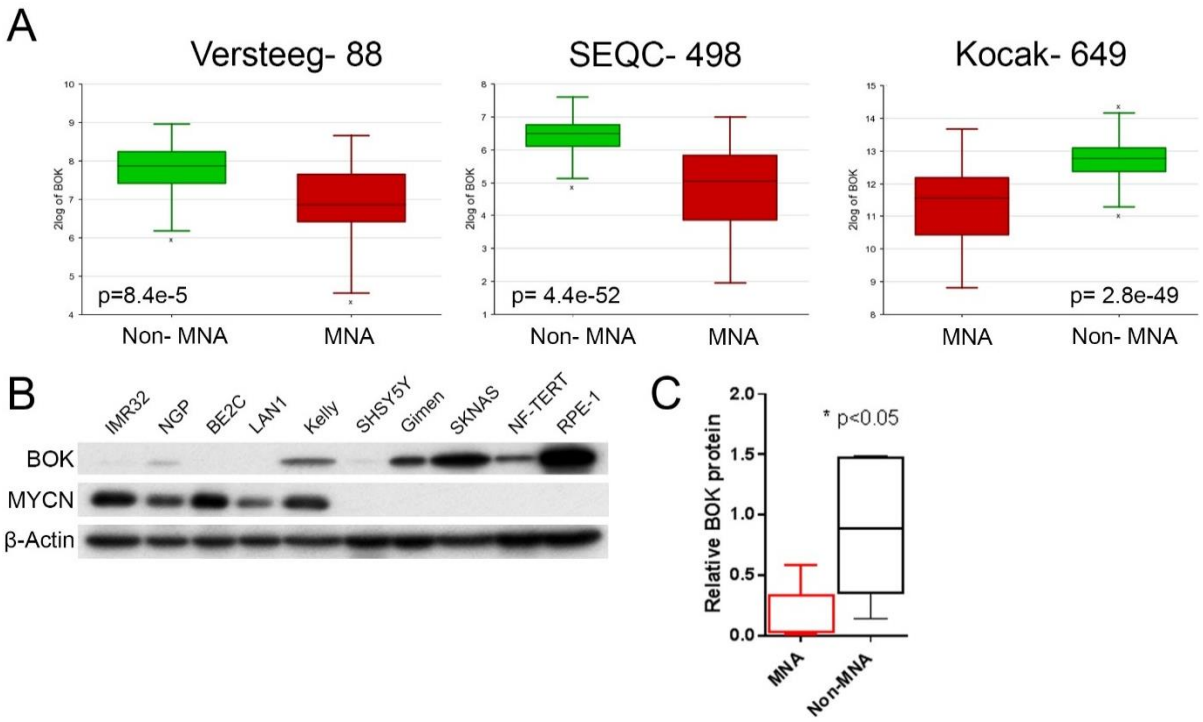

Figure 5.7 – Low BOK protein expression correlates with MYCN protein
A *– Lower BOK mRNA expression is observed in MNA neuroblastoma relative to non MNA. This correlation was shown in three separate named tumour array datasets previously mentioned in Figure 5.4. The red and green colours represent MNA and non MNA respectively. The p-values are calculated by one-way ANOVA (Analysis of Variance) on R2.* ***B*** *– Immunoblot of BOK protein expression in a panel of MYCN- and non-MYCN-amplified neuroblastoma cell lines. β-Actin is used as a loading control. Representative of two biological replicates.* ***C*** *– Relative BOK expression is higher in MNA neuroblastoma. Box plot of relative BOK protein is generated from semi-quantitative densitometry of blot from* ***A****. BOK expression was normalised to β-Actin.*

5.6 BOK depletion rescues Kelly cells treated with UNC0638 from apoptosis

It has been suggested that BOK depletion by short hairpin (sh) RNA in human granulosa tumours is effective at significantly inhibiting caspase-3/7 activation after addition of various apoptosis-inducing factors, thus protecting the cells from apoptotic cell death (322). As the data in this study suggests G9a inhibition by UNC0638 induces apoptosis in *MYCN*-amplified cells, it was therefore hypothesised that BOK depletion may rescue these cells from apoptotic cell death after G9a inhibition; Kelly cells were treated with UNC0638 with and without BOK depletion to assess changes in apoptotic cell death.

DRAQ7 was added to Kelly cells transfected with siNEG and siBOK and treated with DMSO and UNC0638 to assess apoptotic cell death. This was measured by the

IncuCyte imaging system as red object count. The normalised red count shows that whilst there is a very significant increase in siNEG UNC0638 relative to siNEG DMSO control (pink line), there is no significant change between the siBOK DMSO and siBOK UNC0638 treatments over the 48-hour time course (Figure 5.8A).

This is further supported by trypan blue inclusion assay of the harvested cells with the same treatment. In the UNC0638 treated cells with wild type BOK, there was a very significant increase in percentage cell death relative to the negative small molecule inhibitor control DMSO (Figure 5.8B), similar to that seen in the previous chapter. However, in the BOK depleted cells, there was a no significant change in percentage cell death between the siBOK DMSO and siBOK UNC0638 treatments (Figure 5.8B) suggesting BOK depletion has rescued the cells from G9a inhibition-associated apoptosis. This is verified by immunoblot (Figure 5.8C) as there is an increase in BOK and cPARP in the siNEG transfected cells when treated with UNC0638, but no change in either following effective BOK depletion.

Next, other pro-apoptotic factors BAX and BAK were re-probed in the treatments used in the Kelly cells from figure 5.6. This would determine if BOK acted independently of the other factors as highlighted by Einsele-Scholz et al (323) and Llambi et al (38). After 72 hours of UNC0638 treatment, there is no change in either BAX or BAK protein expression despite the obvious increase in BOK and cPARP (Figure 5.8D). This suggests that the mechanistic effect of G9a inhibition on apoptosis is through a pathway that specifically targets BOK.

Therefore, this data suggests that increase in pro-apoptotic factor BOK protein caused by G9a histone methyltransferase activity inhibition is necessary for apoptotic cell death to occur independent of pro-apoptotic factors BAX and BAK.

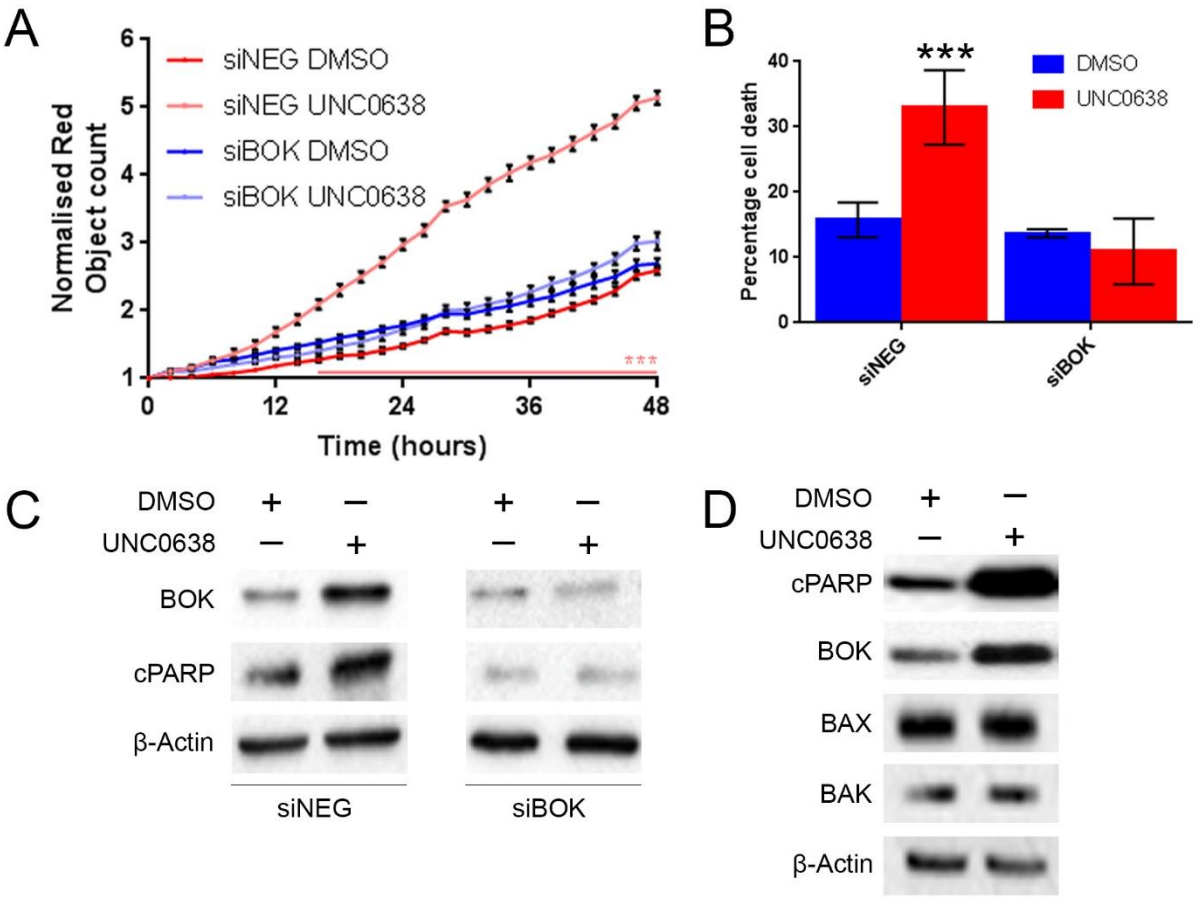

Figure 5.8 – BOK depletion rescues Kelly cells from apoptosis following G9a inhibition
A – *Normalised red object counts between Kelly neuroblastoma cells treated with DMSO and UNC0638 with wild type and depleted BOK. Kelly cells were transfected with siBOK for 36 hours before being treated with negative control DMSO and 5μM UNC0638 for 48 hours. Significance was evaluated at each time point by using T tests (*** p<0.01, n=2). Error bars show the SEM.* ***B*** *– This chart shows the percentage cell death changes. Floating and attached cells were the harvested and trypan blue inclusion assay was performed to count the dead cells. Significance is measured by unpaired T test (n=2, *** p<0.01, ns p>0.05). Error bars show the SEM.* ***C*** *– Immunoblot of treatments from* ***A*** *to confirm BOK depletion and apoptosis induction via cPARP increase. β-Actin was used as a loading control.* ***D*** *– Immunoblot of treatments in Kelly cells from Figure 5.6. These were probed for other pro-apoptotic factors BAX and BAK to determine if these were also increased following UNC0638 inhibition for 72 hours at 5μM. β-Actin was used as a loading control.*

5.7 BOK depletion and inhibits cell proliferation

There was no significant change in the basal percentage cell death between the siNEG and siBOK transfections treated with DMSO despite a suggested decrease in cPARP (Figure 5.8B). This suggests that this increase in BOK expression is driving the apoptotic cell death, and it is not just the mere presence of BOK, as overexpression has been shown to increase its pro-apoptotic function (324-328). Furthermore, it is assumed that BOK is a potential tumour suppressor gene following its induction after G9a inhibition with its role in inducing apoptosis. Therefore, the effect of BOK depletion on cell growth was assessed to determine if BOK is a potential tumour suppressor; cell growth should increase in cells with BOK depleted if BOK acted as a tumour suppressor gene.

BOK was depleted in Kelly and IMR32 cells. There is a significant reduction in percentage confluence in Kelly cells from 88 hours, and very significant from 100 hours (Figure 5.9A). Immunoblot of these lysates shows effective depletion of BOK (Figure 5.9B). Similarly, in IMR32 there is a significant reduction in percentage confluence from 14 hours and very significantly from 58 hours (Figure 5.9C). Effective BOK depletion is confirmed by immunoblot (Figure 5.9D).

This data suggests that BOK depletion, in cell lines with relatively low levels of BOK protein expression, negatively impacts percentage confluence suggesting that BOK not only has a role in promoting cell proliferation, but that its tumour suppressor function is not so clear cut.

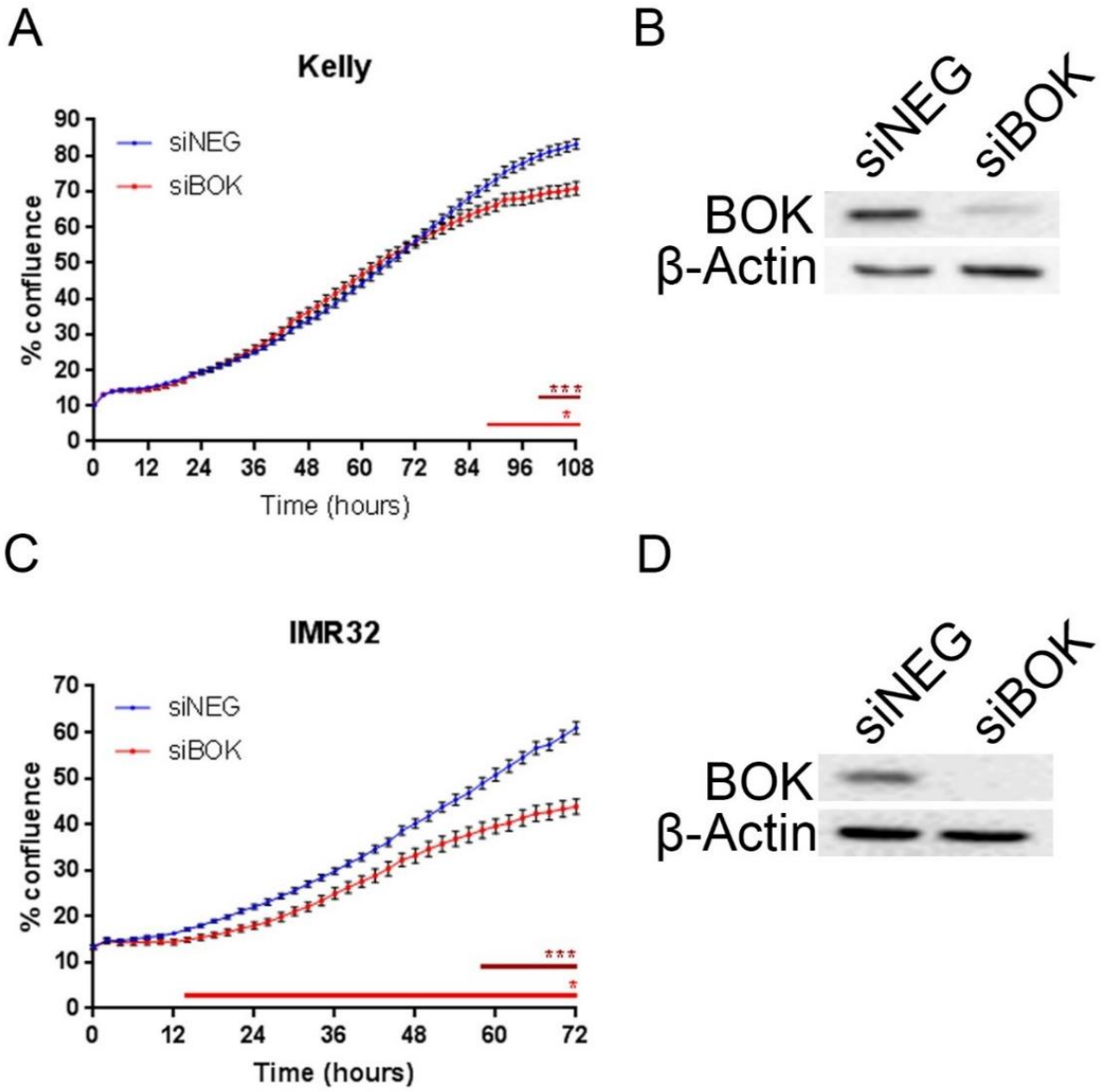

Figure 5.9 – BOK depletion decreases cell proliferation
A *– Graph depicts the normalised percentage phase object confluence as a proxy of cell growth in Kelly cells. The cells were transfected with siRNA at 25nM and incubated for 108 hours. The significant red line below the graph shows significance (n=2, * p<0.05) after 88 hours. After 100 hours, the difference is very significant- maroon line (n=2, *** p<0.01). Error bars show the SEM.* ***B*** *– Immunoblot to confirm BOK depletion. β-Actin is used as loading control.* ***C*** *– Graph depicts the normalised percentage phase object confluence as a proxy of cell growth in IMR32 cells. The cells were transfected with siRNA at 25nM and incubated for 72 hours. The significant red line below the graph shows significance (n=2, * p<0.05) after 14 hours. After 58 hours, the difference is very significant- maroon line (n=2, *** p<0.01). Error bars show the SEM.* ***D*** *– Immunoblot to confirm BOK depletion. β-Actin is used as loading control.*

5.8 BOK is a novel differentiation modulator in Kelly and IMR32 neuroblastoma

When looking at the photomicrographs of IMR32 and Kelly cells with BOK depleted from Figure 5.9, there is a dramatic increase in neuritogenesis in both cell lines; a marker of differentiation.

This differentiation effect is prominent in IMR32 cells with BOK depleted. The photomicrographs (Figure 5.10A) show a marked increase in the neuritogenesis between the negative control and BOK depleted cells. The main body of the cells are smaller, but the neurite lengths are significantly longer. As these cells were imaged using the live cell imaging system IncuCyte Zoom, an analysis job was performed to measure the change in length of these neurites between the negative control and the BOK depleted cells. The change in normalised neurite length is very apparent with normalised neurite length of the BOK depleted cells being nearly two-fold the negative control after 72 hours (Figure 5.10B). There is a significant difference after 50 hours, which is very significant after 56 hours following effective BOK depletion (Figure 5.10C). Moreover, neurite length initially shortens until around 24 hours before they lengthen in both treatments which mirror until around the 48-hour mark. This was consistent across the two biological replicates, suggesting that it takes time for the effect of BOK depletion to manifest itself in this differentiation effect.

In Kelly cells, the morphology of the cells also changes following BOK depletion as they become phenotypically different (Figure 5.11A). The cells with depleted BOK become much thinner and there are more neurites extending from the poles of the cells. This increase is similarly shown in the normalised neurite length graph of the treated Kelly cell lines showing an increase in neuritogenesis and differentiation of the cells (Figure 5.11B). There is no significant change in normalised neurite length until 48 hours when there is a dramatic and significant increase. This becomes very significant after 68 hours. Immunoblot of these cell protein lysates show effective depletion of BOK in these treatments (Figure 5.11C).

This differentiation phenotype was not observed in SKNAS cells effectively depleted of BOK despite showing a decrease in cell proliferation (data not shown). This suggests that BOK has a proliferative effect in cells, and this is not just an artefact of cell size changes following differentiation in BOK depleted samples.

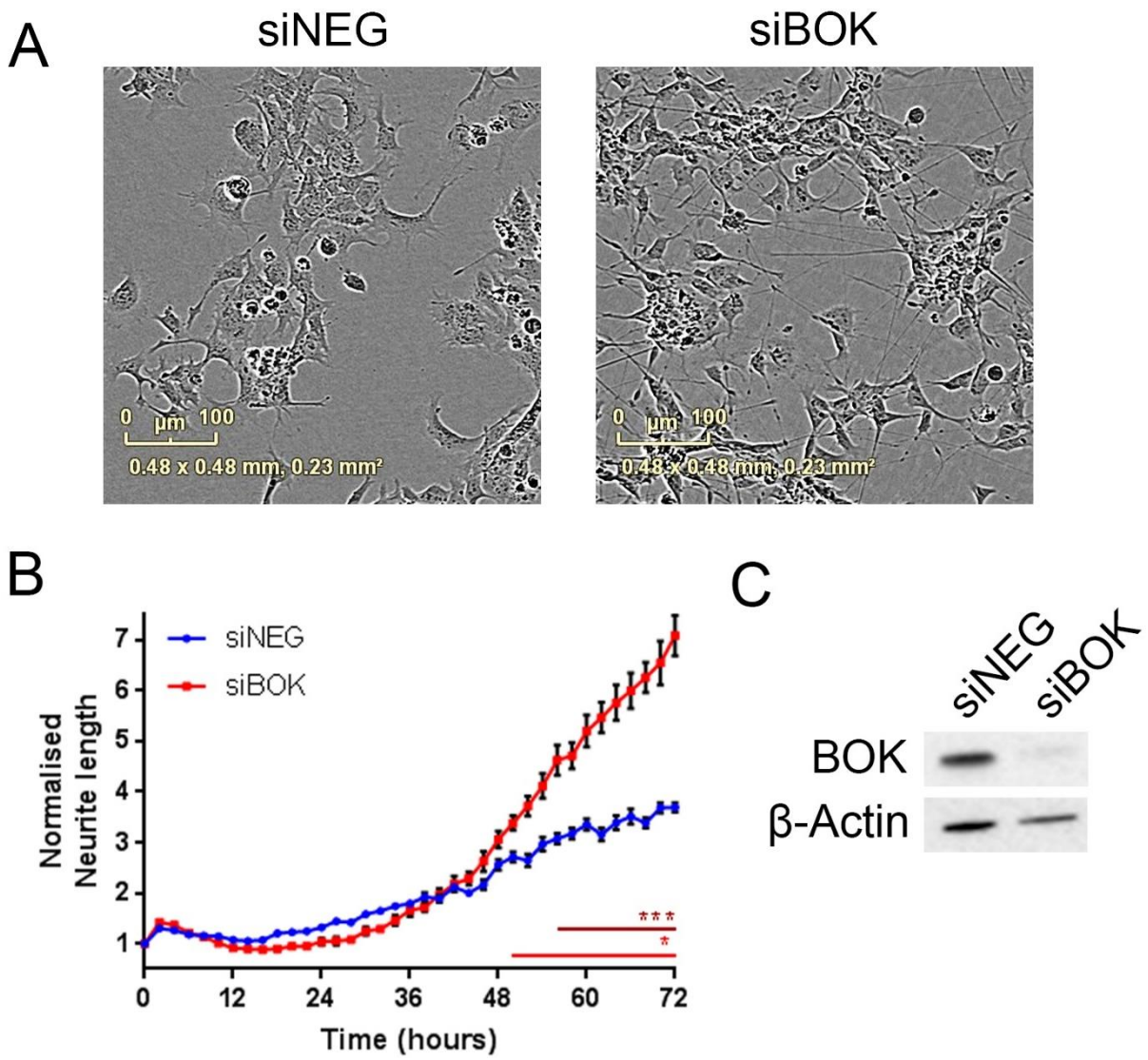

Figure 5.10 – BOK depletion differentiates IMR32 cells after 50 hours
A *– Photomicrographs at 10x objective magnification of IMR32 cells transfected with negative control (siNEG) and BOK siRNA for 72 hours. These show the phenotype of neuritogenesis in the siBOK cells.* ***B*** *– Graph displays normalised neurite length changes over the time course of Kelly cells. There is a significant increase after 50 hours – red line (n=2, * p<0.05), and very significant after 56 hours – maroon line (n=2, *** p<0.01). Error bars show the SEM.* ***C*** *– Immunoblot to confirm BOK depletion. β-Actin is used as loading control.*

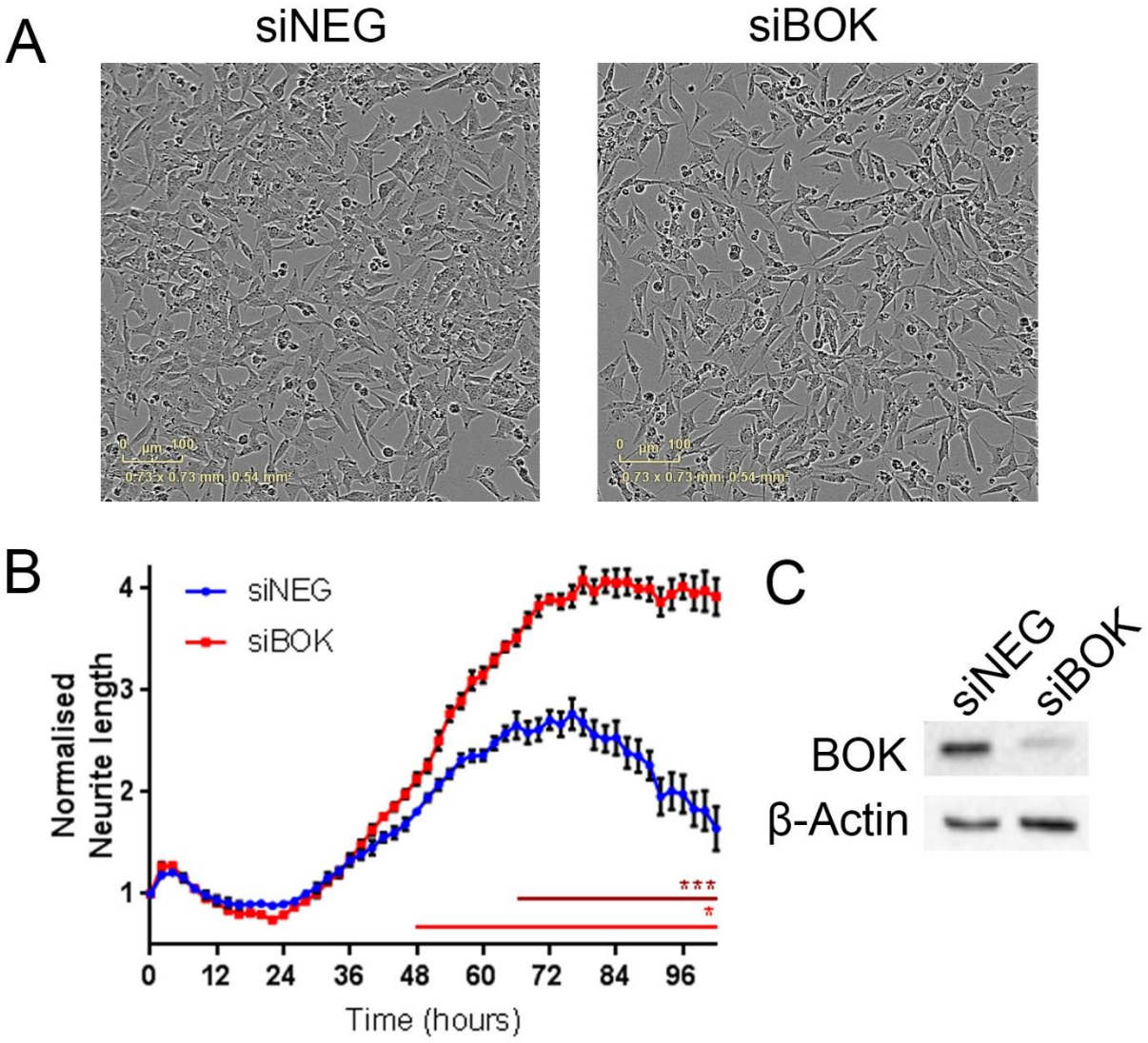

Figure 5.11 – BOK depletion differentiates Kelly cells after 48 hours
A *– Photomicrographs at 10x objective magnification of Kelly cells transfected with negative control (siNEG) and BOK siRNA for 108 hours. These show the phenotype of neuritogenesis in the siBOK cells.* ***B*** *– Graph displays normalised neurite length changes over the time course of Kelly cells. There is a significant increase after 48 hours – red line (n=2, * p<0.05), and very significant after 68 hours – maroon line (n=2, *** p<0.01). Error bars show the SEM.* ***C*** *– Immunoblot to confirm BOK depletion. β-Actin is used as loading control.*

5.9 G9a regulates MYCN protein in Kelly cells

Since there has been shown to be a strong association between G9a and MYCN throughout this study, the effect on MYCN mRNA and protein following G9a depletion was examined.

Effective G9a depletion showed a significant reduction in MYCN at the protein level (Figure 5.12A). However, at the RNA level, despite an effective and significant knockdown of around 50% in two biological replicates, there is not a significant relative fold change in *MYCN* expression (Figure 5.12B). This suggests that the MYCN reduction shown is due to protein regulation by G9a.

To determine if this regulation was necessitated by the histone methyltransferase SET domain of G9a, small molecule inhibitor UNC0638 was added to Kelly and LAN-1 (a progenitor of the LA1-55n cells used by Lu et al) neuroblastoma at 5μM and 10μM respectively for 24 hours (Figure 5.12C). Again, there was a clear decrease in MYCN protein relative to the DMSO control. Furthermore, when looking at the mRNA level, there is no significant change in the relative *MYCN* expression in these cell lines (Figure 5.12D).

Overall, this data suggests that G9a histone methyltransferase domain is necessary for MYCN protein stability and regulation, and inhibition by small molecule inhibitor UNC0638 reduces MYCN protein.

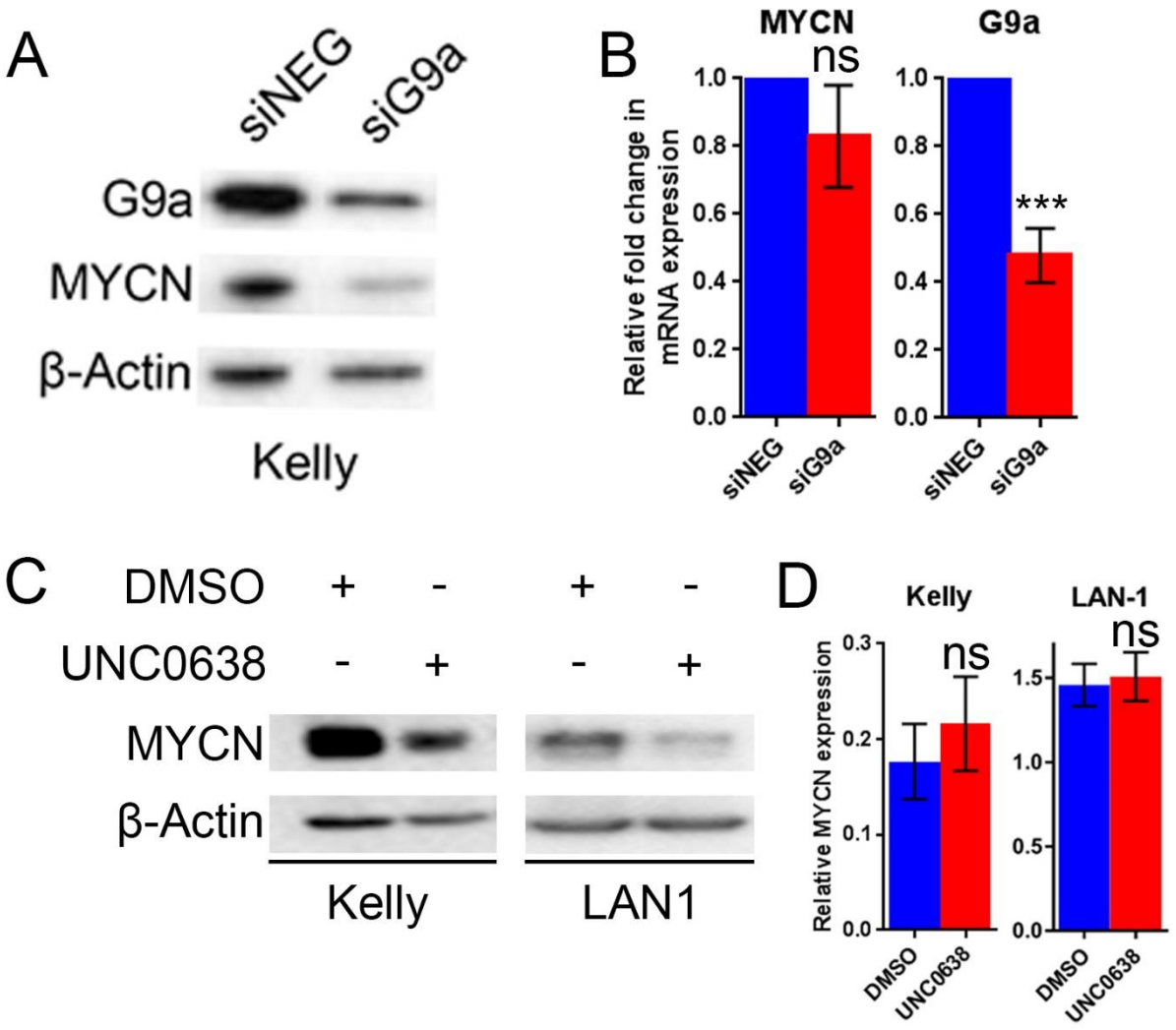

Figure 5.12 – MYCN is regulated by G9a at the protein level

A *– Immunoblot of Kelly cells transfected with siNEG (negative control) and siG9a at a concentration of 25nM for 72 hours. Attached and floating cells were harvested and immunoblotted for G9a and MYCN. β-Actin was used as a loading control.* ***B*** *– qRT-PCR of MYCN and G9a in Kelly cells after 72-hour siG9a transfection. Expression change is relative to TBP. Fold change is relative to negative control. Significance is measured by unpaired T test (*** $p<0.01$, ns $p>0.05$, $n=2$). Error bars show the SEM.* ***C*** *– Immunoblot of Kelly and LAN-1 cells treated with 5μM and 10μM respectively for 24 hours. Attached and floating cells were harvested and immunoblotted for MYCN. β-Actin was used as a loading control.* ***D****- qRT-PCR of MYCN in Kelly and LAN-1 cells treated with 5μM and 10μM respectively for 24 hours cells. Fold change is relative to TBP. Significance is measured by unpaired T test (ns $p>0.05$, $n=3$) Error bars show the SEM.*

5.10 G9a inhibition can regulate MYCN targets

Since MYCN protein was downregulated after inhibition with UNC0638, this suggests that MYCN's ability as a transcriptional regulator may be diminished therefore re-expressing previously repressed targets and repressing induced targets. Therefore, mRNA expression fold change of a few suggested MYCN targets were assessed. The targets tested were Clusterin (CLU), CASP8, and ALK. CLU is a molecular chaperone and tumour suppressor that is downregulated by MYCN binding to *CLU* promoter to recruit repressive complexes (242). CASP8 is a member of the caspase family involved in apoptosis. *CASP8* has been shown to be a direct target of c-MYC in lymphoblastoid cells (329) and MYCN/MAX dimer has been shown to bind to CASP8 promoter after demethylation treatment in LAN-1 cells (330). *ALK* promoter has a non-canonical E-box upstream of the transcription start site which MYCN can bind to upregulate *ALK* transcription (213).

Four neuroblastoma cell lines, Kelly, LAN-1, SKNAS, and Gimen (two *MYCN*-amplified and two non-*MYCN*-amplified respectively) were all treated with UNC0638 for 24 hours. The relative fold change in the mRNA expression of the three genes was then measured (Figure 5.13). In the *MYCN*-amplified Kelly and LAN-1 neuroblastoma, fold change in *CLU* expression increased significantly after G9a inhibition, whereas the was no significant change in the non-*MYCN*-amplified SKNAS and Gimen cells. Similarly, *CASP8* also significantly increases in the Kelly and LAN-1 cells after G9a inhibition. In SKNAS cells, there is a significant decrease in fold expression change, and no significant decrease in Gimen cells. *ALK* fold expression change very significantly decreases in both Kelly and LAN-1, but also in SKNAS cells. Gimen cells have no significant decrease. This all suggests that *CLU* and *CASP8* are upregulated following G9a inhibition in only *MYCN*-amplified cells, suggesting this is due to downregulation of MYCN protein on these promoters. Moreover, *ALK* fold expression change decreases in three of the cell lines (no significant change in Gimen) and there is no pattern between the *MYCN* and non-MYCN-amplified cell lines. This suggests that *ALK* is upregulated by G9a as well as MYCN.

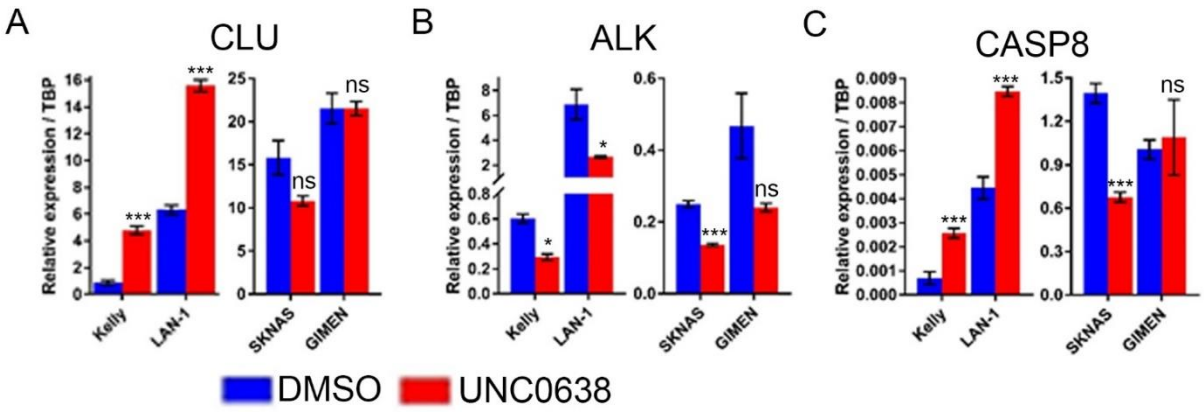

Figure 5.13 – Treatment by G9a small molecule inhibitor regulates suggested MYCN targets
*qRT-PCR of **A** – Clusterin (CLU), **B** – ALK, and **C** – CASP8, in Kelly, LAN-1, SKNAS, and Gimen cells treated 5μM (Kelly) and 10μM (LAN-1, SKNAS, Gimen) UNC0638 for 24 hours cells. Fold change is relative to TBP. Significance is measured by unpaired T test (ns p>0.05, * p<0.05, p<0.01 n=3) relative to DMSO. Error bars show the SEM.*

5.11 Discussion

The aim of this chapter was to assess the gene and protein regulatory effects G9a inhibition has in both *MYCN*-amplified and non-*MYCN*-amplified neuroblastoma. From looking at gene expression changes highlighted by the previous RNAseq analysis, it was verified that G9a has a role gene regulation in neuroblastoma as G9a inhibition was able to up and downregulate expression of certain genes.

There were four groups of genes shown to be regulated by G9a in a heatmap of the RNA sequencing, not shown, with 1) genes upregulated and 2) downregulated following BIX-01294 treatment, and then 3) genes upregulated and 4) downregulated between the *MYCN*-amplified LAN-1 and non-*MYCN*-amplified SKNAS cells. This suggests that G9a not only had its own genes to regulate but could also modulate MYCN repressed and activated targets too. The novel repressed G9a targets in this chapter are *CCBE1*, *FLCN*, *AMHR2*, and *FABP3*. ChIP would be needed to ascertain if the promoters of these genes are directly repressed by G9a or if they are indirect downstream targets.

This chapter has shown that G9a depletion and inhibition in tested *MYCN*-amplified cell lines has the ability to reduce MYCN protein but not *MYCN* mRNA. This suggests that G9a activity can stabilise MYCN at the protein level either through direct

methylation or methylation of a binding partner. In addition, regulation of suggested MYCN targets *ALK, CLU*, and *CASP8* is shown following G9a inhibition suggesting that G9a inhibition can also control expression of MYCN targets. In the context of neuroblastoma, G9a and MYCN regulation has only been suggested in one study Lu et al, as mentioned previously. The data shown in this chapter is more comprehensive and thorough than that currently published as it shows MYCN protein depletion in multiple cell lines after both G9a depletion and inhibition using a more reliable G9a inhibitor. Therefore, this data suggests that G9a is a viable therapeutic target in MYCN-amplified tumours.

MYCN-amplification and overexpression also afflict other types of cancer with an aggressive phenotype. MYCN is found to be overexpressed in a vast majority of retinoblastoma and is amplified in a small subset too (331-333). In addition, *MYCN* is amplified in 15-20% of small-cell lung cancer (334, 335) which are suggested to have a poor response to chemotherapeutic treatments whilst having a very quick growth rate (336). MYCN overexpression has also been reported in a subset of breast cancers (337) and Wilms' Tumour (338). This suggests that *MYCN*-amplification and overexpression is more prevalent than being restricted to high-risk neuroblastoma therefore being able to inhibit and decrease MYCN protein through the use of G9a small molecule inhibitors would benefit a much wider patient set.

G9a has also been shown to stabilise other MYC family member c-MYC (MYC) in Abelson murine leukaemia virus-induced tumour (339). Cycloheximide (CHX) chase assay of MYC in wildtype and G9a depleted Raw264.7 cells also showed the rate of MYC decay was increased four-fold in G9a depleted cells (339). This G9a stabilising effect matches data presented here as there is a decrease in MYCN protein after both G9a depletion and inhibition suggesting G9a has a similar destabilising effect on MYCN. Furthermore, qRT-PCR results have shown an increase in *MYC* expression following G9a knockdown (339), which is similar to the results presented in this chapter as there is no decrease in *MYCN* mRNA expression after separate G9a depletion and inhibition, therefore implying G9a does not regulate gene expression of MYC family members *MYC* and *MYCN*.

This stabilising effect G9a imparts on MYCN would suggest why there is a difference in gene regulation between *MYCN*-amplified LAN-1 and non-*MYCN*-amplified SKNAS

cells following G9a inhibition as G9a inhibition destabilases MYCN protein in amplified cell lines disrupting its regulatory effect on MYCN targets.

The novel tumour suppressor and MYCN-repressed gene shown here to be re-expressed following G9a inhibition is pro-apoptotic factor BOK (BCL-2-related ovarian killer). Whilst it is unknown through which mechanism BOK-driven apoptosis acts in this study, the data in this chapter suggests that the increase in BOK protein expression following G9a inhibition is the driver of apoptosis in *MYCN*-amplified neuroblastoma; there is no BOK induction in non-*MYCN*-amplified neuroblastoma following G9a inhibition and there is also no apoptosis either, whereas in MYCN-amplified cells there were increases in both. Moreover, MYCN depletion also induced BOK gene and protein expression suggesting good prognostic indicator BOK to be a repressed MYCN target. Also, BOK depletion stopped apoptosis in *MYCN*-amplified Kelly cells following UNC0638 treatment. Therefore, this all suggests that BOK is a tumour suppressor and a novel inducer of apoptosis in *MYCN*-amplified neuroblastoma, and this is this potential mechanism for the synthetic lethality relationship between G9a-MYCN.

It was initially reported that BOK-induced apoptosis was BAX/BAK-dependent. Mice deficient in both BAK and BAX are highly resistant to intrinsic apoptosis stimuli (340, 341) even when endogenous BOK is expressed. This suggests it acts upstream of BAX and BAK in the intrinsic pathway (37). Yet, it has recently been demonstrated that BOK can efficiently induce cytochrome c release and apoptosis in the absence of BAK and BAX (323). Furthermore, it has been suggested BOK can influence the apoptotic response to chemotherapeutic drugs in ovarian carcinoma cells suggesting it is a genuine pro-apoptotic factor (323). Results from this chapter agree with this assessment as there is no increase in BAX or BAK protein following UNC0638 inhibition despite the increase in BOK and apoptosis marker cPARP.

Furthermore, the localisation of BOK is different to BAK and BAX as BOK localises mainly to the endoplasmic reticulum (ER) and the Golgi apparatus and only weakly to mitochondria (342). The ER stress pathway was targeted in mouse embryonic fibroblasts from *BOK*-/- animals, with significantly less cell death in the *BOK*-/- relative to wild type cells suggesting BOK promotes apoptosis following ER stress (36). BIX-01294 treatment in bladder cancer cells has also been shown to stimulate ER stress

(305). Therefore mechanistically, this suggests that G9a inhibition increases ER stress in *MYCN*-amplified neuroblastoma and the decrease in MYCN allows for the re-expression of BOK which localises to the ER to drive apoptosis and cell death via MOMP. Moreover, BOK can also be found in the nucleus and its export is regulated by the presence of nuclear export signal (NES) within its BH3 domain (37, 324, 343). This localisation event is suggested to play a big role in its apoptotic function as mutations in this export signal, and inhibition of NES-containing protein exporter Crm1 increases the accumulation of BOK and thus its apoptotic potential (324). This suggests the importance of therapeutically regulating apoptosis through small molecule inhibitors.

The result of differentiation following BOK depletion was very surprising and interesting as the role of the BOK in early development has not been well characterised. As apoptosis is a key process in the stages of development, it is necessary to dispose of unwanted cells and tissues during embryonal growth such as epithelial remodelling during gut development (344). Genetic manipulation in mice, drosophila, and nematodes has shown that the BCL-2 family has a pivotal role in contributing to development, not only by controlling cell death but also in many non-apoptotic functions too (345). For example, BCL-2 proteins localised at the ER membrane can contribute to the control of Ca^{2+} exchanges at the level of the ER/mitochondria interface, or Ca^{2+} hotspots (346). Mitochondria uptake the Ca^{2+} released from the ER, however if mitochondria accumulate Ca^{2+} too quickly, this can lead to mitochondrial Ca^{2+} overload which can cause apoptosis or necrosis (347). This regulation of Ca^{2+} exchange is vital in the development of zebra fish and mice.

In addition, it has recently been shown that anti-apoptotic proteins can act as transcriptional regulators outside of interacting with pro-apoptotic proteins at the outer mitochondrial membrane to promote cancer cell survival and growth. A pro-survival BCL-2 recognition sequence has been identified in the transcriptional regulator SUFU. MCL-1, BCL-2 and BCL-XL can then bind to tumour suppressor SUFU to inhibit its activity and loss of MCL-1, BCL-2 and BCL-XL results in accumulation of SUFU (348). Furthermore, when overexpressed in mesenchymal stem cells, these proteins can induce expression of *BCL2* and *MCL1* in a GLI1/GLI2 dependent manner suggesting that these pro-survival proteins can regulate themselves in a positive feedback loop (348). BOK binds strongly to inositol 1,4,5-trisphosphate receptors (IP_3Rs), proteins

that form tetrameric calcium channels in the ER membrane to direct the release of calcium from the ER. It is suggested that BOK does not affect Ca^{2+} release, instead protecting the IP_3Rs from proteolysis and controlling their expression, at least in mouse embryonic fibroblasts (349). This suggests that, like pro-survival proteins MCL-1, BCL-2, and BCL-XL, pro-apoptotic protein BOK can also act as a transcriptional regulator, although the mechanism for this remains undefined. This may suggest how and why BOK depletion may drive neuritogenesis.

Chapter 6

General discussion and conclusions

6.1 Summary of findings

In this study, the viability of enzyme histone methyltransferase G9a as a neuroblastoma therapeutic target has been assessed. It was determined that G9a is an oncogene in neuroblastoma with increased mRNA and protein in high-risk *MYCN*-amplified correlating with poor prognosis. Depletion of G9a is able to inhibit proliferation in all tested cell lines, as well as inducing apoptotic cell death in MYCN-amplified cell lines.

The efficacy of small molecule inhibitors UNC0638 and UNC0642 was tested in a broad panel of MNA and non-MNA neuroblastoma cell lines with MNA cell lines being pointedly more sensitive to these inhibitors. Furthermore, the viability of disease-free cell lines RPE-1 and NF-TERT was unaffected at the highest concentration suggesting a synthetic lethal relationship between G9a and MYCN.

G9a is shown to be a regulator of MYCN protein and novel repressed G9a targets have also been determined such as *CCBE1*, *FABP3*, and *AMHR2*. Pro-apoptotic and potential tumour suppressor BOK is shown here for the first time to be co-regulated by both G9a and MYCN. G9a depletion and inhibition in MNA cells increases *BOK* mRNA expression and BOK protein and this increase correlates with the increase in apoptotic cell death. Conversely, the depletion of BOK is shown here to help drive differentiation in Kelly and IMR32 cells suggesting there is more to BOK than just being a pro-apoptotic factor.

Furthermore, G9a depletion and inhibition was able to arrest cell proliferation in all neuroblastoma cells tested, irrespective of MYCN-amplification or overexpression therefore suggesting that G9a is a key oncoprotein in neuroblastoma.

6.2 Depletion and inhibition of key oncoprotein G9a is synthetic lethal in MNA neuroblastoma

Synthetic lethality between two genes is defined by the simultaneous loss of both genes is necessary for death to occur; single losses do not affect viability. When comparing the G9a and MYCN potential synthetic lethal relationship with the more established BRCA-PARP synthetic lethality, G9a and MYCN may not appear as straight forward a relationship as this at first glance.

In the BRCA example, mutations in tumour suppressors *BRCA1* and *BRCA2* lead to genetic instability and breast cancers arise (249). These mutations cause these types of breast cancer to be sensitive to PARP inhibitors as PARP plays a key role in the repair of DNA single-strand breaks. The accumulation of these breaks leads to DNA double-strand breaks at the replication forks which are ordinarily repaired by the error-free homologous-recombination double-stranded DNA repair pathway of which key components are the tumour suppressors BRCA1 and 2 (350). Therefore, with BRCA1 and 2 inhibited by the mutations and PARP inhibited therapeutically there is no method for the cell to repair this genomic instability which drives the cell to death.

By comparison, in this thesis G9a depletion and inhibition by SMI UNC0638 is able to induce an apoptotic response selectively in MNA neuroblastoma. However, when depleted and inhibited in non-MNA lines, no apoptosis or cell death was induced (Chapter 3, 4). The apoptosis observed was further preferential to *MYCN*-amplification as engineered S21N cells that can express MYCN dependent on tetracycline exposure, displayed apoptosis only in the presence of MYCN (Chapter 3, 4). This shows how the inhibition of G9a causes apoptosis and cell death.

Furthermore, the results from this study show G9a depletion and inhibition is able to decrease MYCN protein in all MNA cell lines tested. There was no effect on *MYCN* mRNA suggesting that the histone methyltransferase domain of G9a regulates MYCN stability by potentially methylating MYCN (Chapter 4, 5). Post-translational modifications of MYCN protein are required to regulate turnover of MYCN protein, as phosphorylation of serine 62 and threonine 58, and ubiquitination via FBXW7 direct the MYCN for proteosomal degradation (226, 227). Furthermore, arginine methyltransferase PRMT5 has also been shown to methylate MYCN to stabilise the protein (229), although the exact mechanistic reason for this methylation has yet to be elucidated. This reduction in MYCN was able to regulate MYCN targets as there is an increase in repressed targets *CLU* and *CASP8*, as well as a reduction in induction target *ALK* (Chapter 4). This all suggests that in the context of synthetic lethality, G9a inhibition leads to the depletion of MYCN protein which the MNA neuroblastoma cells can’t handle, thus driving them to cell death via apoptosis.

However, it is suggested that the depletion of oncoprotein MYCN in Figure 5.2A leads to an increase in apoptosis indicator cPARP. This would suggest that the singular loss

of MYCN is enough to drive cell death and not the combined loss of G9a and MYCN suggesting oncogene addiction instead. However, it is also suggested in this thesis that in MNA cells there is a significant increase in the amount of G9a transcript and protein. Therefore, this suggests that the depletion of MYCN may lead to a decrease or inhibition of G9a protein which then would suggest a synthetic lethal relationship. This needs to be further examined to further establish the relationship between G9a and MYCN.

6.3 G9a is a novel regulator of gene expression and apoptosis

G9a is a known activator and repressor of gene expression, either directly through depositing repressive methylation marks on H3, or forming repressive complexes. Here novel repressed G9a targets are shown for the first time although it is not known how G9a represses these genes. It is presumed that these genes are potential tumour suppressor genes.

The key novel repressed tumour suppressor gene shown here is *BOK* which is shown to be necessary for G9a-associated apoptosis to occur (Chapter 5). G9a depletion and inhibition was shown to increase *BOK* mRNA and BOK protein expression only in *MNA* neuroblastoma cells. This increase in expression was also exhibited in MYCN depleted cells leading to the hypothesis that MYCN may repress *BOK*, and the decrease in MYCN caused by G9a inhibition may drive *BOK* expression. BOK protein expression was shown to be inversely associated MYCN which supports this notion. LAN-1 saw the biggest increase in *BOK* mRNA when treated with UNC0638 for 24 hours however when protein lysates were tested for BOK, there was no BOK observed. It is suggested that BOK promoter may be methylated however this increase in transcript would suggest there is more regulation in place.

BOK expression was shown to correlate with apoptosis induced by G9a inhibition and depletion. When Kelly neuroblastoma cells depleted of BOK were treated with UNC0638, no cPARP was observed and there was a significant decrease in cell death relative to the BOK wild type. This suggests that BOK is a true pro-apoptotic factor and potential tumour suppressor.

Depletion of BOK also had an unforeseen side effect of helping IMR32 and Kelly neuroblastoma cells to differentiate. It was thought that if BOK acted as a true tumour

suppressor, then depletion of BOK would increase cell growth. However, it had the opposite effect where Kelly and IMR32 cells decreased in percentage phase confluence after BOK depletion. Furthermore, there was a consistent increase neurite length and neuritogenesis, along with a change in morphology in these cells after BOK depletion. These changes became consistently significant after 48 hours suggesting the changes are downstream of BOK depletion and not a direct effect. This seemingly only effected the MYCN-amplified cell lines tested as GIMEN and SKNAS cells were not affected, not shown. This would suggest that despite being repressed by MYCN to begin with, BOK plays a key role as a regulator whether that be through being induced or depleted.

6.4 G9a and MYCN model

Here is shown a graphical model of how G9a and MYCN block apoptotic cell death by repressing pro-apoptotic factor BOK. In wild type *MYCN*-amplified cell lines like Kelly (Figure 6A) it is suggested that G9a stabilises MYCN through an unknown mechanism. It is suggested that MYCN is a non-histone target for G9a and that G9a methylation helps to stabilise MYCN protein similar to that described by Park et al with PRMT5 and MYCN (229). This is then able to represses G9a and MYCN targets. This includes *BOK* expression, again through an unknown mechanism, which then blocks apoptotic cell death.

However, when G9a is either depleted via siRNA interference or inhibited via small molecule inhibitor UNC0638, MYCN is depleted as a result of potentially losing the methylation mark. This destabilisation allows for the re-expression of *BOK* which then leads to apoptotic cell death (Figure 6B). As this is a model explanation, there is still many unknowns which will be further pontificated in the next section.

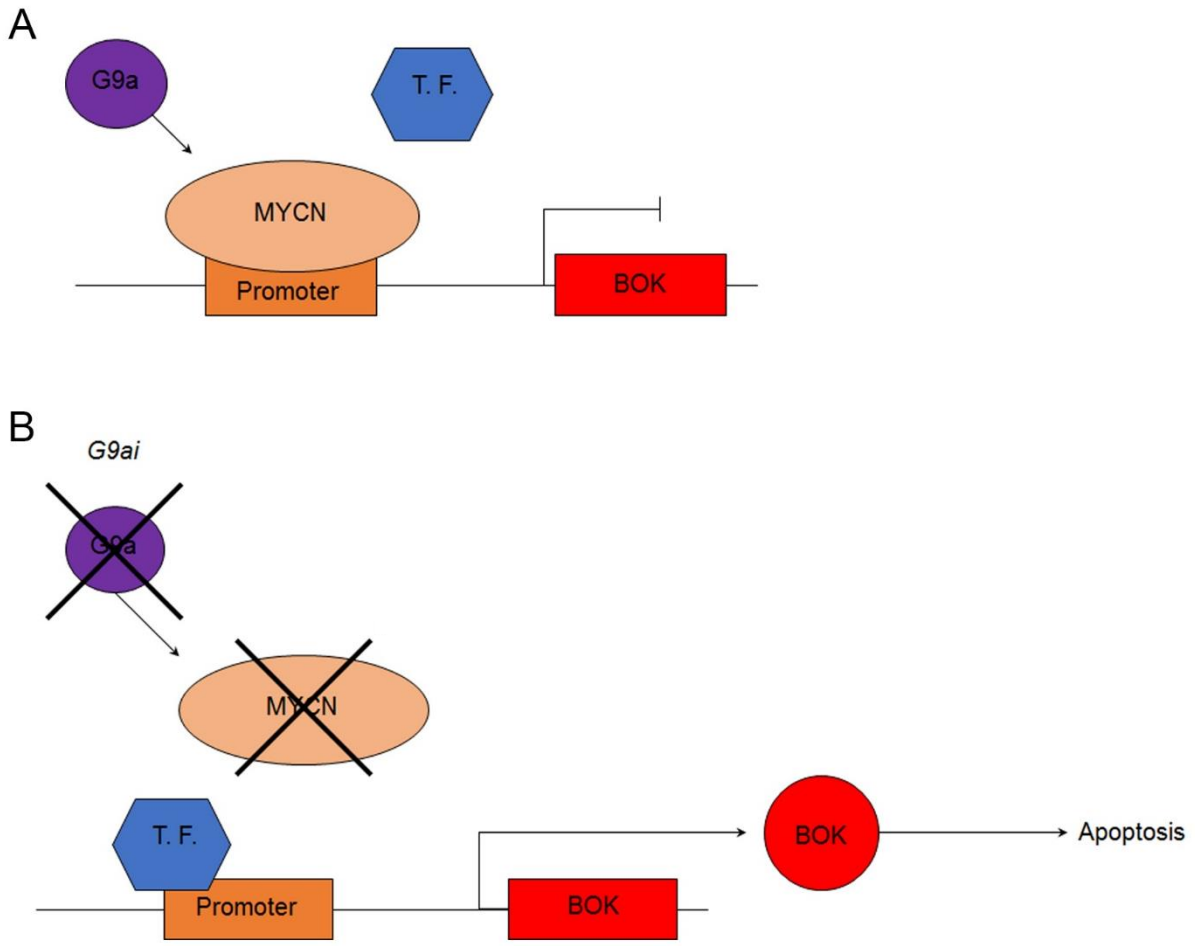

Figure 6 – Model of G9a and MYCN cooperation
A *– G9a may methylate MYCN protein to stabilise it. G9a and MYCN then cooperate to repress BOK expression.* ***B*** *– G9a inhibition and depletion destabilises MYCN to re-express BOK and drive apoptosis via MOMP, as detailed by Llambi et al (38).*

6.5 Future Studies

In this study, a novel decrease in MYCN protein after G9a inhibition was shown. G9a has been shown to bind to c-MYC protein (339), which would suggest that it also binds to MYCN. As well-established post-translational phosphorylation and ubiquitination events of MYCN can regulate proteasomal degradation, it would be of interest to explore the interplay between MYCN and lysine methylation. For example, assessing if MYCN is methylated by G9a using liquid chromatography – tandem mass spectrometry (LC-MS/MS) analysis of immunoprecipitated MYCN protein similar to Park et al (229) and if this protects MYCN from degradation. In addition, the exact mechanism driving synthetic lethality between G9a and MYCN would need to be clarified to further potentiate G9a as a therapeutic target for MYCN-overexpressing cancers.

As current G9a inhibitors block the SET domain, they are not specific to just G9a as they also inhibit GLP. Therefore, understanding if depletion and inhibition of GLP has a similar effect on cell proliferation and apoptosis would be of interest. Furthermore, it would be of interest to determine if the genes shown to be re-expressed following G9a inhibition, would also become re-expressed following GLP inhibition.

G9a is structurally and functionally similar to GLP and the results from this study suggest that wild type GLP is not able to rescue neuroblastoma cells from diminished proliferation and apoptotic cell death after G9a depletion and inhibition. Very little has been written about GLP and neuroblastoma with only one study depleting GLP in neuroblastoma to test the efficacy of their shRNA rather than any phenotypic effect (351). GLP has been suggested to aid the tumour suppressor activity of transcription factor regulator and metallothionein (MT) member MT1h which acts by enhancing the GLP methyltransferase activity on H3 (352). G9a and GLP both methylate H3 however it is suggested that G9a is more important than GLP for the *in vivo* histone methyltransferase function (120). Also, the ankyrin repeat domains of G9a and GLP have been shown to have differing binding affinities towards H3K9me1 and H3K9me2, with G9a preferring to associate with H3K9me2 and GLP associating with H3K9me1 (122). This means the G9a-GLP heterodimer can bind to both H3K9me1 and H3K9me2 marks to recruit G9a-GLP complexes. Therefore, depleting of either G9a or GLP may hinder cell proliferation or drive apoptosis if it is mechanistically driven via these complexes. This suggests that GLP could also play a role as an oncoprotein and this needs to be evaluated to help clarify the mechanistic role of G9a too.

Finally, here novel G9a targets have also been determined such as pro-apoptotic and potential tumour suppressor BOK which is shown for the first time to be co-regulated by both G9a and MYCN. This is potentially through G9a and MYCN protein interaction to form a repressive complex which either binds directly to the *BOK* promoter to block a potential transcription factor, or blocks expression of said transcription factor. Therefore, determining the mechanistic cause for how G9a and MYCN repress BOK protein would be useful for determining how to increase the expression of good prognostic indicator BOK in other cancer cell lines, and if this can be combined with therapeutic treatments. Also determining the role BOK plays in differentiation needs to be elucidated to shed further light on this little-known BCL-2 family member.

References

1. Hanahan D, Weinberg Robert A. Hallmarks of Cancer: The Next Generation. Cell. 2011;144(5):646-74.
2. Greaves M, Maley CC. CLONAL EVOLUTION IN CANCER. Nature. 2012;481(7381):306-13.
3. Croce CM. Oncogenes and Cancer. New England Journal of Medicine. 2008;358(5):502-11.
4. Feinberg AP, Koldobskiy MA, Göndör A. Epigenetic modulators, modifiers and mediators in cancer aetiology and progression. Nature Reviews Genetics. 2016;17:284.
5. Press MF, Bernstein L, Thomas PA, Meisner LF, Zhou JY, Ma Y, et al. HER-2/neu gene amplification characterized by fluorescence in situ hybridization: poor prognosis in node-negative breast carcinomas. Journal of Clinical Oncology. 1997;15(8):2894-904.
6. Baker SJ, Markowitz S, Fearon ER, Willson JK, Vogelstein B. Suppression of human colorectal carcinoma cell growth by wild-type p53. Science. 1990;249(4971):912.
7. Lesko AC, Goss KH, Yang FF, Schwertner A, Hulur I, Onel K, et al. The APC tumor suppressor is required for epithelial cell polarization and three-dimensional morphogenesis. Biochimica et Biophysica Acta (BBA) - Molecular Cell Research. 2015;1853(3):711-23.
8. Chu EC, Tarnawski AS. PTEN regulatory functions in tumor suppression and cell biology. Med Sci Monit. 2004;10(10):RA235-41.
9. Sherr CJ. Principles of Tumor Suppression. Cell. 2004;116(2):235-46.
10. Kastan MB, Lim D-s. The many substrates and functions of ATM. Nature Reviews Molecular Cell Biology. 2000;1:179.
11. Knudson AG. Mutation and Cancer: Statistical Study of Retinoblastoma. Proceedings of the National Academy of Sciences. 1971;68(4):820.
12. Harvey M, Vogel H, Morris D, Bradley A, Bernstein A, Donehower LA. A mutant p53 transgene accelerates tumour development in heterozygous but not nullizygous p53–deficient mice. Nature Genetics. 1995;9:305.
13. Marutani M, Tonoki H, Tada M, Takahashi M, Kashiwazaki H, Hida Y, et al. Dominant-Negative Mutations of the Tumor Suppressor p53 Relating to Early Onset of Glioblastoma Multiforme. Cancer Research. 1999;59(19):4765.
14. Willis A, Jung EJ, Wakefield T, Chen X. Mutant p53 exerts a dominant negative effect by preventing wild-type p53 from binding to the promoter of its target genes. Oncogene. 2004;23:2330.
15. Yoshida BA, Sokoloff MM, Welch DR, Rinker-Schaeffer CW. Metastasis-suppressor genes: a review and perspective on an emerging field. J Natl Cancer Inst. 2000;92(21):1717-30.
16. Mao H, Liu H, Fu X, Fang Z, Abrams J, Worsham MJ. Loss of nm23 expression predicts distal metastases and poorer survival for breast cancer. Int J Oncol. 2001;18(3):587-91.
17. Niu Y, Fu X, Lv A, Fan Y, Wang Y. Potential markers predicting distant metastasis in axillary node-negative breast carcinoma. International Journal of Cancer. 2002;98(5):754-60.
18. Guan-zhen Y, Ying C, Can-rong N, Guo-dong W, Jian-xin Q, Jie-jun W. Reduced protein expression of metastasis-related genes (nm23, KISS1, KAI1 and p53) in lymph node and liver metastases of gastric cancer. International Journal of Experimental Pathology. 2007;88(3):175-83.
19. Katakura H, Tanaka F, Oyanagi H, Miyahara R, Yanagihara K, Otake Y, et al. Clinical significance of nm23 expression in resected pathologic-stage I, non-small cell lung cancer. The Annals of Thoracic Surgery. 2002;73(4):1060-4.
20. Elmore S. Apoptosis: A Review of Programmed Cell Death. Toxicologic pathology. 2007;35(4):495-516.
21. Igney FH, Krammer PH. Death and anti-death: tumour resistance to apoptosis. Nature Reviews Cancer. 2002;2:277.
22. Maiuri MC, Zalckvar E, Kimchi A, Kroemer G. Self-eating and self-killing: crosstalk between autophagy and apoptosis. Nature Reviews Molecular Cell Biology. 2007;8:741.

23. Itoh N, Yonehara S, Ishii A, Yonehara M, Mizushima S-I, Sameshima M, et al. The polypeptide encoded by the cDNA for human cell surface antigen Fas can mediate apoptosis. Cell. 1991;66(2):233-43.
24. Rich T, Allen RL, Wyllie AH. Defying death after DNA damage. Nature. 2000;407:777.
25. Chinnaiyan AM. The apoptosome: heart and soul of the cell death machine. Neoplasia. 1999;1(1):5-15.
26. Gross A, Yin X-M, Wang K, Wei MC, Jockel J, Milliman C, et al. Caspase Cleaved BID Targets Mitochondria and Is Required for Cytochrome c Release, while BCL-XL Prevents This Release but Not Tumor Necrosis Factor-R1/Fas Death. Journal of Biological Chemistry. 1999;274(2):1156-63.
27. Siddiqui WA, Ahad A, Ahsan H. The mystery of BCL2 family: Bcl-2 proteins and apoptosis: an update. Archives of Toxicology. 2015;89(3):289-317.
28. Sato T, Irie S, Krajewski S, Reed JC. Cloning and sequencing of a cDNA encoding the rat Bcl-2 protein. Gene. 1994;140(2):291-2.
29. Huang DCS, Strasser A. BH3-Only Proteins—Essential Initiators of Apoptotic Cell Death. Cell. 2000;103(6):839-42.
30. Gross A, Jockel J, Wei MC, Korsmeyer SJ. Enforced dimerization of BAX results in its translocation, mitochondrial dysfunction and apoptosis. The EMBO Journal. 1998;17(14):3878-85.
31. Wolter KG, Hsu Y-T, Smith CL, Nechushtan A, Xi X-G, Youle RJ. Movement of Bax from the Cytosol to Mitochondria during Apoptosis. The Journal of Cell Biology. 1997;139(5):1281-92.
32. Eskes R, Desagher S, Antonsson B, Martinou J-C. Bid Induces the Oligomerization and Insertion of Bax into the Outer Mitochondrial Membrane. Molecular and Cellular Biology. 2000;20(3):929-35.
33. Hsu Y-T, Wolter KG, Youle RJ. Cytosol-to-membrane redistribution of Bax and Bcl-X(L) during apoptosis. Proceedings of the National Academy of Sciences of the United States of America. 1997;94(8):3668-72.
34. Cuconati A, Mukherjee C, Perez D, White E. DNA damage response and MCL-1 destruction initiate apoptosis in adenovirus-infected cells. Genes Dev. 2003;17(23):2922-32.
35. Hsu SY, Kaipia A, McGee E, Lomeli M, Hsueh AJ. Bok is a pro-apoptotic Bcl-2 protein with restricted expression in reproductive tissues and heterodimerizes with selective anti-apoptotic Bcl-2 family members. Proc Natl Acad Sci U S A. 1997;94(23):12401-6.
36. Carpio MA, Michaud M, Zhou W, Fisher JK, Walensky LD, Katz SG. BCL-2 family member BOK promotes apoptosis in response to endoplasmic reticulum stress. Proceedings of the National Academy of Sciences. 2015;112(23):7201.
37. Echeverry N, Bachmann D, Ke F, Strasser A, Simon HU, Kaufmann T. Intracellular localization of the BCL-2 family member BOK and functional implications. Cell death and differentiation. 2013;20:785.
38. Llambi F, Wang Y-M, Victor B, Yang M, Schneider Desiree M, Gingras S, et al. BOK Is a Non-canonical BCL-2 Family Effector of Apoptosis Regulated by ER-Associated Degradation. Cell. 2016;165(2):421-33.
39. Rodriguez JM, Glozak MA, Ma Y, Cress WD. Bok, Bcl-2 related ovarian killer, is cell cycle regulated and sensitizes to stress-induced apoptosis. The Journal of biological chemistry. 2006;281(32):22729-35.
40. Vaux DL, Cory S, Adams JM. Bcl-2 gene promotes haemopoietic cell survival and cooperates with c-myc to immortalize pre-B cells. Nature. 1988;335:440.
41. Moldoveanu T, Follis AV, Kriwacki RW, Green DR. Many players in BCL-2 family affairs. Trends in biochemical sciences. 2014;39(3):101-11.
42. Bird A. DNA methylation patterns and epigenetic memory. Genes & Development. 2002;16(1):6-21.
43. Prendergast GC, Ziff EB. Methylation-sensitive sequence-specific DNA binding by the c-Myc basic region. Science. 1991;251(4990):186.

44. Yuan G-C, Liu Y-J, Dion MF, Slack MD, Wu LF, Altschuler SJ, et al. Genome-Scale Identification of Nucleosome Positions in S. cerevisiae. Science. 2005;309(5734):626.
45. Gal-Yam EN, Jeong S, Tanay A, Egger G, Lee AS, Jones PA. Constitutive Nucleosome Depletion and Ordered Factor Assembly at the GRP78 Promoter Revealed by Single Molecule Footprinting. PLoS Genetics. 2006;2(9):e160.
46. Schones DE, Cui K, Cuddapah S, Roh T-Y, Barski A, Wang Z, et al. Dynamic Regulation of Nucleosome Positioning in the Human Genome. Cell. 2008;132(5):887-98.
47. Santenard A, Torres-Padilla M-E. Epigenetic reprogramming in mammalian reproduction: Contribution from histone variants. Epigenetics. 2009;4(2):80-4.
48. Jin C, Felsenfeld G. Nucleosome stability mediated by histone variants H3.3 and H2A.Z. Genes & Development. 2007;21(12):1519-29.
49. Luger K, Mäder AW, Richmond RK, Sargent DF, Richmond TJ. Crystal structure of the nucleosome core particle at 2.8 Å resolution. Nature. 1997;389:251.
50. Kouzarides T. Chromatin modifications and their function. Cell. 2007;128(4):693-705.
51. Hong L, Schroth GP, Matthews HR, Yau P, Bradbury EM. Studies of the DNA binding properties of histone H4 amino terminus. Thermal denaturation studies reveal that acetylation markedly reduces the binding constant of the H4 "tail" to DNA. Journal of Biological Chemistry. 1993;268(1):305-14.
52. Lee DY, Hayes JJ, Pruss D, Wolffe AP. A positive role for histone acetylation in transcription factor access to nucleosomal DNA. Cell. 1993;72(1):73-84.
53. Henry KW, Wyce A, Lo W-S, Duggan LJ, Emre NCT, Kao C-F, et al. Transcriptional activation via sequential histone H2B ubiquitylation and deubiquitylation, mediated by SAGA-associated Ubp8. Genes & Development. 2003;17(21):2648-63.
54. Shinkai Y, Tachibana M. H3K9 methyltransferase G9a and the related molecule GLP. Genes Dev. 2011;25(8):781-8.
55. Bannister AJ, Kouzarides T. Reversing histone methylation. Nature. 2005;436:1103.
56. Black Joshua C, Van Rechem C, Whetstine Johnathan R. Histone Lysine Methylation Dynamics: Establishment, Regulation, and Biological Impact. Molecular Cell.48(4):491-507.
57. Shi X, Kachirskaia I, Walter KL, Kuo J-HA, Lake A, Davrazou F, et al. Proteome-wide Analysis in Saccharomyces cerevisiae Identifies Several PHD Fingers as Novel Direct and Selective Binding Modules of Histone H3 Methylated at Either Lysine 4 or Lysine 36. The Journal of biological chemistry. 2007;282(4):2450-5.
58. Barski A, Cuddapah S, Cui K, Roh T-Y, Schones DE, Wang Z, et al. High-Resolution Profiling of Histone Methylations in the Human Genome. Cell.129(4):823-37.
59. Benevolenskaya EV. Histone H3K4 demethylases are essential in development and differentiation. Biochemistry and Cell Biology. 2007;85(4):435-43.
60. Barski A, Cuddapah S, Cui K, Roh T-Y, Schones DE, Wang Z, et al. High-Resolution Profiling of Histone Methylations in the Human Genome. Cell. 2007;129(4):823-37.
61. Steger DJ, Lefterova MI, Ying L, Stonestrom AJ, Schupp M, Zhuo D, et al. DOT1L/KMT4 Recruitment and H3K79 Methylation Are Ubiquitously Coupled with Gene Transcription in Mammalian Cells. Molecular and Cellular Biology. 2008;28(8):2825-39.
62. Rosenfeld JA, Wang Z, Schones DE, Zhao K, DeSalle R, Zhang MQ. Determination of enriched histone modifications in non-genic portions of the human genome. BMC Genomics. 2009;10:143.
63. Koch CM, Andrews RM, Flicek P, Dillon SC, Karaöz U, Clelland GK, et al. The landscape of histone modifications across 1% of the human genome in five human cell lines. Genome Research. 2007;17(6):691-707.
64. Bannister AJ, Schneider R, Myers FA, Thorne AW, Crane-Robinson C, Kouzarides T. Spatial Distribution of Di- and Tri-methyl Lysine 36 of Histone H3 at Active Genes. Journal of Biological Chemistry. 2005;280(18):17732-6.
65. Santos-Rosa H, Schneider R, Bannister AJ, Sherriff J, Bernstein BE, Emre NCT, et al. Active genes are tri-methylated at K4 of histone H3. Nature. 2002;419(6905):407-11.

66. Greer EL, Shi Y. Histone methylation: a dynamic mark in health, disease and inheritance. Nat Rev Genet. 2012;13(5):343-57.
67. Bedford MT, Clarke SG. Protein Arginine Methylation in Mammals: Who, What, and Why. Molecular Cell. 2009;33(1):1-13.
68. Yang Y, McBride Kevin M, Hensley S, Lu Y, Chedin F, Bedford Mark T. Arginine Methylation Facilitates the Recruitment of TOP3B to Chromatin to Prevent R Loop Accumulation. Molecular Cell. 2014;53(3):484-97.
69. Feng Y, Maity R, Whitelegge JP, Hadjikyriacou A, Li Z, Zurita-Lopez C, et al. Mammalian Protein Arginine Methyltransferase 7 (PRMT7) Specifically Targets RXR Sites in Lysine- and Arginine-rich Regions. Journal of Biological Chemistry. 2013;288(52):37010-25.
70. Butler JS, Zurita-Lopez CI, Clarke SG, Bedford MT, Dent SYR. Protein-arginine Methyltransferase 1 (PRMT1) Methylates Ash2L, a Shared Component of Mammalian Histone H3K4 Methyltransferase Complexes. Journal of Biological Chemistry. 2011;286(14):12234-44.
71. Rea S, Eisenhaber F, O'Carroll D, Strahl BD, Sun Z-W, Schmid M, et al. Regulation of chromatin structure by site-specific histone H3 methyltransferases. Nature. 2000;406:593.
72. Rice JC, Briggs SD, Ueberheide B, Barber CM, Shabanowitz J, Hunt DF, et al. Histone Methyltransferases Direct Different Degrees of Methylation to Define Distinct Chromatin Domains. Molecular Cell. 2003;12(6):1591-8.
73. Tachibana M, Ueda J, Fukuda M, Takeda N, Ohta T, Iwanari H, et al. Histone methyltransferases G9a and GLP form heteromeric complexes and are both crucial for methylation of euchromatin at H3-K9. Genes Dev. 2005;19(7):815-26.
74. Collins RE, Tachibana M, Tamaru H, Smith KM, Jia D, Zhang X, et al. In vitro and in vivo analyses of a Phe/Tyr switch controlling product specificity of histone lysine methyltransferases. J Biol Chem. 2005;280(7):5563-70.
75. Kubicek S, O'Sullivan RJ, August EM, Hickey ER, Zhang Q, Teodoro ML, et al. Reversal of H3K9me2 by a small-molecule inhibitor for the G9a histone methyltransferase. Mol Cell. 2007;25(3):473-81.
76. Schultz DC, Ayyanathan K, Negorev D, Maul GG, Rauscher FJ. SETDB1: a novel KAP-1-associated histone H3, lysine 9-specific methyltransferase that contributes to HP1-mediated silencing of euchromatic genes by KRAB zinc-finger proteins. Genes & Development. 2002;16(8):919-32.
77. Loyola A, Bonaldi T, Roche D, Imhof A, Almouzni G. PTMs on H3 Variants before Chromatin Assembly Potentiate Their Final Epigenetic State. Molecular Cell. 2006;24(2):309-16.
78. Wysocka J, Myers MP, Laherty CD, Eisenman RN, Herr W. Human Sin3 deacetylase and trithorax-related Set1/Ash2 histone H3-K4 methyltransferase are tethered together selectively by the cell-proliferation factor HCF-1. Genes & Development. 2003;17(7):896-911.
79. Lee J-H, Tate CM, You J-S, Skalnik DG. Identification and Characterization of the Human Set1B Histone H3-Lys4 Methyltransferase Complex. Journal of Biological Chemistry. 2007;282(18):13419-28.
80. Sun X-J, Wei J, Wu X-Y, Hu M, Wang L, Wang H-H, et al. Identification and Characterization of a Novel Human Histone H3 Lysine 36-specific Methyltransferase. Journal of Biological Chemistry. 2005;280(42):35261-71.
81. Kuo AJ, Cheung P, Chen K, Zee BM, Kioi M, Lauring J, et al. NSD2 links dimethylation of histone H3 at lysine 36 to oncogenic programming. Molecular cell. 2011;44(4):609-20.
82. Feng Q, Wang H, Ng HH, Erdjument-Bromage H, Tempst P, Struhl K, et al. Methylation of H3-Lysine 79 Is Mediated by a New Family of HMTases without a SET Domain. Current Biology. 2002;12(12):1052-8.
83. Min J, Feng Q, Li Z, Zhang Y, Xu R-M. Structure of the Catalytic Domain of Human DOT1L, a Non-SET Domain Nucleosomal Histone Methyltransferase. Cell. 2003;112(5):711-23.

84. Nishioka K, Rice JC, Sarma K, Erdjument-Bromage H, Werner J, Wang Y, et al. PR-Set7 Is a Nucleosome-Specific Methyltransferase that Modifies Lysine 20 of Histone H4 and Is Associated with Silent Chromatin. Molecular Cell. 2002;9(6):1201-13.
85. Schotta G, Lachner M, Sarma K, Ebert A, Sengupta R, Reuter G, et al. A silencing pathway to induce H3-K9 and H4-K20 trimethylation at constitutive heterochromatin. Genes & Development. 2004;18(11):1251-62.
86. Pannetier M, Julien E, Schotta G, Tardat M, Sardet C, Jenuwein T, et al. PR-SET7 and SUV4-20H regulate H4 lysine-20 methylation at imprinting control regions in the mouse. EMBO Rep. 2008;9(10):998-1005.
87. Margueron R, Reinberg D. The Polycomb complex PRC2 and its mark in life. Nature. 2011;469:343.
88. Shen X, Liu Y, Hsu Y-J, Fujiwara Y, Kim J, Mao X, et al. EZH1 Mediates Methylation on Histone H3 Lysine 27 and Complements EZH2 in Maintaining Stem Cell Identity and Executing Pluripotency. Molecular Cell. 2008;32(4):491-502.
89. Kim K-C, Geng L, Huang S. Inactivation of a Histone Methyltransferase by Mutations in Human Cancers. Cancer Research. 2003;63(22):7619.
90. Shi Y, Lan F, Matson C, Mulligan P, Whetstine JR, Cole PA, et al. Histone Demethylation Mediated by the Nuclear Amine Oxidase Homolog LSD1. Cell. 2004;119(7):941-53.
91. Rudolph T, Beuch S, Reuter G. Lysine-specific histone demethylase LSD1 and the dynamic control of chromatin. Biological Chemistry2013. p. 1019.
92. Tsukada Y-i, Fang J, Erdjument-Bromage H, Warren ME, Borchers CH, Tempst P, et al. Histone demethylation by a family of JmjC domain-containing proteins. Nature. 2005;439:811.
93. Frescas D, Guardavaccaro D, Bassermann F, Koyama-Nasu R, Pagano M. JHDM1B/FBXL10 is a nucleolar protein that represses transcription of ribosomal RNA genes. Nature. 2007;450:309.
94. Yamane K, Toumazou C, Tsukada Y-i, Erdjument-Bromage H, Tempst P, Wong J, et al. JHDM2A, a JmjC-Containing H3K9 Demethylase, Facilitates Transcription Activation by Androgen Receptor. Cell. 2006;125(3):483-95.
95. Whetstine JR, Nottke A, Lan F, Huarte M, Smolikov S, Chen Z, et al. Reversal of Histone Lysine Trimethylation by the JMJD2 Family of Histone Demethylases. Cell. 2006;125(3):467-81.
96. Lee MG, Wynder C, Cooch N, Shiekhattar R. An essential role for CoREST in nucleosomal histone 3 lysine 4 demethylation. Nature. 2005;437:432.
97. Walport LJ, Hopkinson RJ, Chowdhury R, Schiller R, Ge W, Kawamura A, et al. Arginine demethylation is catalysed by a subset of JmjC histone lysine demethylases. Nature Communications. 2016;7:11974.
98. Esteller M. Cancer epigenomics: DNA methylomes and histone-modification maps. Nature Reviews Genetics. 2007;8:286.
99. Jones PA, Baylin SB. The Epigenomics of Cancer. Cell. 2007;128(4):683-92.
100. Long C, Yin B, Lu Q, Zhou X, Hu J, Yang Y, et al. Promoter Hypermethylation of the RUNX3 Gene in Esophageal Squamous Cell Carcinoma. Cancer Investigation. 2007;25(8):685-90.
101. Sharma S, Kelly TK, Jones PA. Epigenetics in cancer. Carcinogenesis. 2010;31(1):27-36.
102. Schlesinger Y, Straussman R, Keshet I, Farkash S, Hecht M, Zimmerman J, et al. Polycomb-mediated methylation on Lys27 of histone H3 pre-marks genes for de novo methylation in cancer. Nature Genetics. 2006;39:232.
103. Fraga MF, Ballestar E, Villar-Garea A, Boix-Chornet M, Espada J, Schotta G, et al. Loss of acetylation at Lys16 and trimethylation at Lys20 of histone H4 is a common hallmark of human cancer. Nature Genetics. 2005;37:391.
104. Banister CE. Review of Epigenetics: A Reference Manual: A book edited by Jeffrey M. Craig and Nicholas C. Wong. Epigenetics. 2012;7(8):963-4.
105. Morin RD, Mendez-Lago M, Mungall AJ, Goya R, Mungall KL, Corbett RD, et al. Frequent mutation of histone-modifying genes in non-Hodgkin lymphoma. Nature. 2011;476:298.

106. Béguelin W, Popovic R, Teater M, Jiang Y, Bunting Karen L, Rosen M, et al. EZH2 Is Required for Germinal Center Formation and Somatic EZH2 Mutations Promote Lymphoid Transformation. Cancer Cell. 2013;23(5):677-92.
107. Stransky N, Egloff AM, Tward AD, Kostic AD, Cibulskis K, Sivachenko A, et al. The Mutational Landscape of Head and Neck Squamous Cell Carcinoma. Science. 2011;333(6046):1157.
108. Ntziachristos P, Tsirigos A, Vlierberghe PV, Nedjic J, Trimarchi T, Flaherty MS, et al. Genetic inactivation of the polycomb repressive complex 2 in T cell acute lymphoblastic leukemia. Nature Medicine. 2012;18:298.
109. Ley TJ, Ding L, Walter MJ, McLellan MD, Lamprecht T, Larson DE, et al. DNMT3A Mutations in Acute Myeloid Leukemia. New England Journal of Medicine. 2010;363(25):2424-33.
110. Ribeiro AFT, Pratcorona M, Erpelinck-Verschueren C, Rockova V, Sanders M, Abbas S, et al. Mutant DNMT3A a marker of poor prognosis in acute myeloid leukemia. Blood. 2012;119(24):5824.
111. Kanai Y, Ushijima S, Nakanishi Y, Sakamoto M, Hirohashi S. Mutation of the DNA methyltransferase (DNMT) 1 gene in human colorectal cancers. Cancer Letters. 2003;192(1):75-82.
112. Biegel JA, Zhou J-Y, Rorke LB, Stenstrom C, Wainwright LM, Fogelgren B. Germ-Line and Acquired Mutations of INI1 in Atypical Teratoid and Rhabdoid Tumors. Cancer Research. 1999;59(1):74.
113. Tachibana M, Sugimoto K, Fukushima T, Shinkai Y. Set domain-containing protein, G9a, is a novel lysine-preferring mammalian histone methyltransferase with hyperactivity and specific selectivity to lysines 9 and 27 of histone H3. J Biol Chem. 2001;276(27):25309-17.
114. Milner CM, Campbell RD. The G9a gene in the human major histocompatibility complex encodes a novel protein containing ankyrin-like repeats. Biochemical Journal. 1993;290(Pt 3):811-8.
115. Estève P-O, Patnaik D, Chin HG, Benner J, Teitell MA, Pradhan S. Functional analysis of the N- and C-terminus of mammalian G9a histone H3 methyltransferase. Nucleic Acids Research. 2005;33(10):3211-23.
116. Casciello F, Windloch K, Gannon F, Lee JS. Functional Role of G9a Histone Methyltransferase in Cancer. Front Immunol. 2015;6:487.
117. Zhang Y, Reinberg D. Transcription regulation by histone methylation: interplay between different covalent modifications of the core histone tails. Genes & Development. 2001;15(18):2343-60.
118. Shankar SR, Bahirvani AG, Rao VK, Bharathy N, Ow JR, Taneja R. G9a, a multipotent regulator of gene expression. Epigenetics. 2013;8(1):16-22.
119. Tachibana M, Sugimoto K, Nozaki M, Ueda J, Ohta T, Ohki M, et al. G9a histone methyltransferase plays a dominant role in euchromatic histone H3 lysine 9 methylation and is essential for early embryogenesis. Genes & Development. 2002;16(14):1779-91.
120. Tachibana M, Matsumura Y, Fukuda M, Kimura H, Shinkai Y. G9a/GLP complexes independently mediate H3K9 and DNA methylation to silence transcription. The EMBO Journal. 2008;27(20):2681-90.
121. Ogawa H, Ishiguro K-i, Gaubatz S, Livingston DM, Nakatani Y. A Complex with Chromatin Modifiers That Occupies E2F- and Myc-Responsive Genes in G0 Cells. Science. 2002;296(5570):1132.
122. Collins RE, Northrop JP, Horton JR, Lee DY, Zhang X, Stallcup MR, et al. The ankyrin repeats of G9a and GLP histone methyltransferases are mono- and dimethyllysine binding modules. Nat Struct Mol Biol. 2008;15(3):245-50.
123. Weiss T, Hergeth S, Zeissler U, Izzo A, Tropberger P, Zee BM, et al. Histone H1 variant-specific lysine methylation by G9a/KMT1C and Glp1/KMT1D. Epigenetics & Chromatin. 2010;3:7-.
124. Huret J-L, Ahmad M, Arsaban M, Bernheim A, Cigna J, Desangles F, et al. Atlas of Genetics and Cytogenetics in Oncology and Haematology in 2013. Nucleic Acids Research. 2013;41(D1):D920-D4.
125. Su R-C, Brown KE, Saaber S, Fisher AG, Merkenschlager M, Smale ST. Dynamic assembly of silent chromatin during thymocyte maturation. Nature Genetics. 2004;36:502.

126. Chen X, Skutt-Kakaria K, Davison J, Ou Y-L, Choi E, Malik P, et al. G9a/GLP-dependent histone H3K9me2 patterning during human hematopoietic stem cell lineage commitment. Genes & Development. 2012;26(22):2499-511.
127. Wen B, Wu H, Shinkai Y, Irizarry RA, Feinberg AP. Large histone H3 lysine 9 dimethylated chromatin blocks distinguish differentiated from embryonic stem cells. Nature Genetics. 2009;41:246.
128. Chin HG, Pradhan M, Estève P-O, Patnaik D, Evans TC, Pradhan S. Sequence Specificity and Role of Proximal Amino Acids of the Histone H3 Tail on Catalysis of Murine G9a Lysine 9 Histone H3 Methyltransferase. Biochemistry. 2005;44(39):12998-3006.
129. Chin HG, Estève P-O, Pradhan M, Benner J, Patnaik D, Carey MF, et al. Automethylation of G9a and its implication in wider substrate specificity and HP1 binding. Nucleic Acids Research. 2007;35(21):7313-23.
130. Huang J, Dorsey J, Chuikov S, Zhang X, Jenuwein T, Reinberg D, et al. G9a and Glp Methylate Lysine 373 in the Tumor Suppressor p53. The Journal of Biological Chemistry. 2010;285(13):9636-41.
131. Rathert P, Dhayalan A, Murakami M, Zhang X, Tamas R, Jurkowska R, et al. Protein lysine methyltransferase G9a acts on non-histone targets. Nature chemical biology. 2008;4(6):344-6.
132. Lee JS, Kim Y, Kim IS, Kim B, Choi HJ, Lee JM, et al. Negative Regulation of Hypoxic Responses via Induced Reptin Methylation. Molecular Cell. 2010;39(1):71-85.
133. Chen H, Yan Y, Davidson TL, Shinkai Y, Costa M. Hypoxic Stress Induces Dimethylated Histone H3 Lysine 9 through Histone Methyltransferase G9a in Mammalian Cells. Cancer Research. 2006;66(18):9009.
134. Lee SH, Kim J, Kim WH, Lee YM. Hypoxic silencing of tumor suppressor RUNX3 by histone modification in gastric cancer cells. Oncogene. 2008;28:184.
135. Lu Y, Chu A, Turker MS, Glazer PM. Hypoxia-Induced Epigenetic Regulation and Silencing of the BRCA1 Promoter. Molecular and Cellular Biology. 2011;31(16):3339-50.
136. Casciello F, Al-Ejeh F, Kelly G, Brennan DJ, Ngiow SF, Young A, et al. G9a drives hypoxia-mediated gene repression for breast cancer cell survival and tumorigenesis. Proceedings of the National Academy of Sciences of the United States of America. 2017;114(27):7077-82.
137. Lee JS, Kim Y, Bhin J, Shin H-JR, Nam HJ, Lee SH, et al. Hypoxia-induced methylation of a pontin chromatin remodeling factor. Proceedings of the National Academy of Sciences. 2011;108(33):13510.
138. Melvin A, Rocha S. Chromatin as an oxygen sensor and active player in the hypoxia response. Cellular Signalling. 2012;24(1):35-43.
139. Leutz A, Pless O, Lappe M, Dittmar G, Kowenz-Leutz E. Crosstalk between phosphorylation and multi-site arginine/lysine methylation in C/EBPs. Transcription. 2011;2(1):3-8.
140. Poulard C, Bittencourt D, Wu DY, Hu Y, Gerke DS, Stallcup MR. A post-translational modification switch controls coactivator function of histone methyltransferases G9a and GLP. EMBO Rep. 2017.
141. Bian C, Chen Q, Yu X. The zinc finger proteins ZNF644 and WIZ regulate the G9a/GLP complex for gene repression. eLife. 2015;4:e05606.
142. Lee DY, Northrop JP, Kuo M-H, Stallcup MR. HISTONE H3 LYSINE 9 METHYLTRANSFERASE G9a IS A TRANSCRIPTIONAL COACTIVATOR FOR NUCLEAR RECEPTORS. The Journal of biological chemistry. 2006;281(13):8476-85.
143. Chen M-W, Hua K-T, Kao H-J, Chi C-C, Wei L-H, Johansson G, et al. H3K9 Histone Methyltransferase G9a Promotes Lung Cancer Invasion and Metastasis by Silencing the Cell Adhesion Molecule Ep-CAM. Cancer Research. 2010;70(20):7830.
144. Zhong X, Chen X, Guan X, Zhang H, Ma Y, Zhang S, et al. Overexpression of G9a and MCM7 in oesophageal squamous cell carcinoma is associated with poor prognosis. Histopathology. 2014;66(2):192-200.

145. Mechanic S, Raynor K, Hill JE, Cowin P. Desmocollins form a distinct subset of the cadherin family of cell adhesion molecules. Proceedings of the National Academy of Sciences. 1991;88(10):4476.
146. Wozniak RJ, Klimecki WT, Lau SS, Feinstein Y, Futscher BW. 5-Aza-2'-deoxycytidine-mediated reductions in G9A histone methyltransferase and histone H3 K9 di-methylation levels are linked to tumor suppressor gene reactivation. Oncogene. 2006;26:77.
147. Lin X, Huang Y, Zou Y, Chen X, Ma X. Depletion of G9a gene induces cell apoptosis in human gastric carcinoma. Oncol Rep. 2016;35(5):3041-9.
148. Kondo Y, Shen L, Suzuki S, Kurokawa T, Masuko K, Tanaka Y, et al. Alterations of DNA methylation and histone modifications contribute to gene silencing in hepatocellular carcinomas. Hepatology Research. 2007;37(11):974-83.
149. Cho H-S, Kelly JD, Hayami S, Toyokawa G, Takawa M, Yoshimatsu M, et al. Enhanced Expression of EHMT2 Is Involved in the Proliferation of Cancer Cells through Negative Regulation of SIAH1. Neoplasia. 2011;13(8):676-IN10.
150. Hua K-T, Wang M-Y, Chen M-W, Wei L-H, Chen C-K, Ko C-H, et al. The H3K9 methyltransferase G9a is a marker of aggressive ovarian cancer that promotes peritoneal metastasis. Molecular Cancer. 2014;13:189.
151. Dong C, Wu Y, Yao J, Wang Y, Yu Y, Rychahou PG, et al. G9a interacts with Snail and is critical for Snail-mediated E-cadherin repression in human breast cancer. The Journal of Clinical Investigation. 2012;122(4):1469-86.
152. San José-Enériz E, Agirre X, Rabal O, Roa S, Vilas-Zornoza A, Miranda E, et al. Inhibition of the Methyltransferase G9a with Small Molecules As a New Therapeutic Strategy for Treatment of Hematological Malignancies. Blood. 2014;124(21):3532.
153. Liu S, Ye D, Guo W, Yu W, He Y, Hu J, et al. G9a is essential for EMT-mediated metastasis and maintenance of cancer stem cell-like characters in head and neck squamous cell carcinoma. Oncotarget. 2015;6(9):6887-901.
154. Zhang J, He P, Xi Y, Geng M, Chen Y, Ding J. Down-regulation of G9a triggers DNA damage response and inhibits colorectal cancer cells proliferation2014.
155. Curry E, Green I, Chapman-Rothe N, Shamsaei E, Kandil S, Cherblanc FL, et al. Dual EZH2 and EHMT2 histone methyltransferase inhibition increases biological efficacy in breast cancer cells. Clin Epigenetics. 2015;7:84.
156. Mozzetta C, Pontis J, Fritsch L, Robin P, Portoso M, Proux C, et al. The histone H3 lysine 9 methyltransferases G9a and GLP regulate polycomb repressive complex 2-mediated gene silencing. Mol Cell. 2014;53(2):277-89.
157. Dietrich N, Lerdrup M, Landt E, Agrawal-Singh S, Bak M, Tommerup N, et al. REST–Mediated Recruitment of Polycomb Repressor Complexes in Mammalian Cells. PLOS Genetics. 2012;8(3):e1002494.
158. Roopra A, Qazi R, Schoenike B, Daley TJ, Morrison JF. Localized Domains of G9a-Mediated Histone Methylation Are Required for Silencing of Neuronal Genes. Molecular Cell. 2004;14(6):727-38.
159. Kubicek S, O'Sullivan RJ, August EM, Hickey ER, Zhang Q, Teodoro Miguel L, et al. Reversal of H3K9me2 by a Small-Molecule Inhibitor for the G9a Histone Methyltransferase. Molecular Cell. 2007;25(3):473-81.
160. Chang Y, Ganesh T, Horton JR, Spannhoff A, Liu J, Sun A, et al. Adding a Lysine Mimic in the Design of Potent Inhibitors of Histone Lysine Methyltransferases. Journal of Molecular Biology. 2010;400(1):1-7.
161. Shi Y, Desponts C, Do JT, Hahm HS, Schöler HR, Ding S. Induction of Pluripotent Stem Cells from Mouse Embryonic Fibroblasts by Oct4 and Klf4 with Small-Molecule Compounds. Cell Stem Cell. 2008;3(5):568-74.
162. Shi Y, Tae Do J, Desponts C, Hahm HS, Schöler HR, Ding S. A Combined Chemical and Genetic Approach for the Generation of Induced Pluripotent Stem Cells. Cell Stem Cell. 2008;2(6):525-8.

163. Imai K, Togami H, Okamoto T. Involvement of Histone H3 Lysine 9 (H3K9) Methyltransferase G9a in the Maintenance of HIV-1 Latency and Its Reactivation by BIX01294. The Journal of Biological Chemistry. 2010;285(22):16538-45.
164. Feldman N, Gerson A, Fang J, Li E, Zhang Y, Shinkai Y, et al. G9a-mediated irreversible epigenetic inactivation of Oct-3/4 during early embryogenesis. Nature Cell Biology. 2006;8:188.
165. Chang Y, Zhang X, Horton JR, Upadhyay AK, Spannhoff A, Liu J, et al. Structural basis for G9a-like protein lysine methyltransferase inhibition by BIX-01294. Nat Struct Mol Biol. 2009;16(3):312-7.
166. He Y, Korboukh I, Jin J, Huang J. Targeting protein lysine methylation and demethylation in cancers. Acta Biochimica et Biophysica Sinica. 2012;44(1):70-9.
167. Frye SV. The art of the chemical probe. Nature Chemical Biology. 2010;6:159.
168. Vedadi M, Barsyte-Lovejoy D, Liu F, Rival-Gervier S, Allali-Hassani A, Labrie V, et al. A chemical probe selectively inhibits G9a and GLP methyltransferase activity in cells. Nat Chem Biol. 2011;7(8):566-74.
169. Liu F, Barsyte-Lovejoy D, Li F, Xiong Y, Korboukh V, Huang XP, et al. Discovery of an in vivo chemical probe of the lysine methyltransferases G9a and GLP. J Med Chem. 2013;56(21):8931-42.
170. Liu F, Barsyte-Lovejoy D, Allali-Hassani A, He Y, Herold JM, Chen X, et al. Optimization of Cellular Activity of G9a Inhibitors 7-Aminoalkoxy-quinazolines. Journal of medicinal chemistry. 2011;54(17):6139-50.
171. Sweis RF, Pliushchev M, Brown PJ, Guo J, Li F, Maag D, et al. Discovery and Development of Potent and Selective Inhibitors of Histone Methyltransferase G9a. ACS Medicinal Chemistry Letters. 2014;5(2):205-9.
172. Kondengaden SM, Luo L-f, Huang K, Zhu M, Zang L, Bataba E, et al. Discovery of novel small molecule inhibitors of lysine methyltransferase G9a and their mechanism in leukemia cell lines. European Journal of Medicinal Chemistry. 2016;122:382-93.
173. Wright JH. NEUROCYTOMA OR NEUROBLASTOMA, A KIND OF TUMOR NOT GENERALLY RECOGNIZED. The Journal of Experimental Medicine. 1910;12(4):556-61.
174. Jiang M, Stanke J, Lahti JM. The Connections Between Neural Crest Development and Neuroblastoma. Current topics in developmental biology. 2011;94:77-127.
175. Stiller C. Childhood Cancer in Britain: Incidence, Survival, Mortality2009. 1-288 p.
176. Huang M, Weiss WA. Neuroblastoma and MYCN. Cold Spring Harbor perspectives in medicine. 2013;3(10):a014415-a.
177. Cohn SL, Pearson ADJ, London WB, Monclair T, Ambros PF, Brodeur GM, et al. The International Neuroblastoma Risk Group (INRG) Classification System: An INRG Task Force Report. Journal of Clinical Oncology. 2009;27(2):289-97.
178. Brodeur GM, Seeger RC, Barrett A, Berthold F, Castleberry RP, D'Angio G, et al. International criteria for diagnosis, staging, and response to treatment in patients with neuroblastoma. Journal of Clinical Oncology. 1988;6(12):1874-81.
179. Brisse HJ, McCarville MB, Granata C, Krug KB, Wootton-Gorges SL, Kanegawa K, et al. Guidelines for Imaging and Staging of Neuroblastic Tumors: Consensus Report from the International Neuroblastoma Risk Group Project. Radiology. 2011;261(1):243-57.
180. Monclair T, Brodeur GM, Ambros PF, Brisse HJ, Cecchetto G, Holmes K, et al. The International Neuroblastoma Risk Group (INRG) Staging System: An INRG Task Force Report. Journal of Clinical Oncology. 2009;27(2):298-303.
181. Shohet J, Foster J. Neuroblastoma. BMJ. 2017;357.
182. Maris JM, Hogarty MD, Bagatell R, Cohn SL. Neuroblastoma. The Lancet.369(9579):2106-20.
183. Lawlor ER, Thiele CJ. Epigenetic Changes in Pediatric Solid Tumors: Promising New Targets. Clinical Cancer Research. 2012;18(10):2768.
184. Lázcoz P, Muñoz J, Nistal M, Pestaña Á, Encío I, Castresana JS. Frequent promoter hypermethylation of RASSF1A and CASP8 in neuroblastoma. BMC Cancer. 2006;6:254-.
185. Wang C, Liu Z, Woo CW, Li Z, Wang L, Wei JS, et al. EZH2 Mediates epigenetic silencing of neuroblastoma suppressor genes CASZ1, CLU, RUNX3, and NGFR. Cancer Res. 2012;72(1):315-24.

186. Liu Z, Thiele CJ. ALK and MYCN: when two oncogenes are better than one. Cancer Cell. 2012;21(3):325-6.
187. Morris SW, Kirstein MN, Valentine MB, Dittmer KG, Shapiro DN, Saltman DL, et al. Fusion of a kinase gene, ALK, to a nucleolar protein gene, NPM, in non-Hodgkin's lymphoma. Science. 1994;263(5151):1281.
188. Stoica GE, Kuo A, Aigner A, Sunitha I, Souttou B, Malerczyk C, et al. Identification of Anaplastic Lymphoma Kinase as a Receptor for the Growth Factor Pleiotrophin. Journal of Biological Chemistry. 2001;276(20):16772-9.
189. Stoica GE, Kuo A, Powers C, Bowden ET, Sale EB, Riegel AT, et al. Midkine Binds to Anaplastic Lymphoma Kinase (ALK) and Acts as a Growth Factor for Different Cell Types. Journal of Biological Chemistry. 2002;277(39):35990-8.
190. Trigg RM, Turner SD. ALK in Neuroblastoma: Biological and Therapeutic Implications. Cancers. 2018;10(4):113.
191. Bowden ET, Stoica GE, Wellstein A. Anti-apoptotic Signaling of Pleiotrophin through Its Receptor, Anaplastic Lymphoma Kinase. Journal of Biological Chemistry. 2002;277(39):35862-8.
192. Kuo AH, Stoica GE, Riegel AT, Wellstein A. Recruitment of insulin receptor substrate-1 and activation of NF-κB essential for midkine growth signaling through anaplastic lymphoma kinase. Oncogene. 2006;26:859.
193. Azarova AM, Gautam G, George RE. Emerging importance of ALK in neuroblastoma. Seminars in cancer biology. 2011;21(4):267-75.
194. Mossë YP, Laudenslager M, Longo L, Cole KA, Wood A, Attiyeh EF, et al. Identification of ALK as the Major Familial Neuroblastoma Predisposition Gene. Nature. 2008;455(7215):930-5.
195. Janoueix-Lerosey I, Lequin D, Brugières L, Ribeiro A, de Pontual L, Combaret V, et al. Somatic and germline activating mutations of the ALK kinase receptor in neuroblastoma. Nature. 2008;455:967.
196. Berry T, Luther W, Bhatnagar N, Jamin Y, Poon E, Sanda T, et al. The ALK(F1174L) mutation potentiates the oncogenic activity of MYCN in neuroblastoma. Cancer Cell. 2012;22(1):117-30.
197. Huang FW, Hodis E, Xu MJ, Kryukov GV, Chin L, Garraway LA. Highly recurrent TERT promoter mutations in human melanoma. Science (New York, NY). 2013;339(6122):957-9.
198. Valentijn LJ, Koster J, Zwijnenburg DA, Hasselt NE, van Sluis P, Volckmann R, et al. TERT rearrangements are frequent in neuroblastoma and identify aggressive tumors. Nat Genet. 2015;47(12):1411-4.
199. Frank SR, Parisi T, Taubert S, Fernandez P, Fuchs M, Chan H-M, et al. MYC recruits the TIP60 histone acetyltransferase complex to chromatin. EMBO Reports. 2003;4(6):575-80.
200. Schwab M, Alitalo K, Klempnauer K-H, Varmus HE, Bishop JM, Gilbert F, et al. Amplified DNA with limited homology to myc cellular oncogene is shared by human neuroblastoma cell lines and a neuroblastoma tumour. Nature. 1983;305:245.
201. Malynn BA, de Alboran IM, O'Hagan RC, Bronson R, Davidson L, DePinho RA, et al. N-myc can functionally replace c-myc in murine development, cellular growth, and differentiation. Genes & Development. 2000;14(11):1390-9.
202. Nau MM, Brooks BJ, Battey J, Sausville E, Gazdar AF, Kirsch IR, et al. L-myc, a new myc-related gene amplified and expressed in human small cell lung cancer. Nature. 1985;318:69.
203. Beltran H. The N-myc Oncogene: Maximizing its Targets, Regulation, and Therapeutic Potential. Mol Cancer Res. 2014;12(6):815-22.
204. Knoepfler PS, Cheng PF, Eisenman RN. N-myc is essential during neurogenesis for the rapid expansion of progenitor cell populations and the inhibition of neuronal differentiation. Genes & Development. 2002;16(20):2699-712.
205. Swartling Fredrik J, Savov V, Persson Anders I, Chen J, Hackett Christopher S, Northcott Paul A, et al. Distinct Neural Stem Cell Populations Give Rise to Disparate Brain Tumors in Response to N-MYC. Cancer Cell. 2012;21(5):601-13.

206. Charron J, Malynn BA, Fisher P, Stewart V, Jeannotte L, Goff SP, et al. Embryonic lethality in mice homozygous for a targeted disruption of the N-myc gene. Genes & Development. 1992;6(12a):2248-57.
207. van Bokhoven H, Celli J, van Reeuwijk J, Rinne T, Glaudemans B, van Beusekom E, et al. MYCN haploinsufficiency is associated with reduced brain size and intestinal atresias in Feingold syndrome. Nature Genetics. 2005;37:465.
208. Gherardi S, Valli E, Erriquez D, Perini G. MYCN-mediated transcriptional repression in neuroblastoma: the other side of the coin. Front Oncol. 2013;3:42.
209. Brodeur GM, Seeger RC, Schwab M, Varmus HE, Bishop JM. Amplification of N-myc in untreated human neuroblastomas correlates with advanced disease stage. Science. 1984;224(4653):1121.
210. Seeger RC, Brodeur GM, Sather H, Dalton A, Siegel SE, Wong KY, et al. Association of Multiple Copies of the N-myc Oncogene with Rapid Progression of Neuroblastomas. New England Journal of Medicine. 1985;313(18):1111-6.
211. Brodeur GM. Neuroblastoma: biological insights into a clinical enigma. Nature Reviews Cancer. 2003;3:203.
212. He S, Liu Z, Oh DY, Thiele CJ. MYCN and the epigenome. Front Oncol. 2013;3:1.
213. Hasan MK, Nafady A, Takatori A, Kishida S, Ohira M, Suenaga Y, et al. ALK is a MYCN target gene and regulates cell migration and invasion in neuroblastoma. Scientific Reports. 2013;3:3450.
214. Souttou B, Carvalho NB-D, Raulais D, Vigny M. Activation of Anaplastic Lymphoma Kinase Receptor Tyrosine Kinase Induces Neuronal Differentiation through the Mitogen-activated Protein Kinase Pathway. Journal of Biological Chemistry. 2001;276(12):9526-31.
215. Motegi A, Fujimoto J, Kotani M, Sakuraba H, Yamamoto T. ALK receptor tyrosine kinase promotes cell growth and neurite outgrowth. Journal of Cell Science. 2004;117(15):3319.
216. Giannini G, Cerignoli F, Mellone M, Massimi I, Ambrosi C, Rinaldi C, et al. High Mobility Group A1 Is a Molecular Target for MYCN in Human Neuroblastoma. Cancer Research. 2005;65(18):8308.
217. Sumter TF, Xian L, Huso T, Koo M, Chang YT, Almasri TN, et al. The High Mobility Group A1 (HMGA1) Transcriptome in Cancer and Development. Current molecular medicine. 2016;16(4):353-93.
218. Hatzi E, Murphy C, Zoephel A, Rasmussen H, Morbidelli L, Ahorn H, et al. N-myc oncogene overexpression down-regulates IL-6; evidence that IL-6 inhibits angiogenesis and suppresses neuroblastoma tumor growth. Oncogene. 2002;21:3552.
219. Breit S, Rössler J, Fotsis T, Schweigerer L. N-myc Down-Regulates Activin A. Biochemical and Biophysical Research Communications. 2000;274(2):405-9.
220. Hatzi E, Fotsis T, Murphy C, Breit S, Schweigerer L, Zoephel A, et al. MYCN Oncogene and Angiogenesis: Down-Regulation of Endothelial Growth Inhibitors in Human Neuroblastoma Cells. In: Maragoudakis ME, editor. Angiogenesis: From the Molecular to Integrative Pharmacology. Boston, MA: Springer US; 2000. p. 239-48.
221. Breit S, Ashman K, Wilting J, Rössler J, Hatzi E, Fotsis T, et al. The N-myc Oncogene in Human Neuroblastoma Cells: Down-Regulation of an Angiogenesis Inhibitor Identified as Activin A. Cancer Research. 2000;60(16):4596.
222. Zhang W, Yu Y, Hertwig F, Thierry-Mieg J, Zhang W, Thierry-Mieg D, et al. Comparison of RNA-seq and microarray-based models for clinical endpoint prediction. Genome Biology. 2015;16(1):133.
223. Strieder V, Lutz W. E2F Proteins Regulate MYCN Expression in Neuroblastomas. Journal of Biological Chemistry. 2003;278(5):2983-9.
224. Kapeli K, Hurlin PJ. Differential Regulation of N-Myc and c-Myc Synthesis, Degradation, and Transcriptional Activity by the Ras/Mitogen-activated Protein Kinase Pathway. Journal of Biological Chemistry. 2011;286(44):38498-508.

225. Ikegaki N, Bukovsky J, Kennett RH. Identification and characterization of the NMYC gene product in human neuroblastoma cells by monoclonal antibodies with defined specificities. Proceedings of the National Academy of Sciences of the United States of America. 1986;83(16):5929-33.
226. Sjostrom SK, Finn G, Hahn WC, Rowitch DH, Kenney AM. The Cdk1 Complex Plays a Prime Role in Regulating N-Myc Phosphorylation and Turnover in Neural Precursors. Developmental Cell. 2005;9(3):327-38.
227. Otto T, Horn S, Brockmann M, Eilers U, Schüttrumpf L, Popov N, et al. Stabilization of N-Myc Is a Critical Function of Aurora A in Human Neuroblastoma. Cancer Cell. 2009;15(1):67-78.
228. Brockmann M, Poon E, Berry T, Carstensen A, Deubzer Hedwig E, Rycak L, et al. Small Molecule Inhibitors of Aurora-A Induce Proteasomal Degradation of N-Myc in Childhood Neuroblastoma. Cancer Cell.24(1):75-89.
229. Park JH, Szemes M, Vieira GC, Melegh Z, Malik S, Heesom KJ, et al. Protein arginine methyltransferase 5 is a key regulator of the MYCN oncoprotein in neuroblastoma cells. Molecular Oncology. 2015;9(3):617-27.
230. Sherr CJ, Roberts JM. CDK inhibitors: positive and negative regulators of G1-phase progression. Genes & Development. 1999;13(12):1501-12.
231. Iraci N, Diolaiti D, Papa A, Porro A, Valli E, Gherardi S, et al. A SP1/MIZ1/MYCN repression complex recruits HDAC1 at the TRKA and p75NTR promoters and affects neuroblastoma malignancy by inhibiting the cell response to NGF. Cancer Res. 2011;71(2):404-12.
232. Slack A, Chen Z, Tonelli R, Pule M, Hunt L, Pession A, et al. The p53 regulatory gene MDM2 is a direct transcriptional target of MYCN in neuroblastoma. Proceedings of the National Academy of Sciences of the United States of America. 2005;102(3):731-6.
233. Casciano IDA, Banelli B, Croce M, Ambrosis A, Vinci A, Gelvi I, et al. Caspase-8 Gene Expression in Neuroblastoma. Annals of the New York Academy of Sciences. 2006;1028(1):157-67.
234. Casaccia-Bonnefil P, Kong H, Chao MV. Neurotrophins: the biological paradox of survival factors eliciting apoptosis. Cell death and differentiation. 1998;5(5):357-64.
235. Schulte Johannes H, Pentek F, Hartmann W, Schramm A, Friedrichs N, Øra I, et al. The low-affinity neurotrophin receptor, p75, is upregulated in ganglioneuroblastoma/ganglioneuroma and reduces tumorigenicity of neuroblastoma cells in vivo. International Journal of Cancer. 2009;124(10):2488-94.
236. Veschi V, Petroni M, Cardinali B, Dominici C, Screpanti I, Frati L, et al. Galectin-3 Impairment of MYCN-Dependent Apoptosis-Sensitive Phenotype Is Antagonized by Nutlin-3 in Neuroblastoma Cells. PLoS ONE. 2012;7(11):e49139.
237. Akahani S, Nangia-Makker P, Inohara H, Kim H-RC, Raz A. Galectin-3: A Novel Antiapoptotic Molecule with A Functional BH1 (NWGR) Domain of Bcl-2 Family. Cancer Research. 1997;57(23):5272.
238. Hoyer KK, Pang M, Gui D, Shintaku IP, Kuwabara I, Liu F-T, et al. An Anti-Apoptotic Role for Galectin-3 in Diffuse Large B-Cell Lymphomas. The American Journal of Pathology. 2004;164(3):893-902.
239. Fulda S, Lutz W, Schwab M, Debatin K-M. MycN sensitizes neuroblastoma cells for drug-induced apoptosis. Oncogene. 1999;18:1479.
240. Cotterman R, Jin VX, Krig SR, Lemen JM, Wey A, Farnham PJ, et al. N-Myc regulates a widespread euchromatic program in the human genome partially independent of its role as a classical transcription factor. Cancer research. 2008;68(23):9654-62.
241. Knoepfler PS, Zhang X-y, Cheng PF, Gafken PR, McMahon SB, Eisenman RN. Myc influences global chromatin structure. The EMBO Journal. 2006;25(12):2723-34.
242. Corvetta D, Chayka O, Gherardi S, D'Acunto CW, Cantilena S, Valli E, et al. Physical Interaction between MYCN Oncogene and Polycomb Repressive Complex 2 (PRC2) in Neuroblastoma: FUNCTIONAL AND THERAPEUTIC IMPLICATIONS. The Journal of Biological Chemistry. 2013;288(12):8332-41.

243. Wong M, Tee AEL, Milazzo G, Bell JL, Poulos RC, Atmadibrata B, et al. The Histone Methyltransferase DOT1L Promotes Neuroblastoma by Regulating Gene Transcription. Cancer Res. 2017;77(9):2522-33.
244. Kaelin Jr WG. The Concept of Synthetic Lethality in the Context of Anticancer Therapy. Nature Reviews Cancer. 2005;5:689.
245. O'Neil NJ, Bailey ML, Hieter P. Synthetic lethality and cancer. Nature Reviews Genetics. 2017;18:613.
246. Dobzhansky T. Genetics of Natural Populations. Xiii. Recombination and Variability in Populations of Drosophila Pseudoobscura. Genetics. 1946;31(3):269-90.
247. Bridges CB. The Origin of Variations in Sexual and Sex-Limited Characters. The American Naturalist. 1922;56(642):51-63.
248. Kaiser CA, Schekman R. Distinct sets of SEC genes govern transport vesicle formation and fusion early in the secretory pathway. Cell. 1990;61(4):723-33.
249. Venkitaraman AR. Cancer Susceptibility and the Functions of BRCA1 and BRCA2. Cell. 2002;108(2):171-82.
250. Farmer H, McCabe N, Lord CJ, Tutt ANJ, Johnson DA, Richardson TB, et al. Targeting the DNA repair defect in BRCA mutant cells as a therapeutic strategy. Nature. 2005;434:917.
251. Helleday T. The underlying mechanism for the PARP and BRCA synthetic lethality: Clearing up the misunderstandings. Molecular Oncology. 2011;5(4):387-93.
252. Molenaar JJ, Ebus ME, Geerts D, Koster J, Lamers F, Valentijn LJ, et al. Inactivation of CDK2 is synthetically lethal to MYCN over-expressing cancer cells. Proceedings of the National Academy of Sciences. 2009;106(31):12968.
253. Brockmann M, Poon E, Berry T, Carstensen A, Deubzer HE, Rycak L, et al. Small Molecule Inhibitors of Aurora-A Induce Proteasomal Degradation of N-Myc in Childhood Neuroblastoma. Cancer cell. 2013;24(1):75-89.
254. Müller I, Larsson K, Frenzel A, Oliynyk G, Zirath H, Prochownik EV, et al. Targeting of the MYCN Protein with Small Molecule c-MYC Inhibitors. PLOS ONE. 2014;9(5):e97285.
255. Guo J, Parise RA, Joseph E, Egorin MJ, Lazo JS, Prochownik EV, et al. Efficacy, pharmacokinetics, tisssue distribution, and metabolism of the Myc–Max disruptor, 10058-F4 [Z,E]-5-[4-ethylbenzylidine]-2-thioxothiazolidin-4-one, in mice. Cancer chemotherapy and pharmacology. 2009;63(4):615-25.
256. Puissant A, Frumm SM, Alexe G, Bassil CF, Qi J, Chanthery YH, et al. Targeting MYCN in Neuroblastoma by BET Bromodomain Inhibition. Cancer Discovery. 2013;3(3):308.
257. Henssen A, Althoff K, Odersky A, Beckers A, Koche R, Speleman F, et al. Targeting MYCN-Driven Transcription By BET-Bromodomain Inhibition. Clinical Cancer Research. 2016;22(10):2470.
258. Lochmann TL, Powell KM, Ham J, Floros KV, Heisey DAR, Kurupi RIJ, et al. Targeted inhibition of histone H3K27 demethylation is effective in high-risk neuroblastoma. Science Translational Medicine. 2018;10(441).
259. Ding J, Li T, Wang X, Zhao E, Choi JH, Yang L, et al. The histone H3 methyltransferase G9A epigenetically activates the serine-glycine synthesis pathway to sustain cancer cell survival and proliferation. Cell Metab. 2013;18(6):896-907.
260. Lu Z, Tian Y, Salwen HR, Chlenski A, Godley LA, Raj JU, et al. Histone-lysine methyltransferase EHMT2 is involved in proliferation, apoptosis, cell invasion, and DNA methylation of human neuroblastoma cells. Anticancer Drugs. 2013;24(5):484-93.
261. Ke XX, Zhang D, Zhu S, Xia Q, Xiang Z, Cui H. Inhibition of H3K9 methyltransferase G9a repressed cell proliferation and induced autophagy in neuroblastoma cells. PLoS One. 2014;9(9):e106962.
262. Brodeur GM, Goldstein MN. Histochemical demonstration of an increase in acetylcholinesterase in established lines of human and mouse neuroblastomas by nerve growth factor. Cytobios. 1976;16(62):133-8.

263. Seeger RC, Rayner SA, Banerjee A, Chung H, Laug WE, Neustein HB, et al. Morphology, Growth, Chromosomal Pattern, and Fibrinolytic Activity of Two New Human Neuroblastoma Cell Lines. Cancer Research. 1977;37(5):1364.
264. Tumilowicz JJ, Nichols WW, Cholon JJ, Greene AE. Definition of a continuous human cell line derived from neuroblastoma. Cancer Res. 1970;30(8):2110-8.
265. Biedler JL, Helson L, Spengler BA. Morphology and growth, tumorigenicity, and cytogenetics of human neuroblastoma cells in continuous culture. Cancer Res. 1973;33(11):2643-52.
266. Thiele CJ. Neuroblastoma cell lines. Journal of Human Cell Culture. 1998;1:21-53.
267. Chen L, Rousseau RF, Middleton SA, Nichols GL, Newell DR, Lunec J, et al. Pre-clinical evaluation of the MDM2-p53 antagonist RG7388 alone and in combination with chemotherapy in neuroblastoma. Oncotarget. 2015;6(12):10207-21.
268. Tweddle DA, Malcolm AJ, Bown N, Pearson AD, Lunec J. Evidence for the development of p53 mutations after cytotoxic therapy in a neuroblastoma cell line. Cancer Res. 2001;61(1):8-13.
269. Tweddle DA, Malcolm AJ, Cole M, Pearson AD, Lunec J. p53 cellular localization and function in neuroblastoma: evidence for defective G(1) arrest despite WAF1 induction in MYCN-amplified cells. Am J Pathol. 2001;158(6):2067-77.
270. Cornaglia-Ferraris P, Ponzoni M, Montaldo P, Mariottini GL, Donti E, Di Martino D, et al. A New Human Highly Tumorigenic Neuroblastoma Cell Line with Undetectable Expression of N-myc. Pediatric Research. 1990;27:1.
271. Longo L, Christiansen H, Christiansen NM, Cornaglia-Ferraris P, Lampert F. N-myc amplification at chromosome band 1p32 in neuroblastoma cells as investigated by in situ hybridization. J Cancer Res Clin Oncol. 1988;114(6):636-40.
272. Lutz W, Stohr M, Schurmann J, Wenzel A, Lohr A, Schwab M. Conditional expression of N-myc in human neuroblastoma cells increases expression of alpha-prothymosin and ornithine decarboxylase and accelerates progression into S-phase early after mitogenic stimulation of quiescent cells. Oncogene. 1996;13(4):803-12.
273. Bodnar AG, Ouellette M, Frolkis M, Holt SE, Chiu C-P, Morin GB, et al. Extension of Life-Span by Introduction of Telomerase into Normal Human Cells. Science. 1998;279(5349):349.
274. Schwab M, Alitalo K, Klempnauer KH, Varmus HE, Bishop JM, Gilbert F, et al. Amplified DNA with limited homology to myc cellular oncogene is shared by human neuroblastoma cell lines and a neuroblastoma tumour. Nature. 1983;305(5931):245-8.
275. Mosse YP, Laudenslager M, Longo L, Cole KA, Wood A, Attiyeh EF, et al. Identification of ALK as a major familial neuroblastoma predisposition gene. Nature. 2008;455(7215):930-5.
276. Shahbazi J, Scarlett CJ, Norris MD, Liu B, Haber M, Tee AE, et al. Histone deacetylase 2 and N-Myc reduce p53 protein phosphorylation at serine 46 by repressing gene transcription of tumor protein 53-induced nuclear protein 1. Oncotarget. 2014;5(12):4257-68.
277. Brodeur GM, Green AA, Hayes FA, Williams KJ, Williams DL, Tsiatis AA. Cytogenetic Features of Human Neuroblastomas and Cell Lines. Cancer Research. 1981;41(11 Part 1):4678.
278. George RE, Sanda T, Hanna M, Fröhling S, Luther W, Zhang J, et al. Activating mutations in ALK provide a therapeutic target in neuroblastoma. Nature. 2008;455(7215):975-8.
279. Goldschneider D, Horvilleur E, Plassa L-F, Guillaud-Bataille M, Million K, Wittmer-Dupret E, et al. Expression of C-terminal deleted p53 isoforms in neuroblastoma. Nucleic Acids Research. 2006;34(19):5603-12.
280. M Davidoff A, Pence J, Shorter N, D Iglehart J, R Marks J. Expression of p53 in human neuroblastoma- and neuroepithelioma-derived cell lines1992. 127-33 p.
281. Caren H, Abel F, Kogner P, Martinsson T. High incidence of DNA mutations and gene amplifications of the ALK gene in advanced sporadic neuroblastoma tumours. Biochem J. 2008;416(2):153-9.
282. Ciccarone V, Spengler BA, Meyers MB, Biedler JL, Ross RA. Phenotypic diversification in human neuroblastoma cells: expression of distinct neural crest lineages. Cancer Res. 1989;49(1):219-25.

283. Gilbert F, Balaban G, Moorhead P, Bianchi D, Schlesinger H. Abnormalities of chromosome 1p in human neuroblastoma tumors and cell lines. Cancer Genet Cytogenet. 1982;7(1):33-42.
284. Brodeur GM, Green AA, Hayes FA, Williams KJ, Williams DL, Tsiatis AA. Cytogenetic features of human neuroblastomas and cell lines. Cancer Res. 1981;41(11 Pt 1):4678-86.
285. Hasan MK, Nafady A, Takatori A, Kishida S, Ohira M, Suenaga Y, et al. ALK is a MYCN target gene and regulates cell migration and invasion in neuroblastoma. Sci Rep. 2013;3:3450.
286. Duijkers FA, Gaal J, Meijerink JP, Admiraal P, Pieters R, de Krijger RR, et al. Anaplastic lymphoma kinase (ALK) inhibitor response in neuroblastoma is highly correlated with ALK mutation status, ALK mRNA and protein levels. Cell Oncol (Dordr). 2011;34(5):409-17.
287. Biedler JL, Roffler-Tarlov S, Schachner M, Freedman LS. Multiple neurotransmitter synthesis by human neuroblastoma cell lines and clones. Cancer Res. 1978;38(11 Pt 1):3751-7.
288. Barnes EN, Biedler JL, Spengler BA, Lyser KM. The fine structure of continuous human neuroblastoma lines SK-N-SH, SK-N-BE(2), and SK-N-MC. In Vitro. 1981;17(7):619-31.
289. Cole KA, Huggins J, Laquaglia M, Hulderman CE, Russell MR, Bosse K, et al. RNAi screen of the protein kinome identifies checkpoint kinase 1 (CHK1) as a therapeutic target in neuroblastoma. Proc Natl Acad Sci U S A. 2011;108(8):3336-41.
290. Keshelava N, Zuo JJ, Chen P, Waidyaratne SN, Luna MC, Gomer CJ, et al. Loss of p53 Function Confers High-Level Multidrug Resistance in Neuroblastoma Cell Lines. Cancer Research. 2001;61(16):6185.
291. Cornaglia-Ferraris P, Sansone R, Mariottini GL, Longo L, Tonini GP. Evidence of loss of N-myc amplification during the establishment of a human neuroblastoma cell line. Int J Cancer. 1990;45(3):578-9.
292. Li Z, Takenobu H, Setyawati AN, Akita N, Haruta M, Satoh S, et al. EZH2 regulates neuroblastoma cell differentiation via NTRK1 promoter epigenetic modifications. Oncogene. 2018;37(20):2714-27.
293. Yang Q-W, Liu S, Tian Y, Salwen HR, Chlenski A, Weinstein J, et al. Methylation-associated Silencing of the Thrombospondin-1 Gene in Human Neuroblastoma. Cancer Research. 2003;63(19):6299.
294. Yang Q, Tian Y, Liu S, Zeine R, Chlenski A, Salwen HR, et al. Thrombospondin-1 Peptide ABT-510 Combined with Valproic Acid Is an Effective Antiangiogenesis Strategy in Neuroblastoma. Cancer Research. 2007;67(4):1716.
295. Yang Q, Liu S, Tian Y, Hasan C, Kersey D, Salwen HR, et al. Methylation-Associated Silencing of the Heat Shock Protein 47 Gene in Human Neuroblastoma. Cancer Research. 2004;64(13):4531.
296. Molenaar JJ, Koster J, Zwijnenburg DA, van Sluis P, Valentijn LJ, van der Ploeg I, et al. Sequencing of neuroblastoma identifies chromothripsis and defects in neuritogenesis genes. Nature. 2012;483:589.
297. Valentijn LJ, Koster J, Haneveld F, Aissa RA, van Sluis P, Broekmans MEC, et al. Functional MYCN signature predicts outcome of neuroblastoma irrespective of MYCN amplification. Proceedings of the National Academy of Sciences of the United States of America. 2012;109(47):19190-5.
298. Kocak H, Ackermann S, Hero B, Kahlert Y, Oberthuer A, Juraeva D, et al. Hox-C9 activates the intrinsic pathway of apoptosis and is associated with spontaneous regression in neuroblastoma. Cell Death & Disease. 2013;4(4):e586.
299. Lutz W, Stöhr M, Schürmann J, Wenzel A, Löhr A, Schwab M. Conditional expression of N-MYC in human neuroblastoma cells increases expression of a-prothymosin and ornithine decarboxylase and accelerates progression into s-phase early after mitogenic stimulation of quiescent cells1996. 803-12 p.
300. Huang T, Zhang P, Li W, Zhao T, Zhang Z, Chen S, et al. G9A promotes tumor cell growth and invasion by silencing CASP1 in non-small-cell lung cancer cells. Cell Death &Amp; Disease. 2017;8:e2726.

301. Agarwal P, Jackson SP. G9a inhibition potentiates the anti-tumour activity of DNA double-strand break inducing agents by impairing DNA repair independent of p53 status. Cancer Lett. 2016;380(2):467-75.
302. Woo SM, Seo SU, Min K-J, Kwon TK. BIX-01294 sensitizes renal cancer Caki cells to TRAIL-induced apoptosis through downregulation of survivin expression and upregulation of DR5 expression. Cell Death Discovery. 2018;4(1):29.
303. Kollareddy M, Sherrard A, Park JH, Szemes M, Gallacher K, Melegh Z, et al. The small molecule inhibitor YK-4-279 disrupts mitotic progression of neuroblastoma cells, overcomes drug resistance and synergizes with inhibitors of mitosis. Cancer Letters. 2017.
304. Mair B, Konopka T, Kerzendorfer C, Sleiman K, Salic S, Serra V, et al. Gain- and Loss-of-Function Mutations in the Breast Cancer Gene GATA3 Result in Differential Drug Sensitivity. PLoS Genetics. 2016;12(9):e1006279.
305. Cui J, Sun W, Hao X, Wei M, Su X, Zhang Y, et al. EHMT2 inhibitor BIX-01294 induces apoptosis through PMAIP1-USP9X-MCL1 axis in human bladder cancer cells. Cancer Cell International. 2015;15:4.
306. Jwa M, Chang P. PARP16 is a tail-anchored endoplasmic reticulum protein required for the PERK and IRE1α-mediated unfolded protein response. Nature cell biology. 2012;14(11):1223-30.
307. Wen YY, Yang ZQ, Song M, Li BL, Yao XH, Chen XL, et al. The expression of SIAH1 is downregulated and associated with Bim and apoptosis in human breast cancer tissues and cells. Molecular Carcinogenesis. 2010;49(5):440-9.
308. Kramer JM. Regulation of cell differentiation and function by the euchromatin histone methyltranserfases G9a and GLP. Biochemistry and Cell Biology. 2015;94(1):26-32.
309. Moore KE, Carlson SM, Camp ND, Cheung P, James RG, Chua KF, et al. A general molecular affinity strategy for global detection and proteomic analysis of lysine methylation. Molecular cell. 2013;50(3):444-56.
310. Levy D, Kuo AJ, Chang Y, Schaefer U, Kitson C, Cheung P, et al. Lysine methylation of the NF-κB subunit RelA by SETD6 couples activity of the histone methyltransferase GLP at chromatin to tonic repression of NF-κB signaling. Nature Immunology. 2010;12:29.
311. Xiong Y, Li F, Babault N, Dong A, Zeng H, Wu H, et al. Discovery of Potent and Selective Inhibitors for G9a-Like Protein (GLP) Lysine Methyltransferase. J Med Chem. 2017;60(5):1876-91.
312. Nishio H, Walsh MJ. CCAAT displacement protein/cut homolog recruits G9a histone lysine methyltransferase to repress transcription. Proceedings of the National Academy of Sciences of the United States of America. 2004;101(31):11257.
313. Rao VK, Ow JR, Shankar SR, Bharathy N, Manikandan J, Wang Y, et al. G9a promotes proliferation and inhibits cell cycle exit during myogenic differentiation. Nucleic Acids Res. 2016;44(17):8129-43.
314. Takahashi A, Imai Y, Yamakoshi K, Kuninaka S, Ohtani N, Yoshimoto S, et al. DNA Damage Signaling Triggers Degradation of Histone Methyltransferases through APC/CCdh1 in Senescent Cells. Molecular Cell. 2012;45(1):123-31.
315. Bittencourt D, Wu D-Y, Jeong KW, Gerke DS, Herviou L, Ianculescu I, et al. G9a functions as a molecular scaffold for assembly of transcriptional coactivators on a subset of Glucocorticoid Receptor target genes. Proceedings of the National Academy of Sciences of the United States of America. 2012;109(48):19673-8.
316. Peirce SK, Findley HW. High level MycN expression in non-MYCN amplified neuroblastoma is induced by the combination treatment nutlin-3 and doxorubicin and enhances chemosensitivity. Oncol Rep. 2009;22(6):1443-9.
317. Bouchard C, Dittrich O, Kiermaier A, Dohmann K, Menkel A, Eilers M, et al. Regulation of cyclin D2 gene expression by the Myc/Max/Mad network: Myc-dependent TRRAP recruitment and histone acetylation at the cyclin D2 promoter. Genes Dev. 2001;15(16):2042-7.
318. Luo D, Caniggia I, Post M. Hypoxia-inducible regulation of placental BOK expression. Biochemical Journal. 2014;461(3):391.

319. Luo Y, Wang X, Wang H, Xu Y, Wen Q, Fan S, et al. High Bak Expression Is Associated with a Favorable Prognosis in Breast Cancer and Sensitizes Breast Cancer Cells to Paclitaxel. PLoS ONE. 2015;10(9):e0138955.
320. Carberry S, D'Orsi B, Monsefi N, Salvucci M, Bacon O, Fay J, et al. The BAX/BAK-like protein BOK is a prognostic marker in colorectal cancer. Cell Death & Disease. 2018;9(2):125.
321. Su Z, Fang H, Hong H, Shi L, Zhang W, Zhang W, et al. An investigation of biomarkers derived from legacy microarray data for their utility in the RNA-seq era. Genome Biology. 2014;15(12):3273.
322. Jääskeläinen M, Nieminen A, Pökkylä R-M, Kauppinen M, Liakka A, Heikinheimo M, et al. Regulation of cell death in human fetal and adult ovaries—Role of Bok and Bcl-XL. Molecular and Cellular Endocrinology. 2010;330(1):17-24.
323. Einsele-Scholz S, Malmsheimer S, Bertram K, Stehle D, Johänning J, Manz M, et al. Bok is a genuine multi-BH-domain protein that triggers apoptosis in the absence of Bax and Bak. Journal of Cell Science. 2016;129(11):2213.
324. Bartholomeusz G, Wu Y, Ali Seyed M, Xia W, Kwong K-Y, Hortobagyi G, et al. Nuclear translocation of the pro-apoptotic Bcl-2 family member Bok induces apoptosis. Molecular Carcinogenesis. 2006;45(2):73-83.
325. Igaki T, Kanuka H, Inohara N, Sawamoto K, Núñez G, Okano H, et al. Drob-1, a Drosophila member of the Bcl-2/CED-9 family that promotes cell death. Proceedings of the National Academy of Sciences of the United States of America. 2000;97(2):662-7.
326. Yakovlev AG, Di Giovanni S, Wang G, Liu W, Stoica B, Faden AI. BOK and NOXA Are Essential Mediators of p53-dependent Apoptosis. Journal of Biological Chemistry. 2004;279(27):28367-74.
327. Zhang H, Holzgreve W, De Geyter C. Evolutionarily conserved Bok proteins in the Bcl-2 family. FEBS Letters. 2000;480(2-3):311-3.
328. Inohara N, Ekhterae D, Garcia I, Carrio R, Merino J, Merry A, et al. Mtd, a Novel Bcl-2 Family Member Activates Apoptosis in the Absence of Heterodimerization with Bcl-2 and Bcl-XL. Journal of Biological Chemistry. 1998;273(15):8705-10.
329. Fernandez PC, Frank SR, Wang L, Schroeder M, Liu S, Greene J, et al. Genomic targets of the human c-Myc protein. Genes & Development. 2003;17(9):1115-29.
330. Perini G, Diolaiti D, Porro A, Della Valle G. In vivo transcriptional regulation of N-Myc target genes is controlled by E-box methylation. Proceedings of the National Academy of Sciences of the United States of America. 2005;102(34):12117-22.
331. Lee W-H, Murphree AL, Benedict WF. Expression and amplification of the N-myc gene in primary retinoblastoma. Nature. 1984;309:458.
332. Kim JH, Choi JM, Yu YS, Kim DH, Kim JH, Kim K-W. N-myc amplification was rarely detected by fluorescence in situ hybridization in retinoblastoma. Human Pathology. 2008;39(8):1172-5.
333. MacPherson D, Conkrite K, Tam M, Mukai S, Mu D, Jacks T. Murine bilateral retinoblastoma exhibiting rapid-onset, metastatic progression and N-myc gene amplification. The EMBO Journal. 2007;26(3):784-94.
334. Nau MM, Brooks BJ, Carney DN, Gazdar AF, Battey JF, Sausville EA, et al. Human small-cell lung cancers show amplification and expression of the N-myc gene. Proceedings of the National Academy of Sciences. 1986;83(4):1092.
335. Wong AJ, Ruppert JM, Eggleston J, Hamilton, Baylin SB, Vogelstein B. Gene amplification of c-myc and N-myc in small cell carcinoma of the lung. Science. 1986;233(4762):461.
336. Funa K, Steinholtz L, Nou E, Bergh J. Increased Expression of N-myc in Human Small Cell Lung Cancer Biopsies Predicts Lack of Response to Chemotherapy and Poor Prognosis. American Journal of Clinical Pathology. 1987;88(2):216-20.
337. Mizukami Y, Nonomura A, Takizawa T, Noguchi M, Michigishi T, Nakamura S, et al. N-myc protein expression in human breast carcinoma: Prognostic implications1995. 2899-905 p.
338. Williams RD, Al-Saadi R, Chagtai T, Popov S, Messahel B, Sebire N, et al. Subtype-specific FBXW7 mutation and MYCN copy number gain in Wilms tumour. Clinical cancer research : an official journal of the American Association for Cancer Research. 2010;16(7):2036-45.

339. Liu C, Yu Y, Liu F, Wei X, Wrobel JA, Gunawardena HP, et al. A chromatin activity-based chemoproteomic approach reveals a transcriptional repressome for gene-specific silencing. Nat Commun. 2014;5:5733.
340. Lindsten T, Ross AJ, King A, Zong W-X, Rathmell JC, Shiels HA, et al. The Combined Functions of Proapoptotic Bcl-2 Family Members Bak and Bax Are Essential for Normal Development of Multiple Tissues. Molecular Cell. 2000;6(6):1389-99.
341. Wei MC, Zong W-X, Cheng EHY, Lindsten T, Panoutsakopoulou V, Ross AJ, et al. Proapoptotic BAX and BAK: A Requisite Gateway to Mitochondrial Dysfunction and Death. Science. 2001;292(5517):727.
342. Rabachini T, Fernandez-Marrero Y, Montani M, Loforese G, Sladky V, He Z, et al. BOK promotes chemical-induced hepatocarcinogenesis in mice. Cell Death & Differentiation. 2017:1.
343. Ray JE, Garcia J, Jurisicova A, Caniggia I. Mtd/Bok takes a swing: proapoptotic Mtd/Bok regulates trophoblast cell proliferation during human placental development and in preeclampsia. Cell death and differentiation. 2009;17:846.
344. Abud HE. Shaping developing tissues by apoptosis. Cell death and differentiation. 2004;11:797.
345. Prudent J, Popgeorgiev N, Bonneau B, Gillet G. Bcl-2 proteins, cell migration and embryonic development: lessons from zebrafish. Cell Death & Disease. 2015;6(10):e1910.
346. Rizzuto R, Brini M, Murgia M, Pozzan T. Microdomains with high Ca2+ close to IP3-sensitive channels that are sensed by neighboring mitochondria. Science. 1993;262(5134):744.
347. Rasola A, Bernardi P. Mitochondrial permeability transition in Ca2+-dependent apoptosis and necrosis. Cell Calcium. 2011;50(3):222-33.
348. Wu X, Zhang L-s, Toombs J, Kuo Y-C, Piazza JT, Tuladhar R, et al. Extra-mitochondrial prosurvival BCL-2 proteins regulate gene transcription by inhibiting the SUFU tumour suppressor. Nature Cell Biology. 2017;19:1226.
349. Schulman JJ, Wright FA, Kaufmann T, Wojcikiewicz RJH. The Bcl-2 Protein Family Member Bok Binds to the Coupling Domain of Inositol 1,4,5-Trisphosphate Receptors and Protects Them from Proteolytic Cleavage. The Journal of Biological Chemistry. 2013;288(35):25340-9.
350. Gudmundsdottir K, Ashworth A. The roles of BRCA1 and BRCA2 and associated proteins in the maintenance of genomic stability. Oncogene. 2006;25:5864.
351. Benevento M, Iacono G, Selten M, Ba W, Oudakker A, Frega M, et al. Histone Methylation by the Kleefstra Syndrome Protein EHMT1 Mediates Homeostatic Synaptic Scaling. Neuron. 2016;91(2):341-55.
352. Han Y-C, Zheng Z-L, Zuo Z-H, Yu YP, Chen R, Tseng GC, et al. Metallothionein 1 h tumour suppressor activity in prostate cancer is mediated by euchromatin methyltransferase 1. The Journal of pathology. 2013;230(2):184-93.